Ψ_k Newsletter

AB INITIO (FROM ELECTRONIC STRUCTURE) CALCULATION OF COMPLEX PROCESSES IN MATERIALS

Number 89 October 2008

Editor: Z. (Dzidka) Szotek
E-mail: psik-coord@dl.ac.uk
Sponsored by: UK's CCP9
and ESF Psi-k Programme

Contents

1 Editorial

First of all we would like to turn our readers' attention to the Psi-k Portal about which we write in the General News section.

The most noteworthy item of this newsletter is the 48-page long scientific highlight by Markus E. Gruner and Peter Entel (Duisburg, Germany) on "Simulating functional magnetic materials on supercomputers". In addition, in this newsletter we have three reports on recent meetings, as well as some job and abstract announcements.

The Psi-k's web page is

http://www.psi-k.org.uk/

From this page you can also access the Psi-k Portal and all the information stored there.

Please submit all material for the next newsletters to the email address below.

	function
psik-coord@dl.ac.uk	**messages to the coordinators, editor & newsletter**

Dzidka Szotek, Martin Lüders and Walter Temmerman
e-mail: psik-coord@dl.ac.uk

2 General News

2.1 Psi-k Portal Information Services

It has been brought to our attention that as far as the distribution and sharing of any Psi-k information is concerned, the Psi-k Portal may not be as effective as the old moderated Psi-k mailing list used to be. Thus, if you have any comments, criticism and/or suggestions on the matter we would be happy to hear them. We are very much concerned about improving the range and flow of the Psi-k information for the benefit of the whole Psi-k community.

At the moment we have about 1050 Psi-k Portal members which, however, is only about a half of the old moderated Psi-k mailing list. Therefore, we would like to ask all the members of the Psi-k Portal to encourage their co-workers and colleagues to join the Portal if they have not done it yet.

It is rather straightforward to subscribe to the Portal and on the main Psi-k web page (http://www.psi-k.org) we have a detailed information on how to join and use the Psi-k Portal. Also, on the Psi-k Portal itself there is available some helpful information on this. Of course, in case of any problems we shall be happy to provide further help, if or when we are around.

We welcome all your input and criticism in trying to improve the Psi-k Portal and to make it as easy and efficient to use as possible.

Thank you for your cooperation.

Psi-k Coordinator

3 News from the ESF Programme

"Towards Atomistic Materials Design"

3.1 Reports on the ESF Workshops

3.1.1 Report on Summer School Nanomagnetism and Spintronics

Prague, Czech Republic

September 5–13, 2008

Sponsors

Psi-k Training in Computational Nanoscience
Towards Atomistic Materials Design (Psi-k)

Organizing committee

I. Turek – Charles University, Prague,
and Academy of Sciences of the Czech Republic, Brno
J. Kudrnovský – Academy of Sciences of the Czech Republic, Prague
P. Bruno – European Synchrotron Radiation Facility, Grenoble

http://cmd.karlov.mff.cuni.cz/Spintronics-2008/

Summary

The summer school was organized by the Faculty of Mathematics and Physics, Charles University, Prague, and the Institute of Physics, Academy of Sciences of the Czech Republic, Prague. The scientific part of the school took place in premises of the Faculty of Mathematics and Physics. The school programme, extending over eight days, was based on 28 invited lectures with two inserted poster sessions. The school was attended by more than 120 participants, mostly from Europe (the lists of lecturers and participants are given below).

The purpose of the school was to give an introduction to nanomagnetism and spintronics, with emphasis put on first-principles theoretical methods on the level appropriate to early-stage researchers (last year PhD students, fresh postdocs). Majority of the lecturers and participants came from the community of ab initio electronic structure theory but a part of the talks was devoted to other theoretical approaches (non-equilibrium Green's functions, semiempirical model Hamiltonians) as well as to relevant experimental results and techniques (STM, AFM).

The lectures of the school covered a wide area of theoretical magnetism (the school programme is given below). The particular topics addressed by the speakers included:

- spin-dependent transport properties (P. J. Kelly, S. Sanvito, D. Wortmann, G. E. W. Bauer),
- non-collinear magnetic structures (L. Sandratskii, I. Mertig),
- nanoscale magnetic systems (H. Ebert, C. Carbone, P. Bruno, B. Barbara),
- diluted magnetic semiconductors (B. Gallagher, T. Jungwirth, O. Eriksson, J. Mašek),
- effects of spin-orbit interaction on ground-state properties (G. Bihlmayer, P. Weinberger),
- transport phenomena due to spin-orbit interaction (J. Fabian, J. Wunderlich, J. Sinova, K. Výborný),
- advanced experimental techniques and their theoretical background (S. Blügel, P. Jelínek, W. Wulfhekel),
- electron systems far from thermodynamic equilibrium (B. Velický), with strong electron correlations (S. Biermann), and with more than one order parameter (C. Ederer).

Two lectures by Nobel prize winners (A. Fert, P. Grünberg) provided an excellent overview of development of spintronics from the discovery of the giant magnetoresistance effect towards the very recent and possible future applications.

In addition to the lectures, two poster sessions were organized so that participants could show results of their own research. More than one half of the participants presented a poster; the interesting topics and results displayed led to very lively discussions during both poster sessions (the complete list of posters is given below).

Programme

Saturday, September 6

9:00 P. H. Dederichs: *Opening*

9:00–10:30 P. J. Kelly: *Ab initio scattering theory from wave-function matching*

11:00–12:30 B. Velický: *Introduction to non-equilibrium Green's functions*

14:00–15:30 S. Sanvito: *Magnetic tunnel junctions under finite bias*

16:00–17:30 D. Wortmann: *Complex band structures and all-electron transport calculations for magnetic tunnel junctions*

Sunday, September 7

9:00–10:30 L. Sandratskii: *First-principles study of non-collinear magnetism: Basic principles and applications*

11:00–12:30 H. Ebert: *Finite magnetic metallic clusters*

14:00–15:30 C. Carbone: *Nanoscale magnets at surfaces*

16:00–17:30 I. Mertig: *Non-collinear magnetic nanowires*

Monday, September 8

9:00–10:30 A. Fert: *Variations on themes in spintronics: from the roots to recent developments*

11:00–12:30 G. Bihlmayer: *Spin-orbit effects at magnetic surfaces*

14:00–15:30 P. Weinberger: *Magnetic anisotropies in nanostructured matter*

16:00–17:30 J. Fabian: *Interfaces between ferromagnetic metals and semiconductors: spin-orbit coupling and structural symmetry*

Tuesday, September 9

9:00–10:30 B. Gallagher: *Ferromagnetic semiconductors*

11:00–12:30 T. Jungwirth: *Ferromagnetic semiconductors for spintronics: Theory concepts and experimental overview*

14:00–15:30 O. Eriksson: *Diluted magnetic semiconductors from a first principles point of view*

16:00–17:30 J. Mašek: *Electronic and atomic structure of dilute magnetic semiconductors (some open questions)*

Wednesday, September 10

9:00–10:30 P. Bruno: *Controlling self-organization and magnetism of nanostructures on surfaces by using quantum interferences*

11:00–12:30 G. E. W. Bauer: *Spin transfer by charge and heat currents*

14:00–16:00 poster session I

Thursday, September 11

9:00–10:30 J. Wunderlich: *Voltage controlled spintronics effects based on spin-orbit interaction*

11:00–12:30 J. Sinova: *Anomalous Hall transport: merging semiclassical and microscopic theories*

14:00–15:30 K. Výborný: *Anisotropic magnetoresistance in diluted magnetic semiconductors*

16:00–18:00 poster session II

Friday, September 12

9:00–10:30 S. Blügel: *Spinpolarized scanning tunneling microscopy*

11:00–12:30 W. Wulfhekel: *Spin-polarized scanning tunneling microscopy and spectroscopy: High resolution magnetic imaging and beyond*

14:00–15:30 B. Barbara: *Molecular magnets*

16:00–17:30 S. Biermann: *Electronic correlations in solids beyond the LDA*

Saturday, September 13

9:00–10:30 C. Ederer: *Multiferroic materials*

11:00–12:30 P. Jelínek: *AFM: a tool for surface science*

14:00–15:30 P. Grünberg: *GMR and some of its applications*

The electronic files of the lectures can be downloaded at
`http://kfes-80.karlov.mff.cuni.cz/Spintronics-2008/lectures.php`
using the password: `mellon`

List of posters

- A. Al-Zubi: *Magnetic order and anisotropy of 3d monolayers on Rh(001)*
- C. Ataca: *Magnetism of Transition Metal Nanowires*
- A. Avdonin: *The s,p-d exchange constants in ZnMnTeO alloy*
- M. S. Bahramy: *Theoretical study on phase stability, magnetism and spin-induced transport in $CeMnNi_4$ intermetallic compound*
- P. Balaz: *Current-pulse-induced switching of asymmetric spin valve*
- S. Blizak: *Density Functional Theory of Collinear Magnetism*
- P. Buczek: *Non-adiabatic spin dynamics of complex magnetic structures*
- K. Carva: *Spin-transfer torques in noncollinear spin valves: first principles study*
- K.-W. Chen: *Electron transport through quantum dots with indirect coupling parameter*
- C.-L. Chen: *Persistent spin current and local spin density in a tubular 2DEG with Rashba spin-orbit coupling*
- G. Cheng: *Magnetic-field-induced chains of cobalt nanoparticles*
- F. Cinti: *Monte Carlo Simulations on Thin Rare Earth Films*
- M. Cubukcu: *Study of Ferromagnetic Metal/Semiconductor Bilayers*
- C. Ertler: *Self-sustained magnetoelectric oscillations in magnetic resonant tunneling diodes*
- C. Etz: *Ab-initio magneto-optical properties of bcc Ni/Ni(100)*
- D. Fedorov: *First-principles calculations of spin relaxation time in metals*
- A. Grünebohm: *Ab initio examination of Fe/GaAs(110) interfaces with respect to spin transport*
- R. Hammerling: *Magnetic multipole moments with $\ell > 1$ in ab-initio calculations*
- B. Hardrat: *Unique playground for complex magnetism: Fe on hexagonal transition-metal surfaces*
- S. Heers: *Lifetime reduction of surface states induced by impurity scattering*
- J. Hellsvik: *Dynamics of diluted magnetic semiconductors from atomistic spin dynamics simulations*
- L. Herrera Diez: *Magnetic Anisotropy and Domain Structure in (GaMn)As*
- P. Horley: *Influence of magnetic field pulses with different time profiles on the magnetization dynamics of a monodomain ferromagnetic particle*
- M. Hortamani: *Ab initio study of the exchange interactions and Curie temperature of thin film MnSi/Si(001)*

- D. Iusan: *Theoretical study of Co clustering in ZnO*
- M. James: *Relativistic embedding and surface electronic structure*
- J. Kaczkowski: *Ab initio calculations of magnetic properties of wurzite $Al_{1-x}TM_xN$, (TM = V, Cr, Mn, Fe, Co, Ni)*
- G. Kaur: *Current Induced Dynamic Nuclear Polarization in III-V Semiconductors*
- K. Khazen: *Anisotropic relaxation of magnetization in GaMnAs thin layers*
- L. Kilanski: *Room temperature ferromagnetism in $Zn_{1-x}(Mn,Co)_xGeAs_2$ semiconductor: structural, magnetic and transport properties*
- R. Klepaczko: *The studies of paramagnetic molecules deposited on HOPG (0001) substrates for ESN-STM measurements*
- F. Körmann: *Importance of magnetism for the thermodynamics of bcc iron: an ab initio study*
- A. Kovalev: *Piezospin polarization of currents in nanostructures*
- P. Krukowski: *The studies of organic radical molecules deposited on Au(111) and HOPG (0001) substrates for ESN-STM measurements*
- D. Krychowski: *Spin-polarized transport through T-shaped DQD system in spin-orbital Kondo regime*
- J. Kudrnovský: *Relation of Curie temperature and conductivity: (Ga,Mn)As alloys as a case study*
- D. Legut: *Angular dependence of the Xray circular and linear dichroism in transitional metals from first principles*
- I. Maznichenko: *Electronic and magnetic properties of doped ZnO*
- M. Menzel: *Electronic properties of bi-atomic Fe chains on Ir(001)*
- S. H. Mirhosseini: *Electron correlation effects in the magnetoresistance of Fe/MgO/Fe tunnel junctions: First-principles calculations*
- C. Neise: *Orbital polarization corrections applied to selected uranium compounds*
- C. S. Olariu: *Investigation of Switching Region in SAF System*
- T. Ossowski: *Cohesion and magnetism at grain boundaries in chromium*
- P. Petkova: *Influence of the transition metal impurities on the magnetooptical effect in $Bi_4Ge_3O_{12}$*
- S. Polesya: *Temperature Dependence of Magnetic Order in Fe/(Ga,Mn)As Studied by Monte Carlo Simulation*
- S. Power: *Finite size effects in magnetically doped graphene nanoribbons*
- M. Rasander: *Structural, chemical and magnetic properties of ternary transition metal carbides*
- E. Rozkotová: *Ultrafast laser spectroscopy of GaMnAs*
- F. Römer: *In situ g-factor and magnetic anisotropy determination of Fe/InAs(100)*
- H. Sahin: *Spin-dependent Conductance of Short Graphene Nanoribbons*
- S. Schmaus: *Electron transport across single phthalocyanine molecules*
- S. Schönecker: *fcc - bcc epitaxial Bain path of uranium*
- T. Schuh: *Measuring of magnetic anisotropy of transition metal clusters on Pt(111)*
- V. Sessi: *Magnetism of surface supported 3d and 4d metal nanostructures*
- A. Sidorenko: *NMR study of magnetic properties of thin magnetic layer in various inter-*

faces

- B. Spisak, M. Woloszyn: *Computer simulation of the spin-polarised transport through a nanodevice*
- A. Stroppa: *Hybrid functionals applied to Mn doped III-V semiconductors*
- V. Stsefanovich: *Magnetization process and magnetic anisotropy of (Ga,Mn)As thin films on GaAs (311)A substrate*
- A. Thiess: *Magnetically suppressed chain formation in break junctions*
- S. Trudel: *Amorphous iron oxide: Magnetism and structure*
- I. Turek: *Relativistic electronic structure of (Ga,Mn)As*
- E. Wachowicz: *Cr segregation at Fe* $\Sigma 5(210)$ *and* $\Sigma 3(111)$ *grain boundaries*
- A. Werpachowska: *Spin waves, anisotropies and Curie temperature in ferromagnetic (Ga,Mn)As*
- M. Werwinski: *Ab initio studies of antiferromagnetism in* $UPdAs_2$
- A. Wysocki: *Effect of magnetic short-range order and local moment softening on spin-disorder resistivity*
- P. X. Xu: *Influence of Roughness and Disorder on Spin Transfer Torque in Magnetic Tunneling Junctions*
- A. Zacarias: *DFT approach to molecular electronics*
- M. Zelený: *Ab initio study of structural and magnetic properties of manganese nanowires from one to three dimensions*
- H. Zhang: *Surface magnetic anisotropy in external electric fields: Density functional calculations*

List of lecturers

Albert Fert	Unité Mixte de Physique, CNRS/Thales, Palaiseau, France
Peter Grünberg	Forschungszentrum Jülich, Germany
Gerrit E. W. Bauer	Delft University of Technology, The Netherlands
Hubert Ebert	Ludwig-Maximilian-University, Munich, Germany
Bedřich Velický	Charles University, Prague, Czech Rep.
Gustav Bihlmayer	Forschungszentrum Jülich, Germany
Carlo Carbone	Istituto di Struttura della Materia, Trieste, Italy
Tomáš Jungwirth	Institute of Physics, Acad. Sci. Czech Rep., Prague
Bryan Gallagher	University of Nottingham, UK
Claude Ederer	Trinity College, Dublin, Ireland
Daniel Wortmann	Forschungszentrum Jülich, Germany
Ingrid Mertig	Martin-Luther-University, Halle, Germany
Jan Mašek	Institute of Physics, Acad. Sci. Czech Rep., Prague
Jaroslav Fabian	University of Regensburg, Germany
Karel Výborný	Institute of Physics, Acad. Sci. Czech Rep., Prague
Jairo Sinova	Texas A&M University, USA
Peter Weinberger	Center for Computational Nanoscience, Vienna, Austria
Silke Biermann	CPHT, École Polytechnique, Palaiseau, France
Paul J. Kelly	University of Twente, The Netherlands

Olle Eriksson	Uppsala University, Sweden
Stefano Sanvito	Trinity College, Dublin, Ireland
Leonid Sandratskii	MPI for Microstructure Physics, Halle, Germany
Patrick Bruno	European Synchrotron Radiation Facility, Grenoble, France
Bernard Barbara	Institut Néel, CNRS, Grenoble, France
Jörg Wunderlich	Hitachi Cambridge Laboratory, UK
Stefan Blügel	Forschungszentrum Jülich, Germany
Wulf Wulfhekel	University of Karlsruhe, Germany
Pavel Jelínek	Institute of Physics, Acad. Sci. Czech Rep., Prague

List of participants

Anna Adamska (Prague, CZ)
Ali Al-Zubi (Jülich, DE)
Andrei Avdonin (Warszawa, PL)
Mohammad Saeed Bahramy (Sendai, JP)
Olivier Bengone (Strasbourg, FR)
Sven Bornemann (München, DE)
Karel Carva (Prague, CZ)
Kuo-Wei Chen (Taipei, TW)
Guangjun Cheng (Gaithersburg, US)
Murat Cubukcu (Paris, FR)
Marco Donolato (Como, IT)
Marcus Ekholm (Linköping, SE)
Christian Ertler (Regensburg, DE)
Dmitry Fedorov (Halle, DE)
Nataliya Goncharuk (Prague, CZ)
Anna Grünebohm (Duisburg, DE)
Kjetil Hals (Trondheim, NO)
Björn Hardrat (Hamburg, DE)
Johan Hellsvik (Uppsala, SE)
Lukas Horak (Prague, CZ)
Mahboubeh Hortamani (Halle, DE)
Matthew James (Bath, UK)
Yvonna Jiraskova (Brno, CZ)
Tomas Kana (Brno, CZ)
Khashayar Khazen (Paris, FR)
Rafal Klepaczko (Lodz, PL)
Fritz Körmann (Düsseldorf, DE)
Spiros Krimpalis (Iasi, RO)
Damian Krychowski (Poznan, PL)
Dominik Legut (Uppsala, SE)
Giulia Lorusso (Modena, IT)
Fatih Al (Kocaeli, TR)
Can Ataca (Ankara, TR)
Nadjib Baadji (Dublin, IE)
Pavel Balaz (Poznan, PL)
Salah Blizak (Boumerdes, DZ)
Pawel Buczek (Halle, DE)
Arianna Casiraghi (Nottingham, UK)
Chien-Liang Chen (Taipei, TW)
Fabio Cinti (Modena, IT)
Shafagh Dastjani Farahani (Mainz, DE)
Andrea Droghetti (Dublin, IE)
Pavlina Elstnerova (Brno, CZ)
Corina Etz (Halle, DE)
Andreas Gierlich (Jülich, DE)
Tanja Graf (Mainz, DE)
Lukas Halagacka (Ostrava-Poruba, CZ)
Robert Hammerling (Vienna, AT)
Swantje Heers (Jülich, DE)
Liza Herrera Diez (Stuttgart, DE)
Paul Horley (Lisbon, PT)
Diana Iusan (Uppsala, SE)
Marcela Janatova (Prague, CZ)
Jakub Kaczkowski (Poznan, PL)
Gurneet Kaur (Stuttgart, DE)
Lukasz Kilanski (Warsaw, PL)
Ivo Klik (Taipei, TW)
Richard Korytar (Barcelona, ES)
Pawel Krukowski (Lodz, PL)
Gerhard Kuhn (München, DE)
Maria Longobardi (Baronissi, IT)
Stephan Lowitzer (München, DE)

Martin Magiera (Duisburg, DE)
Silvie Maskova (Prague, CZ)
Matthias Menzel (Hamburg, DE)
Seyed Hossein Mirhosseini (Halle, DE)
Asmund Monsen (Trondheim, NO)
Lea Nichtova (Prague, CZ)
Kamil Olejnik (Prague, CZ)
Kemal Özdogan (Kocaeli, TR)
Anna Pertsova (Dublin, IE)
Nadezda Pizurova (Brno, CZ)
Jana Poltierova-Vejpravova (Prague, CZ)
Tomasz Radzynski (Warsaw, PL)
Florian Römer (Duisburg, DE)
Eva Rozkotova (Prague, CZ)
Hasan Sahin (Ankara, TR)
Magne Saxegaard (Trondheim, NO)
Stephan Schönecker (Dresden, DE)
Alessandro Sena (London, UK)
Andrey Sidorenko (Parma, IT)
Izabela Sliwa (Poznan, PL)
Olha Stelmakhovych (Lviv, UA)
Viktar Stsefanovich (Bialystok, PL)
Alexander Thiess (Jülich, DE)
Takao Tsumuraya (Hiroshima, JP)
Monika Vsianska (Brno, CZ)
Mu Wang (Nottingham, UK)
Agnieszka Werpachowska (Warsaw, PL)
Maciej Woloszyn (Krakow, PL)
Ruijuan Xiao (Dresden, DE)
Dezheng Yang (Trondheim, NO)
Liviu Zarbo (College Station, US)
Jan Zemen (Prague, CZ)
Zhen Gang Zhu (Halle, DE)
Robin Marshall (Nottingham, UK)
Igor Maznichenko (Halle, DE)
Alexey Kovalev (College Station, US)
Pascu Catalin Moca (Oradea, RO)
Carsten Neise (Dresden, DE)
Cristina Stefania Olariu (Iasi, RO)
Tomasz Ossowski (Wroclaw, PL)
Jana Pavlu (Brno, CZ)
Petya Petkova (Shumen, BG)
Svitlana Polesya (München, DE)
Stephen Power (Dublin, IE)
Mikael Rasander (Uppsala, SE)
Pavla Roupcova (Brno, CZ)
Alexandra Rudajevova (Prague, CZ)
Lakshmi Sankaran (Dresden, DE)
Stefan Schmaus (Karlsruhe, DE)
Tobias Schuh (Karlsruhe, DE)
Violetta Sessi (Stuttgart, DE)
Ondrej Sipr (Prague, CZ)
Bartlomiej Spisak (Krakow, PL)
Alessandro Stroppa (Vienna, AT)
Rudolf Sykora (Prague, CZ)
Simon Trudel (Kaiserslautern, DE)
Klara Uhlirova (Prague, CZ)
Elwira Wachowicz (Wroclaw, PL)
Justin Wells (Trondheim, NO)
Miroslaw Werwinski (Poznan, PL)
Aleksander Wysocki (Lincoln, US)
Pengxiang Xu (Enschede, NL)
Angelica Zacarias (Berlin, DE)
Martin Zeleny (Brno, CZ)
Hongbin Zhang (Dresden, DE)

More details on the summer school, including, e.g., full affiliations of the participants, can be found on the school webpage. They will also be given in the full report of the school that will be available on the Psi-k Portal.

3.1.2 Report on 3rd International Workshop and School on Time-Dependent Density Functional Theory: Prospects and Applications

Benasque (Spain), August 31 – September 15, 2008

Organized by
A. Rubio (Univ. País Vasco, ETSF, and DIPC),
E. K. U. Gross (Freie Universität Berlin),
M. A. L. Marques (LPMCN, Universit Lyon I),
F. Nogueira (CFC, Univ. de Coimbra)

Supported by:

Marie Curie Series of Events program: Psi-k Training in Computational Nanoscience
ETSF and NANOQUANTA Network of Excellence
Lightnet Network of Excellence
ESF SimBioMa Programme
CECAM
Spanish Ministry of Science and Technology
Benasque Center for Science
Universities of the Basque Country and Coimbra

The third School and workshop was hosted by the Benasque Center for Science, located at the heart of the Pirinees. The aim of the school was to introduce theoretical, practical, and numerical aspects of Time-dependent-density functional theory (TDDFT) to young graduate students, post-docs and even older scientists that are envisaging a project for which TDDFT would be the tool of choice. During the school we incentivated a close and informal contact between the students and the teachers. Furthermore, the students presented their current research activities and future interests (two of those presentations were selected as oral contributions to the international workshop and were granted with the first Pedro PAscula Prize for the best posters of the school). We felt that this was an important point, since young scientists should be involved in the building up of a strong community. The number of applications (above 190) surpassed all expectations and, of course, the limit of 50 places that we had to satisfy in order for the students to get the maximum benefit from the school, and also due to space and computer resource limitations. The summary for the school is:

Sex	PhD students	Post-docs	Total
Female	9	3	12
Male	27	11	38

Moreover, the students (graduate and postgraduate) also participated in the workshop held just after the 10 days of school. The total number of participants was 104 from all over the world (including 21 females; seven as invited speakers/lectures). The distribution between countries, experience and gender is provided in the following table:

	School	Teachers	Invited	Workshop	Total
Austria			1		1
Belgium	1				1
Brazil	3				3
Canada			1		1
Chile	1	1			2
Colombia	1				1
Czech Republic	1				1
Denmark	1				1
Finland	3		1	3	7
France	1	1			2
Germany	11	4	2	2	19
Greece			1		1
Iran	1				1
Ireland		1	1		2
Israel	1		1	1	3
Italy	8	6	4	3	21
Japan	1	2	1		4
Mexico	2				2
Netherlands	2	1		3	6
Poland	2				2
Portugal	2	3			5
Romania	1				1
South Korea	2				2
Spain	3	4			7
Sweden				1	1
Switzerland	1				1
Taiwan	1				1
UK		1			1
USA		1	3		4
Male PhD	27	2		2	31
Female PhD	9				9
PhD	**36**	**2**		**2**	**40**
Male Post-doc	11	21	13	7	52
Female Post-doc	3	2	3	4	12
Post-doc	**14**	**23**	**16**	**11**	**64**
Male	38	23	13	9	83
Female	12	2	3	4	21
# Participants	**50**	**25**	**16**	**13**	**104**

The aim of the Workshop was to assess the present status of TDDFT approaches to the study of spectroscopic properties of real materials, and explore their capability for applications in further systems with technological and biological interest. The recent developments of TDDFT covered during the workshop include TDDFT versus current-DFT, van der Waals interactions, appli-

cations to biological systems, new functionals, transport phenomena, optical spectra of solids , etc. Due to the different methods used to tackle this problem (Many-Body Theory, Density Functional Theory, Configuration Interaction, semi-empirical approaches), this Workshop was intended as a way to promote links among scientists coming from different communities working or interested in electron excited states. Also it was intended as a follow-up event for the students attending the school as it was a good opportunity for them to see the real implications of the school lectures and get the new theoretical advances in the the development of exchange-correlation functionals as well as applications to complex systems (nanostructures, bio-molecules, interstellar molecular analysis, solids, etc.) Our goal was to bring together scientists working on foundations and different applications of TDDFT and many-body theory, trying to assess the capability of current approximations to be applied to real systems of increasing complexity. The invited and contributed talks covered:

I) Fundamental topics on TDDFT, Many-Body Theory, and electron transport theory.

II) New approximations and techniques.

III) Ab-initio calculations of spectroscopic properties of large scale systens.

IV) Material Science, Nanosciecen, Biology and Chemical applications.

As a consequence, there was a broad variety of participants which helped to get an interdisciplinary vision of the field. Thus, although some of the more specific topics were far from the research interest of many participants, the meeting was an excellent opportunity to see how the same techniques are used by members of other communities

School Program

Day	**Hour**	**Title**	**T/P**
1 (1/9)	9h30 – 10h15	TDDFT I **(EG)**	T
	10h30 – 11h15	TDDFT II **(EG)**	T
	11h30 – 12h15	Overview of spectroscopies I **(MC)**	T
	12h30 – 13h15	Many-Body: GW I **(RG)**	T
	15h00 – 18h30	Introduction to the practical classes	P
2 (2/9)	9h30 – 10h15	Overview of spectroscopies II **(MC)**	T
	10h30 – 11h15	TDDFT III **(EG)**	T
	11h30 – 12h15	Many-Body: GW II **(RG)**	T
	12h30 – 13h15	Theoretical spectroscopy **(SB)**	T
	15h00 – 18h30	Quantum Dots I	P
3 (3/9)	9h30 – 10h15	TDDFT IV **(EG)**	T
	10h30 – 11h15	Overview of spectroscopies III **(MC)**	T
	11h30 – 12h15	Propagation schemes **(AC)**	T
	12h30 – 13h15	Linear response theory **(SB)**	T
	15h00 – 18h30	Quantum Dots II	P

4 (4/9)	9h30 – 10h15	Advanced TDDFT I **(NM)**	T
	10h30 – 11h15	Current DFT I **(CU)**	T
	11h30 – 12h15	Overview of spectroscopies IV **(MC)**	T
	12h30 – 13h15	TDDFT as a tool in chemistry I **(IT)**	T
	15h00 – 18h30	Quantum Dots III	P
5 (5/9)		Free day	
6 (6/9)	9h30 – 10h15	TDDFT as a tool in chemistry II **(IT)**	T
	10h30 – 11h15	Current DFT II **(CU)**	T
	11h30 – 12h15	Many-Body: BSE I **(MG)**	T
	12h30 – 13h15	Advanced TDDFT II **(NM)**	T
	15h00 – 18h30	OCTOPUS I	P
	18h30 – 19h30	Max Planck - A conservative revolutionary **(MC)**	Public talk
7 (7/9)	9h30 – 10h15	TDDFT as a tool in chemistry III **(IT)**	T
	10h30 – 11h15	Many-Body: BSE II **(MG)**	T
	11h30 – 12h15	Current DFT III **(CU)**	T
	12h30 – 13h15	Optimal control theory **(AC)**	T
	15h00 – 18h30	OCTOPUS II	P
	18h30 – 20h00	Posters	
8 (8/9)	9h30 – 10h15	TDDFT versus Many-Body I **(RvL)**	T
	10h30 – 11h15	TDDFT as a tool in biophysics I **(ME)**	T
	11h30 – 12h15	Advanced TDDFT III **(NM)**	T
	12h30 – 13h15	TDDFT as a tool in biophysics II **(ME)**	T
	15h00 – 18h30	YAMBO I	P
	18h30 – 20h00	Posters	
9 (9/9)	9h30 – 10h15	Nonlinear optics **(XA)**	T
	10h30 – 11h15	TDDFT versus Many-Body II **(RvL)**	T
	11h30 – 12h15	TDDFT as a tool in biophysics III **(RS)**	T
	12h30 – 13h15	Fraud in science I **(SO)**	T
	15h00 – 18h30	YAMBO II	P
	18h30 – 19h00	Fraud in science II **(SO)**	T
	19h00 – 19h30	Closing session (organisers: **AR**, **MM**, **FN**, **EG**)	

School Lecturers

Lecturers for the theoretical classes

AC A. Castro (FU Berlin, Germany)
Propagation schemes + Optimal control theory

CU C. Ullrich (Missouri, USA)
Current DFT

EG E. K. U. Gross (FU Berlin, Germany)
TDDFT

IT I. Tavernelli (Lausanne, Switzerland)
TDDFT as a tool in chemistry

MC M. Cardona (Stuttgart, Germany)
Overview of spectroscopies
Public talk: Max Planck - A conservative revolutionary

ME M. Elstner (Braunschweig, Germany)
TDDFT as a tool in biophysics

MG M. Gatti (Paris, France)
Many-Body: BSE

NM N. Maitra (New York, USA)
Advanced TDDFT

RG R. W. Godby (York, UK)
Many-Body: GW

RvL R. van Leeuwen (Groningen, The Netherlands)
TDDFT versus Many-Body

RS R. Send (Irvine, USA)
TDDFT as a tool in biophysics

SB S. Botti (Paris, France)
Linear Response Theory + Theoretical spectroscopy

SO S. Ossicini (Modena, Italy)
Fraud in science

XA X. Andrade (San Sebastian, Spain)
Nonlinear optics

Teachers for `Quantum Dots` and `octopus`

AC Alberto Castro (Berlin, Germany)

AR Angel Rubio (San Sebastian, Spain)

FN Fernando Nogueira (Coimbra, Portugal)

MM Miguel Marques (Lyon, France)

MO Micael Oliveira (Coimbra, Portugal and San Sebastian, Spain)

XA Xavier Andrade (San Sebastian, Spain)

Teachers for `YAMBO`

AM Andrea Marini (Rome, Italy)

CO Conor Hogan (Rome, Italy)

DV Daniele Varsano (Modena, Italy)

PG Pablo Garcia (Madrid, Spain)

SB Silvana Botti (Paris, France)

YP Yann Pouillon (San Sebastian, Spain)

Workshop Program

Day I: Thursday 11th		
Chairperson: E.K.U. Gross		
09h00 - 09h10	Angel Rubio	Opening remarks
09h10 - 10h00	Kieron Burke	Semiclassical origins of density functional theory
10h00 - 10h50	Roi Baer	Dogmatic and Pragmatic Spirits in TDDFT
10h50 - 11h20	Caffeine break	
Chairperson: Neepa Maitra		
11h20 - 12h10	Marc Casida	TDDFT pushing the limits of and going beyond the adiabatic approximation
12h10 - 13h00	S. Kuemmel	Memory effects in real time: Probing the adiabatic approximation in TDDFT
13h00 - 15h00	Lunch break	
Chairperson: Angel Rubio		
15h00 - 15h50	Andreas Goerling	TDDFT with frequency-dependent exchange-correlation kernels
15h50 - 16h40	Kerstin Hummer	Absorption spectra from TDDFT: do hybrid functionals account for excitonic effects?
16h40 - 17h10	Beer break	
Chairperson: Carsten Ullrich		
17h10 - 18h00	John Rehr	Real-time Approaches for Optical and X-ray Spectra
18h00 - 18h50	Xavier Andrade	From TDDFT to Molecular Dynamics

Day II: Friday 12th		
Chairperson: Rex Godby		
09h00 - 09h50	Sohrab Ismail-Beigi	Optical properties of GaN nanotubes from many-body GW-BSE perturbation theory
09h50 - 10h40	Yasutami Takada	The electron self-energy in the Green's-function approach: Beyond the GW approximation
10h40 - 11h10	Caffeine break	
Chairperson: Robert van Leeuwen		
11h10 - 12h00	R.W. Godby	Exchange and correlation in quantum transport
12h00 - 12h50	M. di Ventra	Stochastic TDCDFT: a functional theory of open quantum systems
13h00 - 15h00	Lunch break	
Chairperson: Kieron Burke		
15h00 - 15h50	R. van Leeuwen	Time-Dependence and Interactions in Quantum Transport
15h50 - 16h40	Risto Nieminen	Applications of TDDFT to clusters and nanostructures
16h40 - 17h10	Beer break	
Chairperson: Ivano Tavernelli		
17h10 - 18h00	Claudia Filippi	Autofluorescent proteins: Are first-principle calculations predictive?
18h00 - 18h50	N. Maitra	TDDFT phase-space explorations
20h00	Speakers Dinner	

Day III: Saturday 13th		
Chairperson: Fernando Nogueira		
09h00 - 09h50	Nikos Doltsinis	Nonadiabatic Car-Parrinello MD
09h50 - 10h40	Osamu Sugino	Nonadiabatic dynamics by TDDFT
10h40 - 11h10	Caffeine break	
Chairperson: Osamu Sugino		
11h10 - 12h00	Ivano Tavernelli	Non-adiabatic mixed quantum-classical dynamics using TDDFT
12h00 - 12h50	Kazuhiro Yabana	Dynamics in dielectrics induced by ultrashort laser pulses
13h00 - 15h00	Lunch break	
Chairperson: Massimiliano di Ventra		
15h00 - 15h50	Troy Van Voorhis	Electron Transfer and Electron Transport: Fighting Self-Interaction in TDDFT
15h50 - 16h40	Daniele Varsano	Optical Saturation driven by Exciton Confinement in Molecular Chains
16h40 - 17h10	Beer break	
Chairperson: Massimiliano di Ventra		
17h10 - 18h00	Silvana Botti	Photoelectronic properties of chalcopyrites for photovoltaic conversion: self-consistent GW calculations
18h00 - 20h00	Poster Session	

Day IV: Sunday 14th		
Chairperson: Miguel Marques		
09h00 - 09h20	Ingolf Warnke	*Winner of the school poster session*
09h20 - 09h40	P. Myhnen	*Winner of the school poster session* Quantum transport studies in Kadanoff-Baym approach
09h40 - 10h30	P. Romaniello	Double excitations in finite systems
10h30 - 11h00	Caffeine break	
Chairperson: Miguel Marques		
11h00 - 11h50	Claudio Verdozzi	TDDFT and Strongly Correlated Systems: Insight From Numerical Studies
11h50 - 12h00	Miguel Marques	Closing remarks

List of Students

Ali AKBARI	Centro Joxe Mari Korta, San Sebastin, Spain
Joice ARAJO	UFMG - Universidade Federal de Minas Gerais
Jakub BARAN	Tyndall National Institute, University College Cork
Christophe BERSIER	FU Berlin (freie universitt)
Oana BUNAU	Institut Neel, CNRS Grenoble, France
Letizia CHIODO	National Nanotechnology Laboratory of CNR-INFM
Stefania D'AGOSTINO	CRS NNL, INFM-CNR, Lecce (ITALY)
Fabiana DA PIEVE	Institut Carnot de Bourgogne, Universit de Bourgogne

Florian EICH	Freie Universitaet Berlin, Berlin, Germany
Leonardo ESPINOSA LEAL	Universidad del Pais Vasco
Jos Rui FAUSTINO DE SOUSA	Universidade de Coimbra
Frederico FIORAVANTI	UFMG - Universidade Federal de Minas Gerais
Dietrich FOERSTER	C.P.M.O.H. Universite de Bordeaux I
Giorgia FUGALLO	King's College London
Jos GMEZ MARTNEZ	Universidad Autnoma de Madrid
Michael GAUS	Theoretical Chemistry, TU Braunschweig, Germany
Tamar GERSHON	Hebrew university
Matteo GUGLIELMI	Ecole Polytechnique Federale de Lausanne
Roland GUICHARD	MPIPKS
Matteo GUZZO	Universit Statale di Milano - Bicocca
Ralf HAMBACH	Ecole Polytechnique, Palaiseau, France
Keisuke HATADA	LNF-INFN
Nicole HELBIG	ETSF San Sebastian
Hannes HBENER	LSI, Ecole Polytechnique
Andreas KAROLEWSKI	University of Bayreuth, Germany
Woo Youn KIM	Pohang University of Science and Technology in South Korea
Diemo KOEDDERITZSCH	LMU Muenchen,Dept.Chemie/Biochemie
Karina KORNOBIS	UNIVERSITY OF LOUISVILLE, KY,USA
Petr KOVAL	CPMOH Bordeaux
Olli LEHTONEN	Department of chemistry, University of Helsinki, Finland
Lauri LEHTOVAARA	Helsinki University of Technology
Jian-Hao LI	Center for Condensed Matter Sciences, National Taiwan University
SeungKyu MIN	Pohang University of Science and Technology (POSTECH)
Petri MYHNEN	University of Jyvskyl
Mariana ODASHIMA	Universidade de So Paulo, Brazil
Roberto OLIVARES-AMAYA	Harvard University
Thomas OLSEN	Technical University of Denmark (DTU) - Physics
Max RAMIREZ	Universidad de Chile
Davide SANGALLI	Universit Degli Studi di Milano
Andr SCHLEIFE	Friedrich-Schiller-Universitt, Jena
Mireia SEGADO CENTELLAS	Universitat Rovira i Virgili
Alejandro SOBA	BSC
Lorenzo STELLA	University College London
Huub VAN DAM	STFC Daresbury Laboratory
Matthieu VERSTRAETE	Dept Phys University of York UK
Jos Guilherme VILHENA	Universite Lyon 1
Marius WANKO	BCCMS, University of Bremen
Ingolf WARNKE	University of California, Irvine
Joel YUEN	Harvard University
Martijn ZWIJNENBURG	Universitat de Barcelona

List of School Teachers

Xavier ANDRADE	Universidad del Pais Vasco
Silvana BOTTI	LSI Ecole Polytechnique
Manuel CARDONA	Max-Plack Stuttgart
Alberto CASTRO	Free University of Berlin
Marcus ELSTNER	Theoretical Chemistry, TU Braunschweig, Germany
Pablo GARCIA GONZALEZ	Universidad Nacional de Educacion a Distancia
Matteo GATTI	ETSF - LSI - Ecole Polytechnique
Rex GODBY	University of York
Hardy GROSS	Free Universitat Berlin
Conor HOGAN	Physics Department, University of Rome
Neepa MAITRA	Hunter College of the City University of New York
Andrea MARINI	Physics Department, University of Rome
Miguel MARQUES	LPMCN University Lyon 1
Fernando NOGUEIRA	CFC, University of Coimbra
Micael OLIVEIRA	University of Coimbra
Stefano OSSICINI	Universit di Modena e Reggo Emilia
Yann POUILLON	Universidad del Pas Vasco UPV/EHU
Angel RUBIO	UPV/EHU
Robert SEND	Universitaet Karlsruhe
Osamu SUGINO	ISSP, the University of Tokyo
Ivano TAVERNELLI	EPFL- Lausanne
Carsten ULLRICH	University of Missouri
Robert VAN LEEUWEN	University of Jyvskyl
Daniele VARSANO	Natl. Center S3 INFM-CNR, Modena , ITALY
Kazuhiro YABANA	Center for Computational Sciences, University of Tsukuba

List of Workshop Participants

(besides the students and teachers from the school)

Roi BAER	The Hebrew University of Jerusalem
Arjan BERGER	Ecole Polytechnique, Palaiseau, France
Kieron BURKE	Irvine, USA
Mark CASIDA	Universit Joseph Fourier (Grenoble I)
Massimiliano DI VENTRA	UC, San Diego
Nikos DOLTSINIS	Kings College, London
Jussi ENKOVAARA	CSC - Scientific Computing
Claudia FILIPPI	Universiteit Leiden, Instituut-Lorentz
Klaas GIESBERTZ	VU University
Andreas GOERLING	University of Erlangen-Nuremberg
Maria HELLGREN	Lund University

Dirk HOFMANN	University of Bayreuth, Germany
Kerstin HUMMER	Vienna University
Sohrab ISMAIL-BEIGI	Yale University
Thomas KOERZDOERFER	University of Bayreuth, Germany
Stephan KUMMEL	University of Bayreuth
Ester LIVSHITS	The Hebrew University of Jerusalem
Ilja MAKKONEN	University of Liverpool
Risto NIEMINEN	Helsinki University of Technology
Tapio T. RANTALA	Tampere University of Technology
John REHR	University of Washington
Dario ROCCA	University of California at Davis
Pina ROMANIELLO	Ecole Polytechnique, Palaiseau, France
Gianluca STEFANUCCI	Universita di Roma Tor Vergata
Lorenzo STELLA	University College London
Yasutami TAKADA	Institute for Solid State Physics, Univ. of Tokyo
Meta VAN FAASSEN	VU University
Troy VAN VOORHIS	MIT
Claudio VERDOZZI	Lund University, Sweden

4 News from UK's CCP9 Programme

UK's Collaborative Computational Project 9 (CCP9) on "Computational Studies of the Electronic Structure of Solids"

4.1 Report on the CCP9 Conference

http://www.ccp9.ac.uk/ccp9workshops_2008_cambridge_sept.shtml

Robinson College, Cambridge, 4-5 September 2008

Short report

The Conference was held at the Robinson College in Cambridge on 4th and 5th September 2008 and was attended by 58 participants both from the U. K. and abroad. The scope of the Conference covered all ab-initio and materials specific calculations of the electronic properties of condensed matter systems such as metals, semiconductors, magnets, superconductors, biological systems, minerals, surfaces, etc. Topical areas incorporated in the Conference were magnoelectronics, catalysis, nanotechnology, high temperature superconductors, novel wide band gap semiconductors, etc. Techniques covered by the Conference included QMC, DFT, GW, TDDFT, DMFT, SIC-LSDA, LSDA+U. In general, all the applications dealing with the solution of the Schrödinger/Dirac equation in condensed matter systems were represented.

The Conference was structured around five excellent plenary talks, 9 invited talks, and 21 poster presentations, covering a broad range of ab initio computational topics. The first, very impressive, plenary presentation was by Hardy Gross (FU Berlin, Germany) who talked about density functional theory for superconductors, treating both electrons and ions on equal footing, and demonstrated it on a number of impressive applications. Vladimir Anisimov (Ekaterinberg, Russia) gave a very complete presentation on a practical implementation of the DFT+DMFT method and its application to real d and f electron materials, where electron correlations fall

in the range of moderate to strong and metallic to insulating limits. Gustavo Scuseria (Rice University, USA) presented a nice overview and outlook for the screened hybrid functionals and their applications to solid-state physics and chemistry. Nicola Marzari (MIT, USA) discussed the key challenges for the for the density functional theory in catalysis and electrochemistry. Finally, and David Ceperley (University of Illinois, USA) talked about a new method, called Coupled-Electron Ion Monte Carlo, that allow for simulations in much lower temperatures than with other methods. He discussed an application of the method to the dense Hydrogen.

The first invited talk was by Neil Drummond (University of Cambridge, UK) who talked about an application of Quantum Monte Carlo to the two-dimensional homogeneous electron gas". Leon Petit (University of Aarhus, Denmark) discussed large scale simulations of materials properties through grid applications, based on the study of the whole series of rare earth monopnictides and monochalcogenides using the SIC-LSD method. Marcus Neumann (AVMATSIM) gave a presentation on effective prediction of crystal structures for pharmaceutical industry, combining DFT and tailor-made force fields. Dario Alfe (UCL, UK) talked about the application of Quantum Monte Carlo free energy calculations to melting of iron at Earth's core conditions. Robert Laskowski (TU Wien, Austria) discussed h-BN nanomesh on transition metal surfaces. Jonathan Yates (University of Cambridge, UK) gave a talk with an intriguing title of "Atomic espionage: J-resolved NMR spectroscopy". Hubert Ebert (LMU Muenchen, Germany) presented the first KKR implementation of the LSDA+DMFT method for the application to spectroscopies. Massimiliano Stengel (Santa Barbara, USA) discussed dielectric, piezoelectric and magnetoelectric properties based on first-principles calculations at constant electric displacement. The final invited presentation was by Keith Refson on "Plane-wave Optimised Effective Potential Studies of Transition Metal Oxides".

On both days of the Conference there were poster presentations after lunch and they attracted all the participants, generating a very lively atmosphere of scientific discussions and exchange of opinions. Despite the very unfortunate heavy rain, the conference was very successful and informative to all involved. Considering that at the time of the conference there was a number of similar events happening both in the U. K. and elsewhere, this CCP9 Conference could be considered as very successful.

Conference Programme

Wednesday 3rd September

18.00 - 19.30	REGISTRATION OPEN

Thursday 4th September

08.30 - 09.00	REGISTRATION AND COFFEE
09.00 - 10.00	Hardy Gross (plenary) "Ab-Initio Theory of Superconductivity"
10.00 - 10.25	Neil Drummond "Quantum Monte Carlo Studies of the Two-Dimensional Homogeneous Electron Gas"

10.30 - 10.55 Leon Petit
"Large scale calculations of materials properties through grid applications"

11.00 - 11.30 COFFEE

11.30 - 11.55 Marcus Neumann
"From dispersion corrected DFT to tailor-made force fields - accurate lattice energy calculations for crystal structure prediction"

12.00 - 12.25 Dario Alfe
"Melting of iron at Earth's core conditions from quantum Monte Carlo free energy calculation"

12.30 - 15.30 LUNCH AND POSTER SESSION

15.30 - 16.30 Vladimir Anisimov (plenary)
"Density Functional and Dynamical Mean-Field Theory (DFT+DMFT) method and its applications to correlation effects in electronic structure of real materials"

16.30 - 16.55 Robert Laskowski
"h-BN nanomesh on transition metal surfaces"

17.00 - 17.25 Jonathan Yates
"Atomic espionage: J-resolved NMR spectroscopy"

17.30 MEETING CLOSES FOR THE DAY

Friday 5th September

09.00 - 10.00 Gustavo Scuseria (plenary)
"Screened hybrid functionals for solid-state physics and chemistry"

10.00 - 10.25 Hubert Ebert
"A self-consistent relativistic implementation of the LSDA+DMFT-scheme and its application in spectroscopy"

10.30 - 10.55 Massimiliano Stengel
"Dielectric, piezoelectric and magnetoelectric properties via first-principles calculations at constant electric displacement"

11.00 - 11.30 COFFEE

11.30 - 12.30 Nicola Marzari (plenary)
"DFT challenges in catalysis and electrochemistry"

12.30 - 15.00 LUNCH AND POSTER SESSION

15.00 - 16.00 David Ceperley (plenary)
"Simulation of dense hydrogen using Coupled-Electron Ion Monte Carlo"

16.00 - 16.25 Keith Refson
"Plane-wave Optimised Effective Potential Studies of Transition-Metal Oxides"

16.30 MEETING CLOSES - COFFEE AVAILABLE

List of Posters

Chris Adriaanse (University of Cambridge, U. K.)
"Computation of the free energy change in some steps in the reduction of O_2 in aqueous solution".

Simon Binnie (University College London, U. K.)
"Benchmarking DFT Surface Energies with Quantum Monte Carlo"

Gareth Conduit (University of Cambridge, U. K.)
"DMC calculations in valley degenerate semiconductors"

Calvin Davidson (Sussex University, U. K.)
"A Density Functional Theory Study of the Adsorption of Tetracene on Reconstructed Oxygen Terminated Copper (110) Surfaces"

Giulia C De Fusco (Imperial College London, U. K.)
"Ab Initio Study of the Electronic Structure and Magnetic Properties of the High-Temperature $V(TCNE)_2$ Organic-Based Magnet"

Nicholas Hine (Imperial College London, U. K.)
"Supercell Size Scaling of Formation Energies of Charged Defects"

Leandro Liborio (Imperial College London, U. K.)
"Magneli Phases: An ab initio Approach"

Giuseppe Mallia (Imperial College London, U. K.)
"Doping Titania with transition metal to make a dilute ferromagnetic semiconductor: insights from hybrid density functional simulations"

Andrew Morris (University of Cambridge, U. K.)
"Defects in Semiconductors using Random Structure Searching"

Arash Mostofi (Imperial College London, U. K.)
"Linear-Scaling DFT+U"

Duncan Riley (University of Salford, U. K.)
"Hydrogen Storage in Metal-Organic Frameworks"

Mark Robinson (University of Cambridge, U. K.)
"Ab initio Study of Peptide Stacking in an Amyloid Fibril"

Jon Swaim (Imperial College London, U. K.)
"The Electronic Structure of CrO_2 Revisited: A Hybrid-Exchange Density Functional Theory Study"

Z (Dzidka) Szotek (STFC Daresbury Laboratory, U. K.)
"Application of Local Self-Interaction Correction (SIC) to Transition Metal Oxides"

Walter Temmerman (STFC Daresbury Laboratory, U. K.)
"Finite Temperature Magnetism of Heavy Rare Earths: SIC-DLM Study"

Fabien Tran (Vienna University of Technology, Austria)
"PBE+U Calculations of the Jahn-Teller Effect in PrO_2"

Claudia Utfeld (University of Bristol, U. K.)

"$Co_xFe_{1-x}S_2$: How close to half-metallicity?"

Rebecca Varns (University of Kent, U. K.)
"A First Principles Study of Group 13 Simple Metal Clusters: Superatom or Cluster?"

Rebecca Varns (University of Kent, U. K.)
"A First Principles Study of the Electronic Structure and Chemical Bonding of Neutral and Charged Boron Clusters"

Rudolf Zeller (Institut fuer Festkoerperforschung, Juelich, Germany)
"A Reformulation of the KKR Green-Function Method for Large-Scale Density-Functional Calculations"

Nicholas Zonias (University of Southampton, U. K.)
"Large-Scale DFT Calculations on Silicon Nanocrystals"

List of Participants

Title	First Name	Surname	Affiliation
Mr	Chris	Adriaanse	University of Cambridge
Prof	Dario	Alfe	University College London
Prof	Vladimir	Anisimov	Institute for Metal Physics
Prof	James	Annett	University of Bristol
Mr	Albert	Bartok-Partay	University of Cambridge
Mr	Simon	Binnie	University College London
Prof	David	Ceperley	University of Illinois
Mr	Gareth	Conduit	University of Cambridge
Dr	Gabor	Csanyi	University of Cambridge
Mr	Calvin	Davidson	Sussex University
Ms	Giulia C	De Fusco	Imperial College London
Dr	Neil	Drummond	University of Cambridge
Prof	Paul	Durham	STFC Daresbury Laboratory
Prof	Hubert	Ebert	Ludwig-Maximilians-University of Munich
Dr	Asier	Eiguren	Donostia International Physics Center
Prof	Matthew	Foulkes	Imperial College London
Prof	Michael	Gillan	University College London
Prof	Hardy	Gross	FU Berlin
Mr	Nic	Harrison	STFC Daresbury Laboratory
Dr	Philip	Hasnip	University of York
Prof	Volker	Heine	University of Cambridge
Mr	Tilina	Herath	University of Warwick
Dr	Nicholas	Hine	Imperial College London
Mr	Damian	Jones	STFC Daresbury Laboratory
Dr	Thomas	Kuehne	ETH Zurich
Dr	Robert	Laskowski	TU Wein
Dr	Leandro	Liborio	Imperial College London
Dr	Giuseppe	Mallia	Imperial College London

Prof	Nicola	Marzari	Massachusetts Institute of Technology
Dr	Victor	Milman	Accelrys Inc.
Dr	Carla	Molteni	King's College London
Mr	Andrew	Morris	University of Cambridge
Prof	Ian	Morrison	University of Salford
Dr	Arash	Mostofi	Imperial College London
Dr	Andres	Mujica Fernaud	Universidad de La Laguna
Prof	Richard	Needs	University of Cambridge
Dr	Marcus	Neumann	Avant-Garde Materials Simulation
Prof	Mike	Payne	University of Cambridge
Dr	Alexander	Perlov	Accelrys Inc.
Dr	Leon	Petit	University of Aarhus
Dr	Chris	Pickard	"SUPA, University of St Andrews"
Dr	Keith	Refson	STFC Daresbury Laboratory
Dr	Duncan	Riley	University of Salford
Mr	Mark	Robinson	University of Cambridge
Prof	Gustavo E.	Scuseria	Rice University
Dr	Chris-Kriton	Skylaris	University of Southampton
Dr	Michiel	Sprik	University of Cambridge
Dr	Massimiliano	Stengel	University of California
Prof	Paul	Strange	University of Kent
Mr	Jon	Swaim	Imperial College London
Prof	Z (Dzidka)	Szotek	STFC Daresbury Laboratory
Prof	Walter	Temmerman	STFC Daresbury Laboratory
Dr	Fabien	Tran	Vienna University of Technology
Ms	Claudia	Utfeld	University of Bristol
Ms	Rebecca	Varns	University of Kent
Dr	Jonathan	Yates	University of Cambridge
Dr	Rudolf	Zeller	Institut fuer Festkoerperforschung
Mr	Nicholas	Zonias	University of Southampton

Conference Organizers:

Prof James F. Annett (Bristol University)
Prof Mike C. Payne (Cambridge University)
Prof Walter M. Temmerman (STFC Daresbury Laboratory)

Local Organizers:

Damian Jones (STFC Daresbury Laboratory)
Shirley Miller (STFC Daresbury Laboratory)

5 General Job Announcements

Ph.D / M.Sc. Studentships
Nanoscience Center, University of Jyväskylä, Finland

Newly founded Nanoscience Center at the Department of Physics, University of Jyväskylä, Finland, is looking for motivated Ph.D. and M.Sc. students to work on some of the most active fields in theoretical condensed matter physics.

The main projects are (1) quantum optimal control of dynamical processes in nanostructures, (2) quantum transport in low-dimensional systems, and (3) development of density functionals in reduced dimensions. The general goal is to design coherent quantum gates and charge/current switches, thereby aiming at novel applications in quantum information. International collaboration with several groups worldwide is an important part of the research.

We offer an active and enthusiastic research environment at the Nanoscience Center in Jyväskylä, a lively university city located in the Finnish Lakeland. The Nanoscience Center brings together expertise in theory, experiments, and industry in various disciplines.

A successful applicant for the Ph.D. studentship must hold a M.Sc. degree in physics and good general knowledge of quantum mechanics and desirably electronic-structure theory. Programming skills (e.g. Fortran/C/C++) are highly beneficial. From the M.Sc. students hired for Master's thesis projects we require excellent performance in undergraduate studies.

The appointment for the Ph.D. studentship is made for the full course of the Ph.D. work with a trial period. The minimum starting salary is 1800 EUR/month, and participation in teaching is paid separately. M.Sc. studentships are approximately 1500 EUR/month for a fixed period of six months. Screening of candidates will start immediately and will continue until the positions are filled. To apply, please contact Dr. Esa Räsänen, esa.rasanen(at)jyu.fi, and attach your CV, a brief statement of your research interests, and contact information of 2-3 referees.

PhD and/or Postdoc position in Computational Materials Theory

School of Physics, Trinity College Dublin, Ireland

Funding is available for two positions (either as PhD studentships or on the postdoctoral level) in the group of Dr. Claude Ederer in the School of Physics at Trinity College Dublin, Ireland. The successful applicants will perform research in one of the following areas (depending on previous qualifications and interest):

1. First principles modeling of functional complex oxide heterostructures, in particular combinations of magnetic and ferroelectric materials.

2. Combining density functional theory with many-body approaches such as dynamical mean field theory (DMFT), and application to functional transition metal oxides.

Candidates for a postdoc position are expected to have previous research experience in either first principles techniques or computational many-body physics. Candidates for a PhD studentship are required to have at least a 2.1 honors degree from an Irish university or an equivalent or higher qualification. In all cases a fluent command of the English language, a strong overall motivation, and a keen interest in theory and computation as well as in addressing specific materials science problems is required. Experience in working with UNIX/Linux environments and programming in either Fortran or C/C++ is beneficial.

Trinity College is located in the heart of Dublin, one of Europe's most vibrant capital cities. The School of Physics at Trinity College has a very strong research program in computational materials science and maintains close links with several on-campus interdisciplinary research centers, such as CRANN (Center for Research on Adaptive Nanostructures and Nanodevices) or TCHPC (Trinity Center for High Performance Computing).

Applications containing cover letter, CV, list of references, and a short statement of research interests should be sent to (pdf format preferred):

Dr. Claude Ederer, School of Physics, Trinity College, Dublin 2. Ireland
email: edererc@tcd.ie

There is no deadline for these positions. Screening of applications will start immediately and will continue until the positions are filled. For further information please contact Dr. Ederer directly (see also: www.tcd.ie/Physics/People/Claude.Ederer).

6 Abstracts

Spin-mixing conductances: The influence of disorder

K. Carva[1,2] and I. Turek[2]

[1] *Department of Physics, Uppsala University, Sweden*

[2] *Dept. Condensed Matter Physics, Charles University, Prague, Czech Republic*

Abstract

Spin-transfer torque exerted on a magnetic layer can be viewed as a linear response to the spin accumulation inside an adjacent non-magnetic layer, information about their response coefficient is provided by the complex spin-mixing conductance C^{mix}. Substitutional disorder is known to affect the spin-dependent charge conductances and often reduces strongly the magnetoresistance. Here we examine its impact on C^{mix} of several selected realistic systems. Recently predicted oscillations of C^{mix} as a function of ferromagnetic layer thickness in Ni based junctions might be suppressed by interface interdiffusion, but presented ab initio calculations disprove this possibility. Halfmetallic character of the Heusler compound Co_2MnSi is destroyed by often encountered antisite disorder; however the impact of this disorder to the predicted C^{mix} is rather weak. Diluted magnetic semiconductor (Ga,Mn)As is an intrinsically disordered system, the analysis of calculations shows that the variation of C^{mix} with substitutional Mn content can be understood in terms of the associated change of the number of carriers, whereas the variation with lattice defects is more complex.

Published in: Physica Status Solidi A 205 (2008) 1805.

Contact person: Karel Carva (karel.carva@fysik.uu.se)

Electronic, magnetic, and transport properties and magnetic phase transition in quaternary (Cu,Ni)MnSb Heusler alloys

J. Kudrnovský[1,2], V. Drchal[1], I. Turek[3] and P. Weinberger[4]
[1] *Institute of Physics, ASCR, Prague, Czech Republic*
[2] *MPI for Microstructure Physics, Halle, Germany*
[3] *Dept. Condensed Matter Physics, Charles University, Prague, Czech Republic*
[4] *Center for Computational Nanoscience, Vienna, Austria*

Abstract

The electronic properties, finite-temperature magnetism, and transport properties of semi-Heusler quaternary alloys (Cu,Ni)MnSb are studied theoretically by means of ab initio calculations as a function of the alloy composition. As documented by experiment, the transition from the ferromagnetic state (NiMnSb) to the antiferromagnetic state (CuMnSb) gives rise to an abrupt change in the magnetic moments and resistivities at about $x_{\mathrm{Cu}} \approx 0.7$, while the Curie temperature exhibits a smooth behavior with the Cu content. We explain this peculiar behavior with the onset of disorder in orientations of the Mn spins at $x_{\mathrm{Cu}} \approx 0.7$. A simple account of magnetic disorder based on the so-called uncompensated disordered local-moment picture provides a good quantitative understanding of available experimental data. An origin of the observed magnetic phase transition is also discussed.

Published in: Physical Review B 78 (2008) 054441.
Contact person: Josef Kudrnovský (kudrnov@fzu.cz).

Electronic structure and magnetism of $MnFeP_{1-x}Si_x$ alloys from first-principles calculations

M. Diviš and I. Turek
Dept. Condensed Matter Physics, Charles University, Prague, Czech Republic

Abstract

First-principles calculations of electronic structure and magnetic properties based on density-functional theory were performed for $MnFeP_{1-x}Si_x$ ($0.44 \leq x \leq 0.60$) alloys which are considered as promising magnetocaloric refrigerants. We used the full-potential APW+lo method and treated the random order of P(Si) atoms in the ZrNiAl-type structure in a virtual-crystal approximation. A non-monotonic behavior of the alloy magnetization as a function of x was obtained, in qualitative agreement with experiment, and explained in terms of the spin-polarized densities of states.

Published in: Physica B 403 (2008) 3276.
Contact person: Martin Diviš (divis@mag.mff.cuni.cz)

Transition-Metal Substituted Indium Thiospinels as Novel Intermediate-Band Materials: Prediction and Understanding of Their Electronic Properties

P. Palacios[1,2], I.Aguilera[1], K. Sánchez[1], J.C. Conesa[2], P. Wahnón[1]
[1]*Instituto de Energía Solar & Dpt. Tecnologías Especiales*
ETSI Telecomunicación, UPM, Ciudad Universitaria, Madrid 28040, Spain
[2]*Instituto de Catálisis y Petroleoquímica,CSIC.Cantoblanco, 28049, Madrid, Spain*

Abstract

Results of density-functional calculations for indium thiospinel semiconductors substituted at octahedral sites with isolated transition metals (TM=Ti, V) show an isolated partially-filled narrow band containing three t_2g-type states per TM atom inside the usual semiconductor band-gap. Thanks to this electronic structure feature, these materials will allow the absorption of photons with energy below the band-gap, in addition to the normal light absorption of a semiconductor. To our knowledge, we demonstrate for the first time the formation of an isolated intermediate electronic band structure through TM substitution at octahedral sites in a semiconductor, leading to an enhancement of the absorption coefficient in both infrared and visible ranges of the solar spectrum. This electronic structure feature could be applied for developing a new third-generation photovoltaic cell.

(Phys. Rev. Lett. **101** 046403)
Contact person: P. Wahnón - perla@etsit.upm.es

Towards a linear-scaling algorithm for electronic structure calculations with the tight-binding Korringa-Kohn-Rostoker Green-function method

Rudolf Zeller
Institut für Festkörperforschung, Forschungszentrum Jülich GmbH, D-52425 Jülich, Germany

Abstract

The proposed algorithm is based on the exponential decay of the screened structure constants in the tight-binding (TB) Korringa-Kohn-Rostoker (KKR) Green-function method and on a spatial truncation of the Green function in the spirit of Kohn's principle of nearsightedness of electronic matter. The KKR matrix equations are solved iteratively and non-zero electronic temperatures are used to accelerate the iterations. The dependence of the total energy accuracy on the size of the truncation region was investigated for large Cu and Pd supercells and it was found that total energy errors smaller than 2 meV could be achieved if the truncation region contained a few thousand atoms.

Published in J. Phys.: Condens. Matter, 20, 294215 (2008).

Phonon transport in isotope-disorder carbon and boron-nitride nanotubes: is localization observable?

Ivana Savić[1], Natalio Mingo[2,3], and Derek A. Stewart[3]
[1] LITEN, CEA-Grenoble, 17 rue des Martyrs, 38054 Grenoble Cedex 9, France
[2] UC Santa Cruz, Santa Cruz, CA 95064 USA
[3] Cornell Nanoscale Facility, Cornell University, Ithaca, NY 14853, USA

Abstract

We present an *ab initio* study which identifies dominant effects leading to thermal conductivity reductions in carbon and boron-nitride nanotubes with isotope disorder. Our analysis reveals that, contrary to previous speculations, localization effects cannot be observed in the thermal conductivity measurements. Observable reduction of the thermal conductivity is mostly due to diffusive scattering. Multiple scattering induced interference effects were found to be prominent for isotope concentrations $\geq$10%; otherwise, the thermal conduction is mainly determined by independent scattering contributions of single isotopes. We give explicit predictions of the effect of isotope disorder on nanotube thermal conductivity that can be directly compared with experiments.

Accepted by *Physical Review Letters*; estimated publication date Oct. 10th, 2008
Contact person: Ivana Savić (ivana.savic@cea.fr)

7 SCIENTIFIC HIGHLIGHT OF THE MONTH: "Simulating functional magnetic materials on supercomputers"

Simulating functional magnetic materials on supercomputers

Markus E. Gruner and Peter Entel
Physics Department and Center for Nanointegration CENIDE
University of Duisburg-Essen, Duisburg Campus, 47048 Duisburg, Germany

Abstract

The recent passing of the petaflop/s landmark by the Roadrunner project at the Los Alamos National Laboratory marks the preliminary peak of an impressive world-wide development in the high-performance scientific computing sector. Also purely academic state-of-the-art supercomputers as the IBM Blue Gene/P at Forschungszentrum Jülich allow nowadays to investigate large systems of the order of 10^3 spin polarized transition metal atoms by means of density functional theory. Three applications will be presented where large scale *ab initio* calculations contribute to the understanding of key properties emerging from a close interrelation between structure and magnetism. The first two examples discuss the size dependent evolution of equilibrium structural motifs in elementary iron and binary Fe-Pt and Co-Pt transition metal nanoparticles, which are currently discussed as promising candidates for ultra-high-density magnetic data-storage media. However, the preference for multiply twinned morphologies at smaller cluster sizes counteracts the formation of a single-crystalline $L1_0$ phase which alone provides the required hard magnetic properties. The third application is concerned with the magnetic shape memory effect in the Ni-Mn-Ga Heusler alloy, which is a technologically relevant candidate for magneto-mechanical actuators and sensors. In this material strains of up to 10 % can be induced by external magnetic fields by the field-induced shifting of martensitic twin boundaries, requiring an extremely high mobility of the martensitic twin boundaries, but also the selection of the appropriate martensitic structure from the rich phase diagram.

1 Introduction

Not at last due to the increasing trend towards miniaturization of everyday-life goods, smart materials tend to play an increasingly important role for technological applications. A specific group of smart materials are functional magnetic materials, where in the widest sense of the definition the magnetic properties decide over the functional applications. In many cases the desired functional magnetic properties of these materials are connected with a specific structural conformation relying on the absence and sometimes also the presence of structural defects (for

an overview, see, e.g., [1]). The detailed understanding of the specific interplay of magnetic and structural properties is thus decisive for the optimization of functional materials or even the design of new alloys and compounds for a given purpose.

Magnetic nanoparticles, for instance, play an important role in biomedical applications, as carriers for targeted drug delivery within the human body or as heating agent for local hypothermic cancer treatment strategies [2–4]. Other potential applications envisage their use as building blocks for ultra-high density magnetic data storage media [5, 6]. Here, in particular, a large magneto-crystalline anisotropy is required, assuring a stability of the stored information in the order of decades. For the case of Fe-Pt and Co-Pt, the largest magnetocrystalline anisotropy is expected for single-crystalline particles of the $L1_0$ phase, which exhibits extremely large values in the bulk [7]. The occurrence of so-called multiple twinning, which is induced by a competition between surface and core energies and typical for small particle sizes, counteracts the required large magnetocrystalline anisotropy and thus the miniaturization of the bits by reducing the particle sizes down to a few nanometers. On the contrary, in magnetic shape memory materials, a prerequisite for their functional purpose is the existence of a martensitic phase and in consequence the presence of internal interfaces as twin boundaries (see, e.g., [1, 8–10]). Their extremely large mobility in combination with a considerable magnetocrystalline anisotropy allows shifting by moderate magnetic fields of the order of one Tesla, which in consequence leads to a huge macroscopic change of shape in the range of several percent in the lateral dimensions.

The investigation of atomistic processes in the above mentioned materials should cover at least a few nanometers, requiring system sizes of the order of 10^2 to 10^3 atoms. Traditionally, this is the realm of classical statistical methods as molecular dynamics simulations using empirical inter-atomic potentials or semi-empirical quantum-mechanical approaches such as tight-binding schemes (e. g. [11–16]). These methods usually rely on careful fitting procedures to material specific quantities, which must be obtained from experiment or *ab initio* calculations, and lack in general the accuracy to give a definitive account on the interrelation of the electronic and structural properties. This is especially true for systems with strong interrelation between magnetic and structural properties as those which are the main topic of this review. *Ab initio* calculations in the framework of the density functional theory provide this accuracy but are on the other hand computationally expensive and thus traditionally limited to rather small system sizes. Therefore, in recent times, efforts have been made to improve the classical simulation schemes, e.g., by incorporating magnetic degrees of freedom into classical simulations of real materials on a systematic basis [17, 18]. A very promising route is the development of so-called $\mathcal{O}(N)$ DFT methods [19–22]. These provide as classical molecular dynamics a linear increase of the computational demands with the system size, allowing system sizes N larger than 10^5 to be considered. Most of these approaches work best for semiconductors and insulators, as they require a rather close localization of orbitals at the atomic positions. Investigations of structural properties of large transition metal systems have not been reported, so far.

For problems like the ones discussed in this review, it is therefore still unavoidable to come back to the traditional DFT implementations, although they are hampered by a much worse scaling behavior. For the example discussed in Sec. 4 this is shown in Fig. 1 (left side). A full structural optimization of a Fe-Pt nanocluster with 561 atoms would require several years of computing time, if performed on a single processor machine, a particle of the order of 10^3 atoms

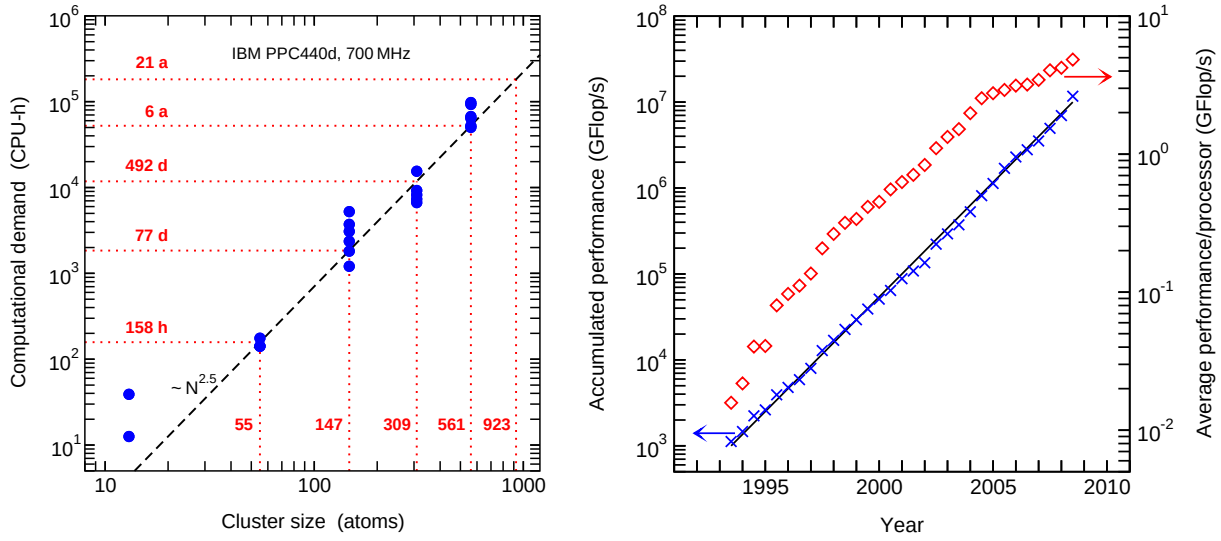

Figure 1: Left: Double logarithmic plot of the computation time per CPU needed on JUBL for a full geometric optimization of Fe-Pt nanoclusters of magic cluster sizes according to Eq. (1). Originally published in [23]. Right: Evolution of the accumulated available theoretical performance (maximum measured linpack power in units of 10^9 floating point operations per second) and averaged performance per processor (as given by the accumulated performance divided by total number of processors) of the world's 500 fastest supercomputers within the last 15 years (data by kind permission of the TOP500 project). The collection comprises academic as well as non-academic (e.g., commercial and military) sites, see the TOP500 web-site for more information [24].

would even take decades. This clearly demonstrates that such calculations are only possible on massively parallel supercomputers, using 1000 processors or more at the same time. This has become possible by the recent development in the supercomputing sector over the last 15 years leading to an amazing exponential overall increase in capacity, doubling the world-wide available computing power nearly every 13 months (c.f. Fig. 1, right side). Another important trend visible from Fig. 1 is that the improvement in the average performance per processor lost momentum during the past years in favor of massively parallelized machines containing thousands of processor cores.

The increasing availability of large computational resources has allowed the physical problems to grow larger, as several examples from materials science impressively demonstrate, e.g., the investigation of Pd-nanowire self-assembly from individual Pd_{225} nanoparticles [25], the simulation of structural phase transitions in Ge/Sb/Te phase-change materials for optical data recording purposes [26, 27] with up to 460 atoms or the exemplary electronic structure calculation of a supercell containing 1000 Molybdenum atoms [28, 29]. Another outstanding work is the determination of structural and electronic properties of a boron-nitride nano-mesh placed on a Rh substrate considering more than 1100 atoms within a full potential approach [30, 31].

Within this contribution we will present three more showcases, where large-scale DFT calculations contribute to the advance in the field of materials science, with a special emphasis on functional magnetic materials. The calculations were performed on more than 1000 proces-

sors on the IBM Blue Gene installations of the John von Neumann Institute for Computing at Forschungszentrum Jülich and cover *ab initio* structure optimizations of up to 923 spin-polarized transition metal atoms.

2 Technical details and performance

The calculations were carried out in the framework of the density functional theory [32] using the Vienna Ab-initio Simulation Package (VASP) [33], which expands the wavefunctions of the valence electrons in a plane wave basis set. The interaction with the nuclei and the core electrons is described within the projector augmented wave (PAW) approach [34] yielding an excellent compromise between speed and accuracy (for an overview on the current state of the code and a review of recent applications, see [35]). For the accurate description of structural properties of ferrous alloys, the use of the generalized gradient approximation (GGA) for the representation of the exchange-correlation functional is mandatory. For the metallic nanoparticles, the formulation of Perdew and Wang [36, 37] in connection with the spin interpolation formula of Vosko, Wilk and Nusair [38] was used. Since the objects under consideration are zero-dimensional and thus non-periodic, k-space sampling was restricted to the Γ-point. The description of the electronic properties with a plane wave basis requires a periodic setup, thus the clusters were placed in a cubic supercell, with a sufficient amount of vacuum separating the periodic images. The supercells for the smaller systems were cubic, with a typical edge length of 22 Å, 28 Å and 32 Å for systems containing 147, 309 and 561 atoms, respectively, warranting a separation of about 9 Å of the periodic images. In order to check the convergence of the results with the supercell size, selected $N = 561$ clusters were studied within a 35 Å supercell, leading to an overall change of the absolute energy per atom of about 0.1 meV/atom. The effect on the energy difference between the clusters, was of one order of magnitude smaller. The clusters with $N = 923$ were placed in a unit cell with fcc basis vectors (lattice constant: 38.1 Å). This provides a more efficient use of resources as it allows a smaller volume of the simulation cell, while maintaining sufficient separation of the periodic images. A cutoff for the plane wave energy of 268 eV was used for the ferrous systems. Gaussian finite temperature smearing with $\sigma = 50$ meV was used to speed up convergence. For the isomers with competitive energies, σ was reduced to $\sigma = 10$ meV in a second step. The $3d^6\,4s^1$, $3d^7\,4s^1$, $3d^8\,4s^1$ electrons were treated as valence for Mn, Fe, Co and $3d^9\,4s^1$ for Pt, respectively. In most of the calculations, the symmetrization of wavefunctions and forces was switched off allowing for symmetry-lifting changes of the structure. The geometrical optimizations were carried out on the Born-Oppenheimer surface using the conjugate gradient method. The structural relaxations were stopped when the energy difference between two consecutive relaxations was less than 0.1 meV leading to a convergences of forces down to the order of 10 meV/Å.

The phonon dispersions in Sec. 5 have been obtained within the direct force-constant approach using the PHONON package by Krzysztof Parlinski [39]. By this, an orthorhombic supercell was constructed consisting of 40 atoms formed by five tetragonal unit cells stacked in [110] direction. This corresponds to the direction along which the phonon softening of the TA_2 branch is found in experiment. The dynamical matrix is constructed from the Hellmann-Feynman forces obtained by *ab initio* calculations from specific displacements of the atoms in the supercell using the

VASP code. For the $1 \times 5 \times 1$ supercell the mesh for the integration in reciprocal space was reduced to $10 \times 2 \times 8$ Monkhorst-Pack grid points. All phonon dispersions were calculated for the volume corresponding to the equilibrium lattice constant at zero magnetic field and zero temperature, $a_0 = 5.8067\,\text{Å}$. We used pseudopotentials with $3d^9 4s^1$ as valence for Ni, $3d^6 4s^1$ for Mn and $4s^2 4p^1$ for Ga and a cut-off energy $E_{\text{cut}} = 353\,\text{eV}$. For the simulation of the twin boundary motion processes, k-point integration was restricted to the Γ-point only as a consequence of the large simulation cell. The plane wave cutoff was set to 337 eV and exchange correlation potential in the formulation of Perdew, Burke and Ernzerhoff [40] was used. Again, the geometric relaxations performed using the conjugate gradient method were carried out until difference between total energies of two consecutive steps fell below 0.1 meV.

Parallelization is implemented in the VASP code using calls to the Message Passing Interface (MPI) library. Parallel linear algebra routines (e.g., eigensolver) are used from the ScaLAPACK library. The installation on the IBM Blue Gene did not require major changes in the code. The peculiarity of the IBM Blue Gene/L concept is the huge packing density, which allows 1024 double processor (700 MHz PowerPC 440d) nodes with a peak performance of 5.6 GFlop/s to be placed into one rack (for an overview, see [41]). Its successor, the Blue Gene/P provides 4096 cores per rack (850 MHz PowerPC 450d), where four cores make up one node. To allow sufficient air cooling, power consumption was kept low by reducing the clock frequency of the CPUs and providing only a limited amount of main memory 512 MB per node (2 GB for the Blue Gene/P).[1] The Blue Gene/L hardware allows the memory to be divided between both CPUs ('virtual node' mode) or to be dedicated to one processor alone, while the other takes care of the communication requests ('communication coprocessor' mode), while the Blue Gene/P provides for each node true four-fold symmetrical multiprocessing on request. To increase scalability, a threefold high-bandwidth, low-latency network is implemented. In fact, the quality of the high-speed interconnect plays a decisive role for the successful usage of the DFT code on a massively parallel system, which is demonstrated by scaling benchmarks in Fig. 2.

Although DFT calculations are generally considered to be demanding with respect to memory and I/O bandwidth, we can show that large systems can be handled efficiently on the Blue Gene despite its severe restrictions concerning operating system, partitioning and main memory per node. So far, systems of up to 923 spin polarized transition metal atoms, corresponding to 8350 valence electrons have been successfully treated on the Blue Gene/P. First tests confirmed that systems up to $N = 1415$ atoms will be possible to calculate. The left diagram of Fig. 2 demonstrates that the VASP code can achieve 69 % of the ideal performance on 1024 processors of the Blue Gene/L for a Fe_{561} cluster; in this case, the coprocessor mode was used to make use of the full memory per node on one processor. Especially the optimization of the trial wavefunctions according to the residual vector minimization scheme (labeled 'RMM-DIIS' in Fig. 2) scales nearly perfectly, even at the largest processor numbers under consideration. However, with increasing number of processors, its computation time gets outweighed by other routines ('EDDIAG' and 'ORTCH') providing the calculation of the electronic eigenvalues, subspace diagonalization and orthonormalization of the wavefunctions, making use of linear algebra routines from the ScaLAPACK library and performing fast Fourier transforms. The scaling of

[1] The numbers for the main memory provided here apply to the Blue Gene installations at Forschungscentrum Jülich, the maximum memory configurations available from IBM are actually twice as large.

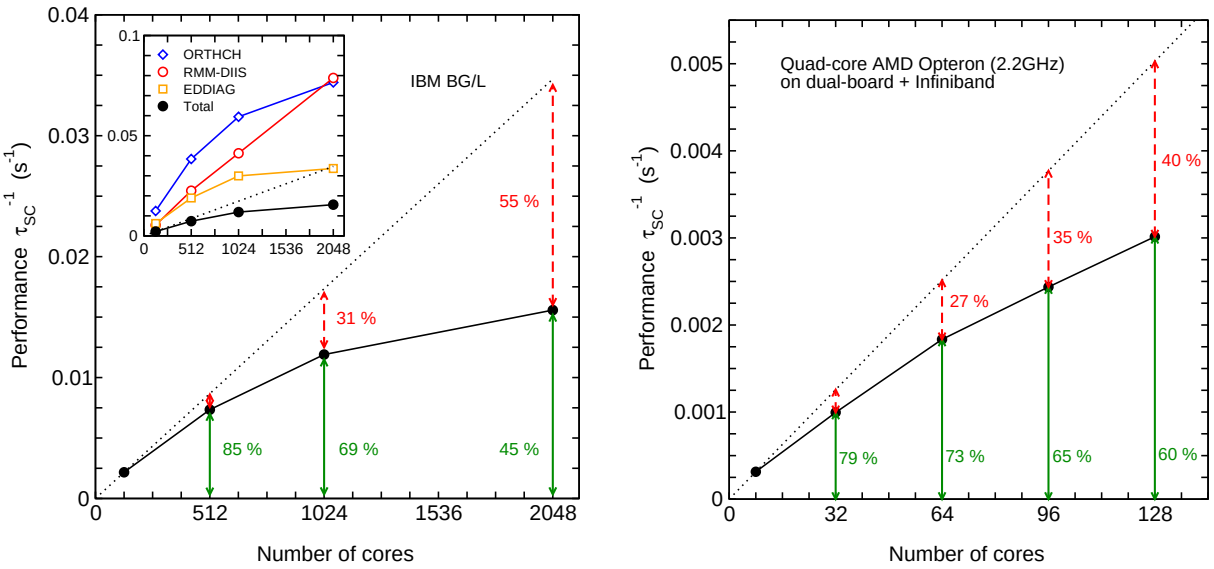

Figure 2: Left: Scaling behavior of a nanocluster with 561 Fe atoms on the IBM Blue Gene/L obtained with the VASP code. The performance given by the inverse average computation time for an electronic self-consistency step, τ_{SC}^{-1}, is shown as a function of the number of cores (black circles). The dashed lines describe the ideal scaling behavior. The inset shows a double logarithmic plot of τ_{SC}. The open symbols in the inset refer to the scaling of the most time consuming subroutines. Right: Scaling behavior of a nano-cluster with $Fe_{265}Pt_{296}$ (561 atoms) on a contemporary PC-cluster (eight boards with $2 \times 2.2\,\mathrm{GHz}$ quad-core Opteron processors and Infiniband interconnect). The performance data were obtained with the same code in the same fashion as for the Blue Gene/L.

these routines may become the primary obstacle, when attempting to run the VASP code on $\mathcal{O}(10^4)$ processors as provided by next-generation supercomputers.

A comparable benchmark of the VASP code on contemporary off-the-shelf PC-hardware, however, lead to a rather disillusioning result (Fig. 2, right side). Despite extensive tuning, acceptable scaling was achieved only with up to 100 cores. This demonstrates, that it is not the code alone which should be made responsible for a dissatifying parallel performance. When attempting to touch the current limits, special care must be taken in the selection of the appropriate computer hardware, too.

3 Structure and magnetism of elemental nanoclusters

Although elemental $3d$ transition metal nanoclusters – in contrast to binary or multimetallic systems – hardly fulfill the criteria for functional magnetic materials even in the widest sense, we will devote our first section to this topic as structure and magnetism may be delicately related even in these seemingly simple systems (for recent reviews in this field, see, e.g., [42–45]). Elemental nanoparticles have raised much attention since they allow, e.g., in gas phase experiments, the direct observation of the crossover from bulk to atomic properties, circumventing the two- and one-dimensional (surface and chain) cases, which require substrates to stabilize

the low dimensional structures experimentally. Prominent examples are the crossover behavior of magnetic moments observed in 3d transition metal nano-clusters as a function of the cluster size, which was studied in the seminal experiments of Billas *et al.* [46–48] or the discovery of significant magnetic moments in small gold nanoparticles or clusters of 4d transition metals as Rh or Pd, which are all non-magnetic in their bulk phases. Not only magnetism, but also the structure of small nanoparticles is strongly affected by the increased surface-to-volume ratio at smaller sizes. This leads to a competition between surface energies and contributions arising from the core structure and internal interfaces and consequently to a crossover between different structural motifs as a function of the cluster size. This has been extensively studied and understood in the framework of simple model systems such as Lennard-Jones-clusters [49–52], which can be easily handled in the framework of classical molecular dynamics and also with empirical model potentials [43, 53]. Here, multiply twinned icosahedral and decahedral structures are favored at smaller sizes, while single crystalline morphologies prevail for larger sizes.

Heavier elements as Au and Pt furthermore form planar or even amorphous structures at smaller cluster sizes. Especially for these elements, but also for systems which are expected close to magnetic or magneto-structural instabilities, it may be doubted whether classical molecular dynamics based on empirical pair potentials can give a reliable account on their structural properties without benchmarks against parameter-free first-principles calculations.

Due to the large computational demands, most of these calculations have been performed for small systems with around 50 atoms or less or without structural optimizations (e.g. [54–58] for the case of iron). Nevertheless a couple of early exceptions exist, e.g., for Pd_{147} [59] and Sr_{147} [60]. Calculations of Pd isomers with size $N = 309$ in an icosahedral and octahedral symmetry have also been reported using the Turbomol package [61]. Recently, a report on the size dependence of magnetism in unrelaxed Fe-clusters of up to 400 atoms has been published [62] reproducing the experimental results in the considered size range as it was also found previously from semi-empirical (tight-binding) calculations [63, 64]. A later result from our group covering structurally optimized Fe-clusters with sizes of up to 641 atoms [65], in contrast, showed strong deviations from the experimental data for larger cluster sizes in agreement with atomic shell models [42, 66, 67] which were developed to describe the oscillatory variations found in experiment. Xie and Blackman [68, 69] argued that the neglect of the magnetocrystalline anisotropy of the clusters and thus the coupling of magnetism to the rotational degrees of freedom can lead to a significant underestimation of the moments in the analysis of the time of flight experiments and may thus account for the observed behavior. Our investigations, on the other hand, give evidence that the experimental trend may be also related to the occurrence of a previously unreported shell-wise Mackay-transformed modification at icosahedral magic cluster numbers. This structure is characterized by an icosahedral outer shape, bcc-like coordinated outer shells and a ferrimagnetic face centered cubic (fcc) cluster core [23, 65, 70] and is possibly kinetically stabilized during the gas phase growth process [71]. The next subsection is devoted to discuss these results in detail, as these findings can be understood from the electronic structure.

3.1 Structure and magnetism of iron clusters

Iron is certainly one of the most important materials of our time. Not only that it is omnipresent as one of the central constituents of our planets but also due to its manifold applications arising not at least from its unusual allotropy. Iron possesses a complex structural phase diagram, with the body centered cubic (bcc) α- and δ-phases below 1185 K and above 1167 K, the face centered cubic (fcc) γ-phase in between and the hexagonal close packed (hcp) ϵ-phase at high pressures. In the fcc γ-phase a variety of competing magnetic states have been discovered, which were brought in connection with magneto-structural anomalies as the Invar effect and the magnetic shape memory behavior in Fe-rich Fe-Ni, Fe-Pd and Fe-Pd alloys, where the fcc structure is also present at ambient conditions. Also in the form of nanoparticles, iron provides a lot of interesting applications, especially in the field of biomedicine (for an overview, see, e.g. [72]).

The systematic scan of the potential energy surface in order to find the most stable morphologies is a very demanding task even for small clusters containing a hand full to few tens of atoms. But the numerical effort increases exponentially with the size and becomes hopeless in the nanometer range. Therefore, it is necessary to restrict the investigation to a subset of paradigmatic morphologies. As a consequence, so-called magic-number clusters have evolved as the Drosophila of size dependent structural investigations in nanoparticle physics. Their size N is a function of the number n of closed geometric shells:

$$N = 1/3\left(10n^3 + 15n^2 + 11n + 3\right) = 13, 55, 147, 309, 561, 923, 1415, \ldots \tag{1}$$

Magic cluster sizes appear to be particularly stable for the late $3d$ elements [73], especially Ni and Co. Magic number clusters according to Eq. (1) allow for a comparison of several paradigmatic geometries: Single-crystalline cuboctahedra with face centered cubic (fcc) structure, perfect Mackay-icosahedra [74] and Ino-decahedra [75], i.e., pentagonal bi-pyramids with symmetrical truncations of their ten faces. Isomers with a body centered cubic (bcc) lattice, which are indispensable for ferrous systems, can be obtained from cuboctahedra by a Bain-transformation [76].

In contrast to the ideal morphologies according to Eq. (1), the geometries observed in experiments are often showing modifications which reflect the competition between obtaining spherical shape and a favorable ratio between facets with different crystallographic orientations and different surface energies. Improved fcc isomers can be constructed according to a Wulff construction [77]. Also, Marks-decahedra [78] with smaller truncations and reentrant cuts at the edges are often found to be more favorable than Ino-decahedra. The optimized morphologies usually harbor a different number of atoms for each geometrical motif. For a quantitative prediction of the most likely surface truncations improving the relative stability, the ratio of the surface energies of the competing facets needs to be known in detail. However, the accurate determination of these quantities is a methodologically and computationally demanding task, especially for the case of materials with a strong interdependence between structure and magnetism as iron or in binary alloys. Magic cluster sizes, on the other hand, allow for the direct comparison of the most important structural motifs and are thus at least good for drawing a coarser, more qualitative picture.

Until recently, the structural evolution of iron clusters as a function of particle size had not

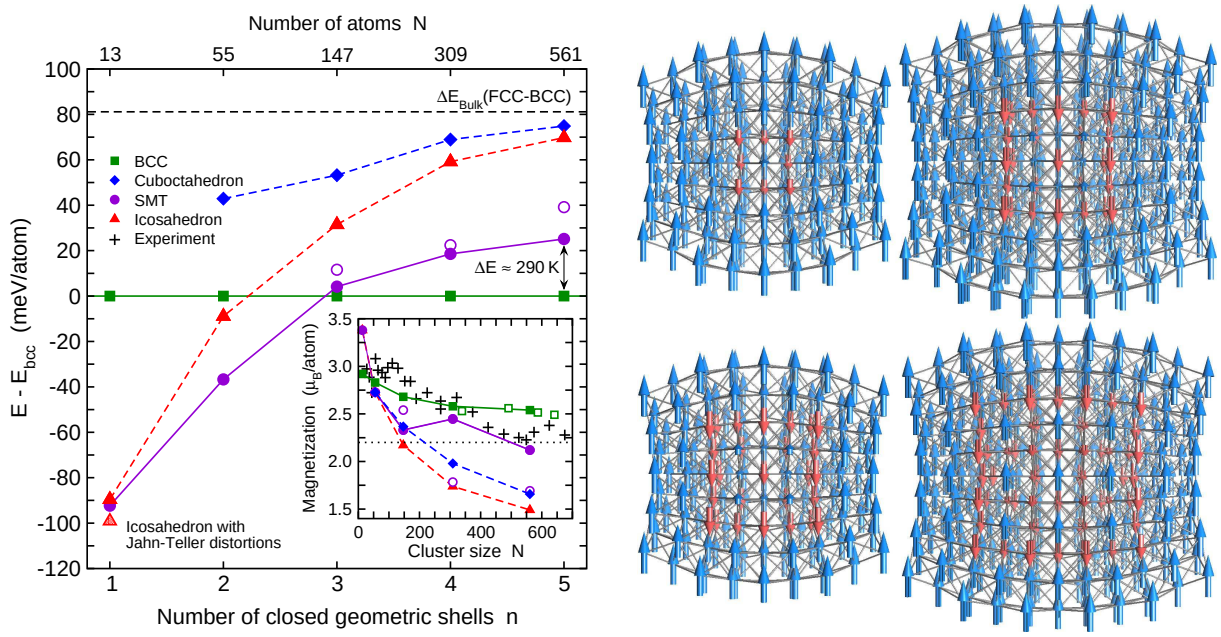

Figure 3: Left: Comparison of the energies of various isomers of elemental iron nanoclusters as a function of the number of closed geometric shells n (data from [65]). The bcc isomer has been chosen as reference and thus represents the abscissa. Open circles denote SMT isomers with alternative magnetic configurations which are not lowest in energy. The lines are intended as guide to the eye, broken lines refer to instable structures. The horizontal dashed line marks the bulk value for the fcc-bcc energy difference [79]. The inset shows the variation of the average magnetic moment of the different isomers as a function of the cluster size (experimental moments taken from [47]). Open squares represent non-magic number bcc isomers. Right: Ferrimagnetic spin configurations of the Fe_{309} and Fe_{561} SMT isomers ($n = 4$ and 5, respectively) shown as cross sections. The arrows refer in length and orientation to the atomic moments. The upper isomers correspond to the high-moment structures with the lowest energy. The isomers on the bottom correspond to low magnetization structures marked by the open circles in the diagram on the left.

been resolved: Transmission electron micrographs (TEM) of 6 nm particles suggest a bcc structure [80], while for 13 atoms, first principles calculations predict a Jahn-Teller distorted icosahedron [81, 82]. For the next closed-shell magical number, i.e. 55 atoms, a previously unreported morphology was found to provide a good candidate for the ground state [65, 71]. Based on this discovery, the concept of the so-called shell-wise Mackay-transformed (SMT) morphologies was introduced by Georg Rollmann and Alfred Hucht, which will be explained in more detail below.

On a larger size scale, estimations of the energetic order between the different paradigmatic cluster morphologies were only available from structure optimizations with classical empirical potentials [83], predicting a crossover between icosahedral and bcc morphologies at sizes around 2000 atoms, while the binding energies were reported to be comparatively close for these morphologies. Keeping in mind that these calculations largely neglect the influence of magnetism on structure, which is especially important in the case of iron, this result cannot be considered conclusive. A detailed analysis based on first-principles electronic structure methods was thus

launched by us to settle this fundamental question [65]. The investigation comprised icosahedral, cuboctahdral and bcc (Bain-transformed cuboctahedra) clusters with up to five completed geometrical shells according to Eq. (1), i.e. $N = 561$ atoms corresponding to, approximately, 2.5 nm in diameter. In addition, more spherical bcc geometries were considered with non-magic sizes up to $N = 641$ atoms. Technically, the calculations were carried out using the VASP code in the fashion described in the preceding section including unconstrained geometric optimizations on the Born-Oppenheimer surface. The total energies resulting for different geometries as a function of the number of closed geometric shells displayed in Fig. 3 reveal that for three closed shells (147 atoms) and larger, the bcc isomer clearly marks the lowest energy conformation, especially in comparison to (high-symmetry) icosahedral and the cuboctahedral isomers, which rapidly approach with increasing n the energy difference between the bcc and fcc phases obtained by bulk *ab initio* calculations [79]. An extensive comparison between the total energies of a vast number of unrelaxed geometries at intermediate sizes obtained with the PARSEC real space DFT method suggests that bcc isomers supersede icosahedral and fcc motifs already below $N = 100$ [62, 65]. The average magnetic moments obtained by both approaches agree well for the bcc case, while for cuboctahedra and icosahedra, the fully optimized structures rather exhibit an onion-type ferrimagnetic ordering of the closed geometric shells reducing the average moment shown in the inset of Fig. 3 considerably. The magnetic ordering of Fe cuboctahedra as a function of the lattice spacing has been investigated recently in more detail [84, 85]. Compared with the experimental data of Billas *et al.* [46, 47], the theoretical data follow the experimental trend up to sizes of $N = 400$ atoms but deviate significantly beyond. This also applies for magic number clusters as well as for more compact bcc clusters up to $N = 641$ atoms, which possess an improved surface-to-volume ratio as compared to the Bain-transformed cuboctahedra, and is in accordance to previous results obtained by other approaches [42].

For all sizes, cuboctahedral and icosahedral shapes are only maintained during the optimization procedure, if the atoms are strictly kept in their symmetric positions and additional symmetry constraints for charge densities and forces are imposed. Already small distortions along the Mackay-path [74] are sufficient to induce a transformation, which finally leads to the above mentioned shell-wise Mackay-transformed conformation. The SMT state is very robust and can be obtained from different initial configurations [86] and has recently also been reproduced by classical molecular dynamics simulations with empirical EAM potentials [87] for clusters with up to 15 closed geometric shells [88].

The Mackay-path is analogously to the Bain-path [76], which connects fcc and bcc bulk phases by changing the extension of the c-axis with respect to the equal a and b axes of the crystal, a diffusionless, displacive mechanism relating the cuboctahedron with a single-crystalline fcc structure to the non-crystallographic icosahedron. During this process twelve pairwise adjacent triangular (111)-faces of the icosahedron stretch along their common edge and turn into the same plane to form the six square (100)-faces of the cuboctahedron. An illustration of this process is given in Fig. 4 for the case of the $N = 561$ isomers. The original Mackay process affects all shells simultaneously. Such homogenous transformations have been recently studied in detail for magic number Pb clusters of different sizes with *ab intio* methods [89]. In the SMT isomers, however, the degree of transformation varies gradually from shell to shell, from a perfect cuboctahedron in the particle core, to a nearly icosahedral shape of the surface shell. This is

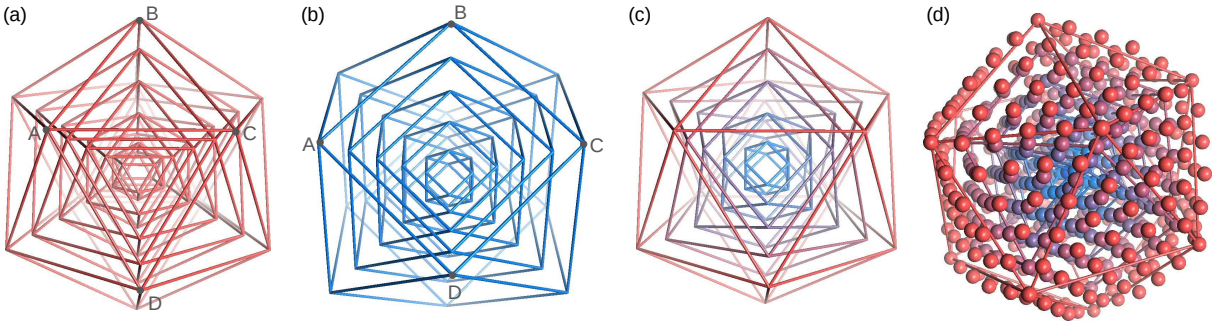

Figure 4: Edge models of the optimized Fe_{561} icosahedron (a), cuboctahedron (b) and SMT isomer (c). Separately for each shell, the corner atoms of the faces are connected by lines, the atoms themselves are omitted for clarity. The complete SMT isomer including all atomic positions is shown in (d). For icosahedra and cuboctahedra, shells of the same shape but different sizes are stacked into each other. For the SMT isomer, the shape of the outermost shell is icosahedral and continuously changes towards the inside along the Mackay-path to a cuboctahedron, which represents the shape of the innermost shell, which is reflected by the gradual change of color from red to blue in (c) and (d). The Mackay transformation works by stretching the bond $\overline{AC}$ of the icosahedron and turning the two adjacent triangular faces ABC and ACD into the same plane producing the square face $ABCD$ of the cuboctahedron.

slightly distorted by the inward bending of the common edge between the two triangular facets which correspond to the square face of the cuboctahedron. The SMT represents the lowest energy isomer for $n=2$ and is only slightly higher in energy than the Jahn-Teller distorted icosahedron with only one closed shell for $N=13$. For $n\geq 3$, however, the bcc isomers form the ground state. Nevertheless, the energy of the SMT is largely reduced compared to the symmetric icosahedra and cuboctahedra and still in the range of thermal energies to the bcc isomer for $N=561$. Also the magnetic structure differs: While still being ferrimagnetic with an onion-type (shell-wise) alternating arrangement of layers in the particle core, the average moment of the SMT is systematically larger than the moment of icosahedra and cuboctahedra: For the SMT the outermost three shells are ferromagnetically aligned (cf. right side of Fig. 3), while for the latter only surface and sub-surface shells have the same magnetization direction. Due to its ferrimagnetic spin structure, the average moment of the SMT isomer is considerably smaller than the average bcc moment and agrees therefore much better with the experimental data. It is certainly too speculative to conclude from this evidence that the occurence of SMT isomers around $N=561$ explains the dip in the cluster moments in the experiments of Billas *et al.*, but it should be kept in mind, that icosahedral features are frequently observed in many materials during solidification from the melt or during gas phase synthesis [90]. Also, from recent DFT calculations, icosahedral or, respectively, SMT-growth has been proposed as a likely growth mode for small Fe-clusters from the gas phase [71].

The search for the origin of this unusual transformation requires a more detailed structural analysis. For several hundred atoms, the inspection of the structural environment at the atomistic level may, however, become a tedious and fallible task without appropriate statistical means. A well corroborated approach has been developed in the classical molecular dynamics community

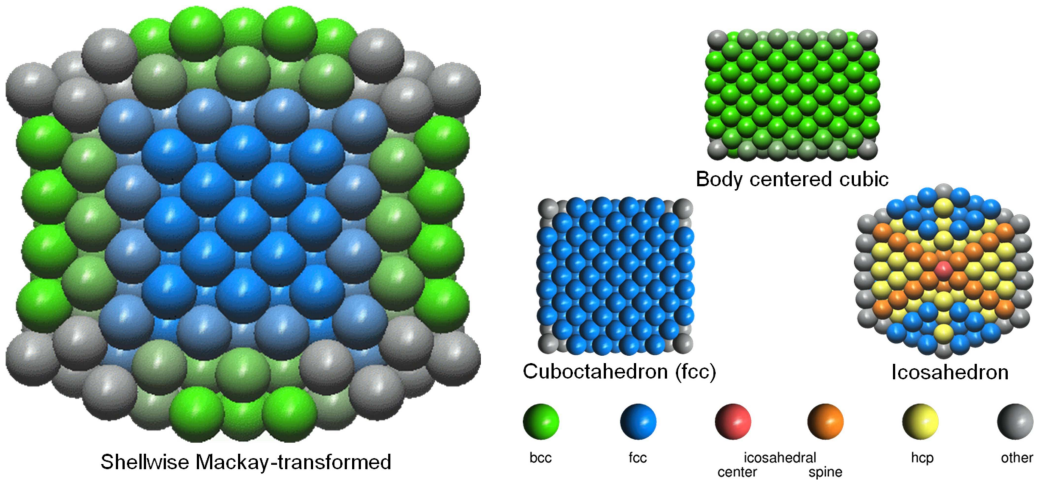

Figure 5: Cross sections of optimized geometries of 561-atom iron nanoparticles. The color coding describes the local coordination of the atoms obtained by a common neighbor analysis. Bright colors refer to perfect matching of the CNA-signatures with the ideal bulk and surface configurations. With increasing number of deviations the colors turn into grey.

where the classification of structural transformations in large systems is a common request. The so-called common neighbor analysis (CNA) [91, 92] allows a comprehensive comparison of the SMT structure with other morphologies. If we restrict ourselves to the first (for bcc up to the second) neighbor shell, a set of three-index-signatures provides a classification of the local structural environments of the atoms in the cluster. The indices refer – in the respective order – to the number of nearest neighbors both atoms have in common, the number of bonds between those neighbors, and the longest chain of bonds connecting them. Each ideal bulk structure is characterized by a specific set of 12 to 14 individual signatures. For surface and sub-surface atoms different signatures apply. A comparison of the CNA of atoms of the SMT with the respective positions in the other, ideal isomers can now attribute for each atom a specific characterization of the local environment. Figure 5 shows the result of a CNA applied to the optimized isomers, the colors indicating the local structural environment. In many cases, the coincidence is not perfect and few signatures differ with respect to the ideal cases. Here, the colors turn into grey with increasing number of non-matching signature, which marks an unidentified environment. While the bcc and fcc clusters are uniform in structure, we find for the icosahedron the typical mixture of fcc, hcp and – along the five-fold symmetry axes – icosahedral environments. The SMT isomer, however, shows a rather unexpected pattern: While the central atoms are fcc coordinated according to the nearly completed Mackay-transformation of these shells, we find no trace of the typical icosahedral signatures in the outermost shells which, however, retain their overall icosahedral shape. Instead, their signatures show typical signs of the energetically favorable bcc-like coordination, suggesting that the affinity of bulk-Fe to form a bcc lattice at low temperatures is also responsible for the stabilization of SMT structures in nanoparticles. In this case bcc-specific features should also show up in the electronic density of states (DOS).

A comparison of the DOS for different $N = 561$ morphologies is presented in Fig. 6. For the bcc isomer, the partial DOS of the core and subsurface atoms exhibit the typical valley in the

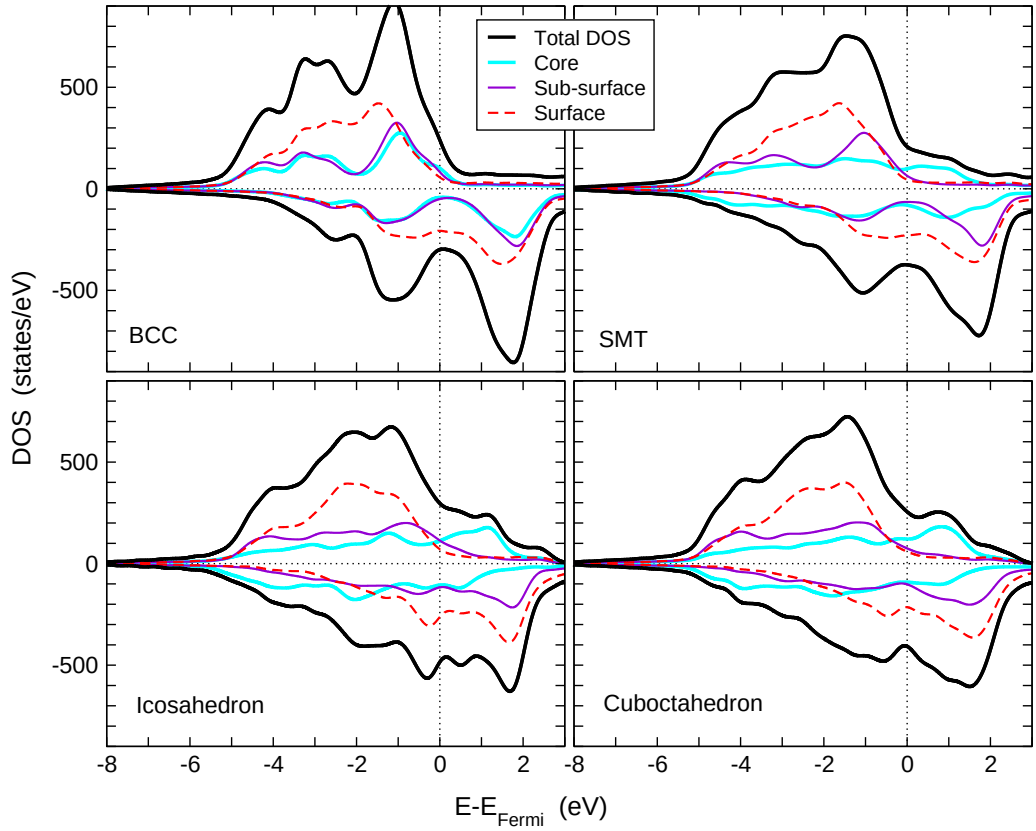

Figure 6: Total electronic density of states of the four Fe_{561} morphologies (thick black lines). Positive densities refer to the majority-spin states, negative to the minority-spin channel. The colored lines mark the shell-resolved partial contributions. Thick bright blue lines denote the DOS of the innermost three shells (147 atoms), thin violet lines the sub-surface shell (162 atoms) and the broken red lines refer to the surface shell (252 atoms). In order to concentrate on the essential features, the curves have been artificially broadened according to a Gaussian distribution with $\sigma = 0.2\,\mathrm{eV}$.

center of the d band – a characteristic feature for bulk bcc alloys. While the majority d band is nearly filled, the Fermi level locks into this valley in the minority channel, providing a motivating argument for the extraordinary stability of the ferromagnetic α-phase of bulk iron [93]. In fact, the partial contributions of sub-surface and surface shells bear strong similarities to the bcc case, while the partial contributions of the core atoms with their ferrimagnetic alignment rather resemble the result for the cuboctahedral or icosahedral morpholgies.

While the density of states can in priciple be detected by photoemission experiments, the particular examples provided in Fig. 6 may – except for the case of the bcc cluster – not provide sufficiently distinctive features to discriminate between the structural motifs. An experimentally accessible quantity, which is directly related to the structure, is the pair distribution function (PDF). The inhomogeneous structural environment of the SMT results in a PDF which is qualitatively different from the other morphologies (Fig. 7). It neither compares well to a linear combination of fcc and bcc PDF, as could have been guessed from the CNA, results but rather to the experimental results of Ichikawa *et al.* [94] obtained from a thin film produced by low-temperature condensation of evaporated iron. These exhibit features which are typical for

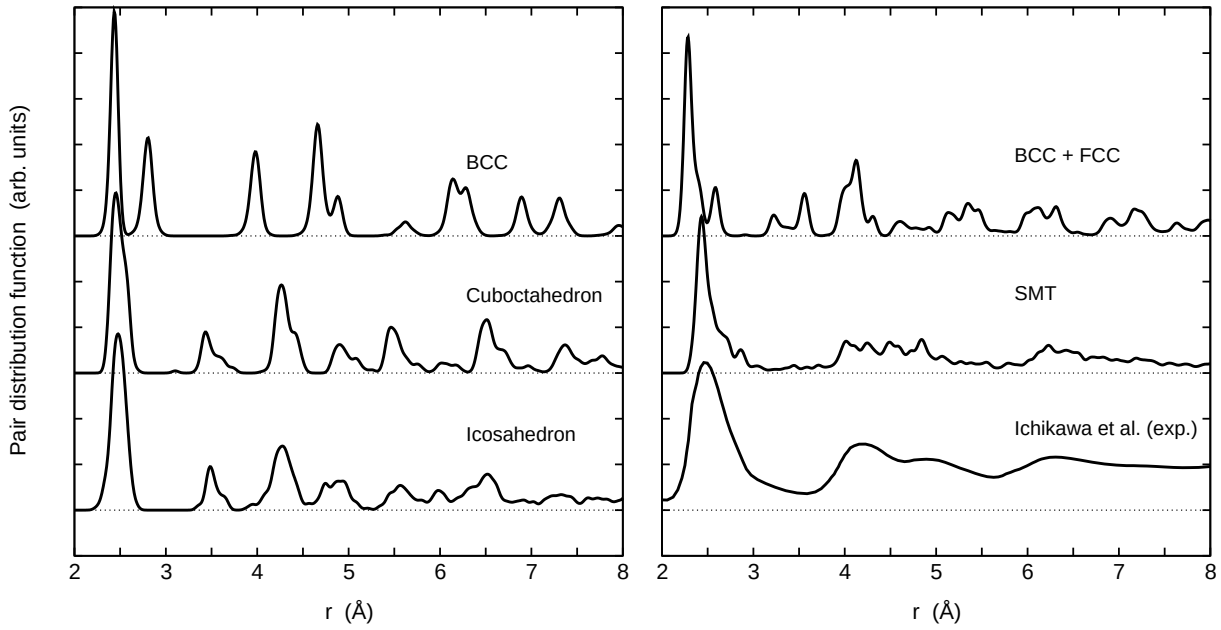

Figure 7: Pair distribution functions (PDF) of the Fe_{561} isomers discussed in Fig. 5. For comparison also a linear combination of the bcc and the cuboctahedral PDF (top right) as well as the experimental PDF (bottom right) of an Fe-film produced condensation of evaporated iron [94] is shown (theoretical data from [70]).

amorphous alloys and were thus interpreted in this sense. Other related experiments are based on a sonochemical approach [95].

It has to be noted at this point, that while the existence of certain amorphous Fe-based alloys is well established in literature (see, e.g., [96] and references herein), the possiblity of amorphous pure iron is highly debated. While the SMT isomer is not amorphous in a literal sense, the transformation may be compared to the rosette-like structural excitations which were recently discussed as amorphization mechanism for Pt and Au nanoclusters [97]. Recently, an intermediate amorphous-like phase was reported from empirical molecular dynamics simulations of 2.5 nm $Fe_{80}Ni_{20}$ clusters [98], which shows striking similarities concerning its PDF and other structural motifs as the wave-like bending of atomic columns and planes, which is visible in Fig. 4. This can be seen as a further indication that SMT morphologies may in fact be realized in the experiment under certain environmental conditions.

3.2 Cobalt and nickel nanoparticles

Due to the multitude of different possible bulk phases with distinct magnetic properties, iron is certainly an exceptional case, also with respect to its properties on the nanoscale. For the other elements showing ferromagnetism in the bulk phase, a comparably rich behavior is not expected. Figure 8 compares thus only the two most important magic number morphologies, icosahedra and cuboctahedra. For Ni and Co, icosahedra are strongly preferred over the whole size range, the energy difference being much larger as compared to Fe, especially in the case of Co. The magnetic properties approach the bulk values faster with increasing cluster size as

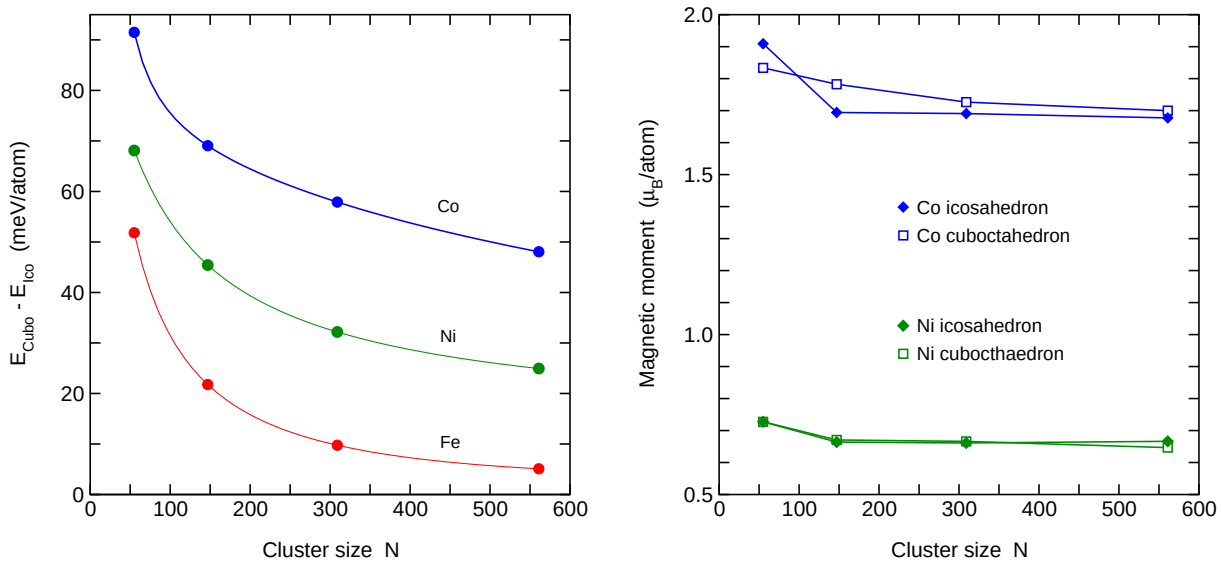

Figure 8: Left: Energy difference between cuboctahedra and icosahedra of Co, Ni and Fe as a function of the cluster size. Right: Size dependece of the averaged magnetic moment of Co and Ni clusters.

it is the case for iron, agreeing well with combined time-of-flight mass-spectroscopy and Stern-Gerlach measurements [48] and the results of the extensive tight-binding studies of Xie and Blackman [15,99,100]. This makes these elements appear more suited for a successful description with emprirical potentials. Especially in the case of Ni, the calculated energy differences between icosahedra and cuboctahedra coincide from $N = 147$ atoms upwards surprisingly well with the early results of Cleveland and Landman [53] based on empirical pair potentials.

From the electronic structure point of view, it is tempting to classify the preference for the icosahedral structure in terms of the electronic density of states. From Fig. 9 it becomes evident that the core and sub-surface contribution do not differ significantly between the two morphologies of the same element and only slightly between the elements (except for the different exchange splitting). The most distinctive changes are visible with respect to the DOS of the surface atoms suggesting that – in contrast to iron – the surface energy contributions play the dominant role in the determination of the particle shape.

4 Binary transition metal nanoparticles – in search of ultrahigh density magnetic recording materials

In the field of ultra-high density magnetic recording (for an overview, see, e.g. [101]), the long-lasting exponential increase in storage density over time still seems unbroken: While about a decade ago, densities of 35 GBit/in^2 were state-of-the-art [7], the manufacturers hope to go up to 10 to 50 TBit/in^2 in the future. However, to reach this goal, it is necessary to switch to new types of recording media. Magnetic data storage as in conventional hard disk drives currently relies on thin CoCrPtB microstructured magnetic films consisting of single crystalline grains with polydisperse size distribution. To average out the noise, the information has to be stored

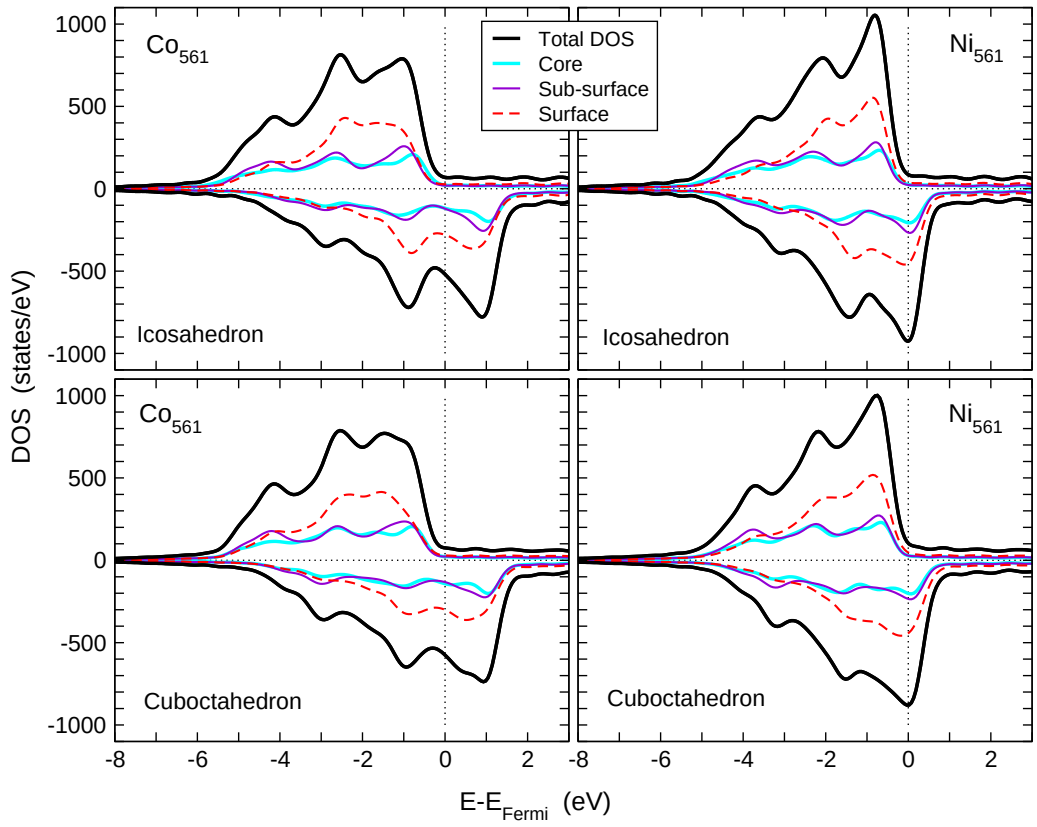

Figure 9: Electronic density of states of Co_{561} and Ni_{561} icosahedra and cuboctahedra. Lines and colors have the same meaning as in Fig. 6.

in the different magnetization directions of around 50 to 100 of loosely coupled grains.

The main obstacle to further miniaturization is the so-called superparamagnetic limit, which threatens the long-time stability of the information stored. The Néel relaxation time of a macrospin with uniaxial anisotropy, representing the recording media grain, has an exponential dependence on the product of anisotropy constant and volume divided by temperature. This imposes a lower boundary for the possible size of a grain which keeps its magnetization unaffected by thermal relaxation processes at room temperature for a sufficiently long period of time (usually decades). Today, two approaches beyond current technologies are discussed:

- Replacement of polycrystalline films by patterned media, where each bit is represented by a single thermally stable magnetic particle. This reduces dramatically the area needed for one bit and also the interaction between neighboring grains but demands high standards with respect to monodispersity, magnetic properties and arrangement of the particles. Remarkable progress has been made in this field in the past years [5, 6, 102].

- Use of high-anisotropy materials. This allows a reduction of the grain size stability limit inversely proportional to the increase in the anisotropy constant [7, 101]. Materials, which are currently widely discussed in this respect are Fe-Pt and Co-Pt [103]. Several studies had suggested that particles sizes as small as 3 nm (for Fe-Pt, inferred from the bulk anisotropy constant) could be sufficient for thermally stable storage of information [5, 104, 105] (for a comparison of several possible materials, see Tab. 3).

Alloy	K_u (10^7 erg/cm^3)	H_C (kOe)	D_p (nm)
CoCrPtB	0.33	20	9.1
Co	0.45	6	8.0
FePd	1.8	33	5.0
FePt	6.6 – 10	116	≈3.0
CoPt	4.9	123	3.6
MnAl	1.7	69	5.1

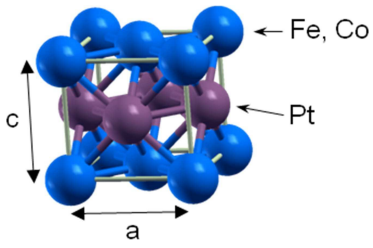

Table 3: Collection of characteristic properties of contemporary and future storage media materials capable of storing information over a decade in grain sizes smaller than 10 nm (taken from [7]). Listed are: Uniaxial anisotropy K_u, coercitive field H_C, critical particle size D_p. The figure on the right visualizes the $L1_0$ structure of FePt, FePd, CoPt and MnAl.

Structural and magnetic properties of binary nanoparticles formed of the transition metal alloy Fe-Pt have been subject to a considerable number of investigations during the past years (for a recent overview, see, e.g. [106]). The stoichiometric $L1_0$-phase FePt, CoPt and FePd is characterized by a face centered tetragonal (fct) lattice with a layer-wise stacking of $3d$ and fourth- and fifth row transition metals along the shortened axis. The alternation of the elemental constituents gives rise to the unusually large magnetocrystalline anisotropy – rather than the slight tetragonal distortion of a few percent [107]. Current production routes for Fe-Pt nanoparticles are to fabricate disordered fcc particles from gas phase experiments [108, 109] or wet-chemical production routes [5,110,111] and to obtain the ordered $L1_0$ phase in a further annealing step [6]. However, in recent times it was reported that $L1_0$ particles with a sufficient magnetocrystalline anisotropy may be difficult to obtain in the interesting size range [110, 112–115]. Recently, improved results have been reported after embedding the particles in a matrix, in micelles or by irradiating them with ions [116–118]. In most cases, however, compared to the coercivity of the bulk materials in Table 3 the results obtained for small nanoparticles are rather disappointing (e. g. [119]). Part of the experimental studies relate this to the incomplete order in these systems as there is a critical particle size, below which sufficient ordering cannot be achieved for thermodynamical reasons. Another possible explanations, which also accounts for larger particle sizes, is related to the appearance of domains with different orientations of $L1_0$ structure in the same particle, counteracting the development of one stable easy axis. Indeed, high resolution transmission electron microscopy (HRTEM) showed the occurrence of multiply twinned morphologies such as icosahedra and decahedra already at particle sizes around 6 nm [120–122] consisting of several strained twins (20 in the case of Mackay-icosahedra and 5 in the case of decahedra). Therefore such morphologies cannot be expected to exhibit a large uniaxial magnetocrystalline anisotropy, even if the individual twins are perfectly $L1_0$-ordered, because of their different crystallographic orientations.

As the crossover effects between different geometries at small particle sizes can be traced back to a competition between surface and core energies, two possible routes open up to suppress unwanted multiply twinned morphologies – either by changing the ratio of the surface energy of different faces, which can be effectively done by suitable ligands in wet-chemical approaches,

or, on the other side, by increasing the energy related to internal lattice defects, such as twin boundaries, which could be achieved, e.g., by alloying.

4.1 Fe-Pt and Co-Pt nanoparticles for data recording applications

In many elementary nanoparticles with fcc ground state in bulk, a competition between different morphologies is observed owing to the favorable (111)-surfaces of the icosahedron, which gives the dominating energetic contribution at small particle sizes. In binary systems like Fe-Pt, segregation and ordering tendencies have to be considered, too. In this respect, we distinguish three different classes: Disordered structures, ordered isomers and core-shell structures, corresponding to perfect surface segregation, with all Pt placed on the surface or in the shell below. The composition was fixed to the near-stoichiometric perfectly $L1_0$ ordered cuboctahedra which are the most relevant isomers from the technological point of view. Although orbital magnetism is not explicitely included in our calculations, it is obvious from geometric considerations that the multiply twinned morphologies, even if the individual twins are $L1_0$ ordered, will not show the desired uniaxial magnetic anisotropy due to the multiple orientations of the twins in the nanoparticles. A deep understanding of the interplay between geometric structure, chemical ordering and magnetic properties will therefore be an important step towards the production of high anisotropy nanomaterials for ultra-high density magnetic data recording.

So far, most *ab initio* studies of binary transition metal clusters were restricted to rather small sizes (for a recent review, see [123]). Thus, most theoretical investigations of Fe-Pt and Co-Pt nanoparticles have been carried out using continuum models [124], classical Monte-Carlo and molecular dynamics simulations with empirical model potentials [125–130] or semi-empirical methods [131, 132]. The magnetism of spherical 2.5-5 nm $L1_0$ Fe-Pt nanoparticles embedded in a disordered alloy matrix has been investigated by means of the locally self-consistent multiple scattering (LSMS) method [133].

In order to shed more light on the origin of the experimental problems from the electronic structure point of view, we started *ab initio* calculations of Fe-Pt and Co-Pt nanoparticles with up to 923 atoms (≈ 3.0 nm in diameter), comparing more than 60 configurations of particles of both materials with different sizes [134–136]. Although the largest particles are still too small to avoid superparamagnetism, general trends can be formulated from the results, as the largest clusters already possess a balanced surface-to-volume ratio (45 % at 2.5 nm as compared to 32 % at 4 nm).

The systematic investigation of binary alloy clusters raises more complications due to the additional compositional degree of freedom. Apart from the competition of various geometries, also order-disorder and surface segregation effects must be taken into account. Therefore, we must restrict ourselves, again, to a small number of paradigmatic morphologies. In addition, perfectly chemically ordered or segregated structures exist only for particular compositions and this usually depends on the particular distribution motif of the elements, such as a layered or shell-wise ordering or a perfect core-shell like configuration. Comparing perfect motifs would require to relate calculations for different compositions, which hampers the direct comparison of the relative stability of the isomers. In order to avoid these problems, we will chose one specific composition and most compositional motifs will consequently be approximated by randomly

distributing the atoms of the excess species on the designated sites of the short element. As the central concern of our work is related to nanoparticles for ultra-high-density recording purposes, the stoichiometric $L1_0$ fct isomer with alternating Fe and Pt layers along the shortened c-axis is a distinguished case, since this is the closest approximant of the bulk alloy structure and thus expected to show the desired large magnetocrystalline anisotropy. Due to the symmetry of the structure, the two (001)-surfaces of the $L1_0$ cuboctahedra have to be terminated by one species, either completely with iron or with platinum, respectively. This results in a slight off-stoichiometry which decreases with increasing cluster size. For the Pt-rich case, the size dependence of the composition is given by the following relations

$$\begin{aligned} N_{\mathrm{Fe}} &= \tfrac{1}{3}\left(5n^3+6n^2+4n\right) &&= 5,24,67,144,265,440,\ldots \quad , \\ N_{\mathrm{Pt}} &= \tfrac{1}{3}\left(5n^3+9n^2+7n+3\right) &&= 8,31,80,165,296,483,\ldots \quad , \end{aligned} \tag{2}$$

where n is again the number of complete geometric shells. Exemplary *ab initio* calculations of $Fe_{265}Pt_{296}$ clusters [135] demonstrate that in comparison to the perfectly $L1_0$ ordered Fe-covered isomer, a redistribution of the atoms in connection with covering the surface with Pt leads to a considerable gain in energy despite the imperfection of the order by placing the excess Fe on the Pt-antisites. Therefore, in thermodynamic equilibrium, the Pt-dominated morphologies should dominate and we consequently focused on the isomers with predominately Pt-covered surfaces. This reasoning comes closest to the gas phase production route; for wet chemical processes the kinetics of formation plays a much bigger role, which we currently cannot cover by *ab initio* simulations.

4.1.1 Size dependent properties of Fe-Pt nanoparticles

The investigated isomers are categorized in three major groups, ordered structures, disordered structures and core-shell motifs, which are symbolized by the colored boxes in Fig. 10. The ordered morphologies (blue box) refer to the structures which reflect the strong tendency towards $L1_0$ ordering in bulk Fe-Pt. These comprise the $L1_0$ ordered cuboctahedron as the reference structure and an Ino-decahedron with its five twins individually $L1_0$ ordered and Pt-terminated (001)-surfaces. The ordered icosahedron was obtained by applying a full transformation along the Mackay-path [74] on the positions of the $L1_0$ cuboctahedron, while keeping the occupancy of the sites by the atomic species fixed, since this largely preserves the local chemical enviroment of the atoms. In fact, the multiply twinned ordered morphologies turn out to be lower in energy than the reference isomer, supporting the experimentally observed trends. This is especially significant for small clusters, with decreasing tendency towards larger sizes. For the ordered icosahedron a crossover to the single crystalline $L1_0$ morphology is taking place around 600 atoms, which is in excellent agreement with the cross-over size predicted on the basis of continuum-models for a related icosahedron with 20 individually ordered $L1_0$ twins with random orientation of the c-axis [124]. It should be kept in mind, that the nominal composition is varying with cluster size, which affects mainly the smallest investigated sizes.

For comparison, the three paradigmatic cluster shapes have also been studied as chemically disordered isomers (green box). The icosahedral morpholgies are again preferred over the decahedral and single crystalline structure, but all corresponding energies are considerably above the values of the ordered morphologies, which is expected due to the strong ordering tendencies

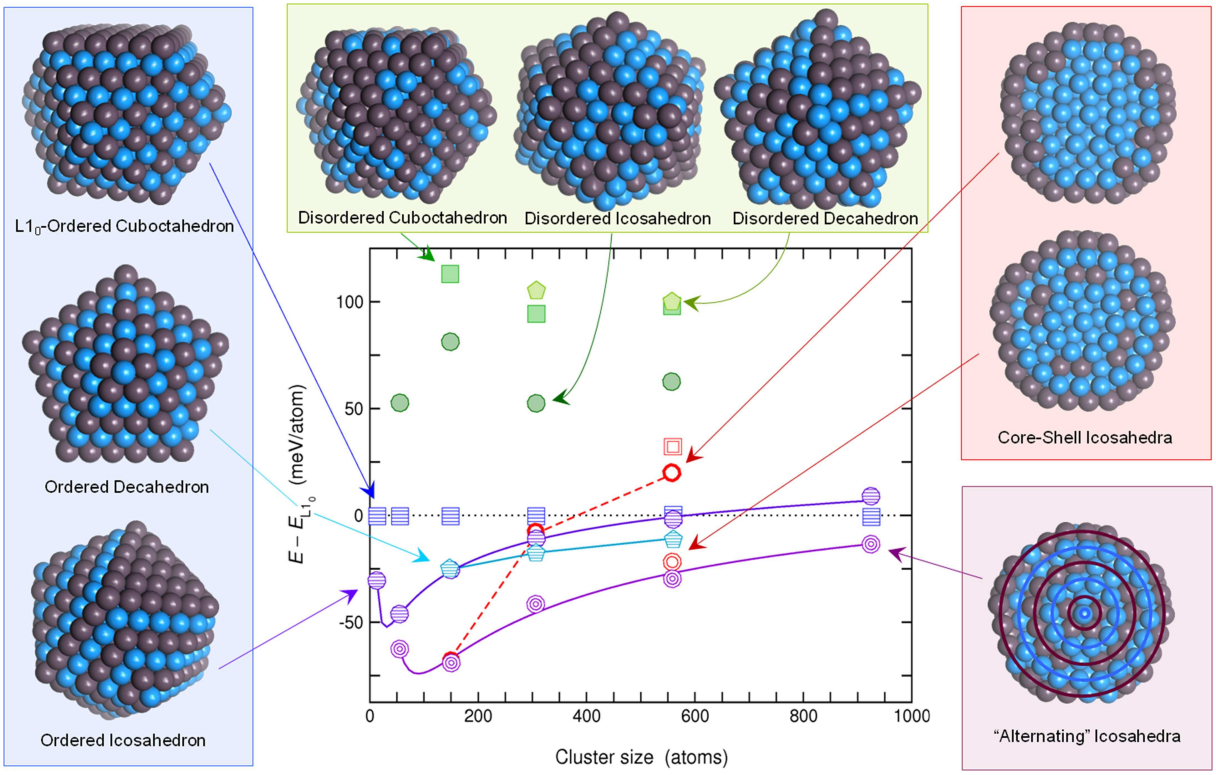

Figure 10: Morphologies of Fe-Pt nanoparticles and their corresponding energies as a function of the cluster size. The data up to $N = 561$ are taken from [134]. In the diagram, cuboctahedra are represented by squares, icosahedra by circles and decahedra by pentagons; the lines are guides to the eye. The energy reference is defined by the $L1_0$ cuboctahedron. Shaded (green) symbols denote disordered isomers, hatched (blue) symbols ordered structures, thick and nested symbols core-shell (red) icosahedra and cuboctahedra as well as icosahedra with shell-wise ordering tendencies (violet). Around the diagram, examples of the simulated cluster structures are shown. Only the structures with $N = 561$ atoms (265 Fe and 296 Pt) are depicted. Blue spheres refer to Fe atoms, brown spheres to Pt. The icosahedral core-shell structures on the right are shown as cross sections, visualizing the inner arrangement of the atomic species. The circles drawn on top of the lowest-energy icosahedron (right bottom) visualize the alternating, onion-type arrangement of Fe- and Pt-rich shells.

in bulk Fe-Pt. In order to obtain a quantitative estimate, configurational averaging over a large number of distributions would be necessary, especially for the smaller sizes, which has been omitted in the present study.

The third important class (red box) represents the core-shell morphologies. Again, Pt atoms are expected to segregate to the surface, while the Fe-atoms occupy predominately the core sites. For $N = 147$, where Pt covers 80 of the 92 surface sites, this is a very favorable arrangement. For larger clusters, the number of Pt atoms exceeds the number of surface sites, for $N = 309$ by 3 atoms and 44 atoms for $N = 561$. Placing these atoms into the subsurface shell, which corresponds to complete segregation, is obviously becoming a much less advantageous structural configuration as demonstrated by the broken red line in Fig. 10. However, if the subsurface shell is kept Pt-depleted and the Pt atoms occupy sites of the third shell instead, the energy

is decreased by sizeable 42 meV/atom. This isomers can also be understood as a shell-wise alternating arrangement of pure Fe and Pt-enriched closed geometric shells with an extreme concentration gradient in the Pt-enriched layers ranging from 0 % from the center to 100 % on the surface. In fact, icosahedral configurations with a concentration gradient have been proposed recently to explain high-resolution transmission electron micrographs of larger icosahedral Fe-Pt clusters with a diameter around 6 nm [122]. A configuration in which all Pt-containing shells have the same relative composition refers to another limiting case. Such isomers are depicted in Fig. 10 by triply nested circles and mark the lowest energy isomers throughout the whole investigated size range. This morphology marks an intermediate between core-shell and ordered structures with an incomplete $L1_1$ ordering within each of the 20 twins. The $L1_1$ structure is defined by a layer-wise alternation of [111] planes of the fct lattice occupied by different elements, terminated in our case by the 20 (111)-surfaces of the icosahedra. Structures with $L1_1$ ordering are known from the bulk Cu-Pt alloy [137] but not from bulk Fe-Pt or Co-Pt. Here, obviously the low surface energy of the Pt-terminated (111) surfaces overcompensate the energy contributions due to twinning and the strained $L1_1$ arrangement of the core atoms. As a consequence, the energetic advantage over the single crystalline $L1_0$ isomer is decreasing with increasing particle size. A tentative extrapolation leads to the expectation that the crossover between these two structural motifs will occur around 8 closed shells or a diameter around 4 nm, respectively.

Isomers with $N = 147$ atoms or larger show a more or less uniform, size independent behavior for average magnetization per atom [134], which takes values in a corridor of about $\pm 0.1\,\mu_B$ around the average bulk value [138], which is in good agreement with previous DFT studies of unrelaxed Fe-Pt clusters with up to 135 atoms [58]. Exceptions are observed for the core-shell isomers, which show a reduced average moment due to ferrimagnetic alignment of the spins in the Fe-rich core. From DFT calculations it has been predicted [139–142], that the ordered $L1_0$ phase is close to an instability towards an antiferromagnetic (AF) structure described by ferromagnetic (FM) Fe-layers alternating along the c-axis. The origin has been traced back to a competition between a Pt-mediated ferrmomagnetic coupling and a direct antiferromagnetic exchange between the layers [141,143], similar to the α-FeRh alloy which in fact shows a temperature induced AF-FM metamagnetic transition [144]. The hypothetic AF phase is characterized by a slightly increased tetragonal distortion with nearly the same atomic volume [142]. In fact, AF isomers which are nearly degenerate in energy can be stabilized in calculations. Disorder and magnetocrystalline anisotropy, however, are expected to work in favor of the FM phase [135,139,140,145]. Entropic arguments may also play a role [143,146–148].

From experimental side, it has been argued that an inhomogeneous distribution of the Fe- and Pt-species may lead to local deviations from the stoichiometric compositions which can decisively influence the magnetic properties of these isomers [106]. A more detailed analysis of the distribution of the magnetic moments with respect to their structural enviroment is given in Fig. 11. Here, the site-specific magnetic moments of all Fe and Pt atoms in selected $Fe_{265}Pt_{296}$ are plotted versus their distance to the center of the particle. To provide further information on the structural environment, we use open and filled symbols, alternating with the index n of the geometric shells according to Eq. (1), to which the respective atoms belong to. For all isomers, there is a continuous increase of the iron mangnetic moment from the center of the cluster towards the surface, while the induced Pt-moments appear to be nearly constant or

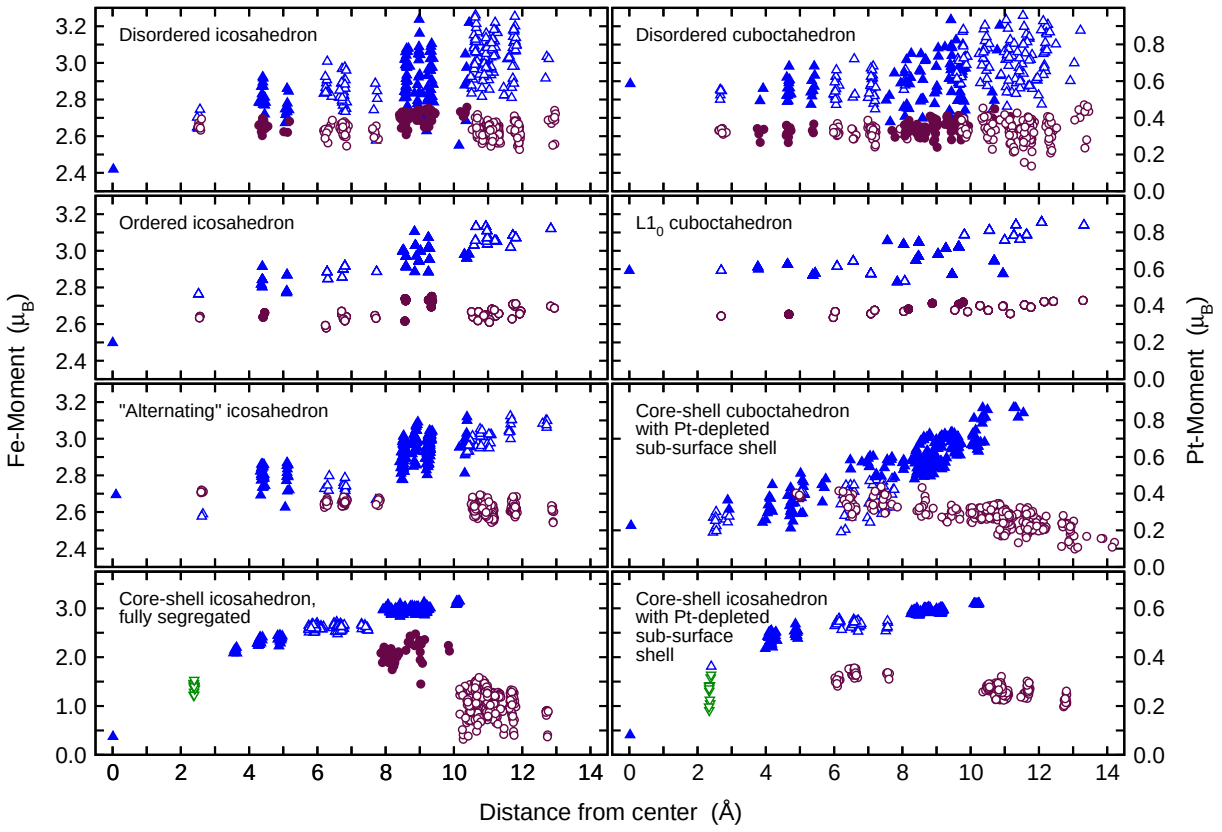

Figure 11: Spatial distributions of the element specific magnetic spin-moments of several $Fe_{265}Pt_{296}$ nanoparticles from Fig. 10. In addition to these, also a core-shell cuboctahedron with Pt-depleted subsurface shell has been considered. Fe-moments are represented by triangles, pointing upwards (blue) for alignment parallel the total magnetization, downwards (green) for antiferromagnetic alignment. Pt-moments are depicted by brown circles. Moments belonging to geometric shells with even index number n are marked by open symbols, atoms belonging to shells with odd n by filled symbols.

even decrease, as for the core-shell morphologies. For the disordered isomers, there are large fluctuations in the Fe- and Pt-moments owing to the inhomogeneous chemical environment of the Fe atoms. This is largely reduced for the ordered structures, as there are many equivalent sites consequently characterized the same magnetic moment and distance from the center. The moment of the central atom is significantly lower in the icosahedral structure, as this position is strongly compressed by the surrounding atoms, which are much closer than in the cuboctahedral structures. This is a consequence of the fact that that the inter-shell atomic distances are by about 5 % smaller than the intrashell distances in ideal icoshaedra, because all of its neigbors are located in the first shell, so that for symmetry reasons there is no possibility for a compensation. This compression is strongest in the case of core-shell isomers which are characterized by a pure iron core with an antiparallel orientation of the first shell. Consequently, the overall diameter of the core-shell icosahedra is about 1-2 % smaller than, e.g., for the disordered isomer.

For some of the isomers, the distribution of the positions in Fig. 11 displays marked deviations from the patterns typical for a given morphology. This applies to the fully segerated $Fe_{265}Pt_{296}$ icosahedron and the core shell cuboctahedron, and is an indication of structural changes. Both

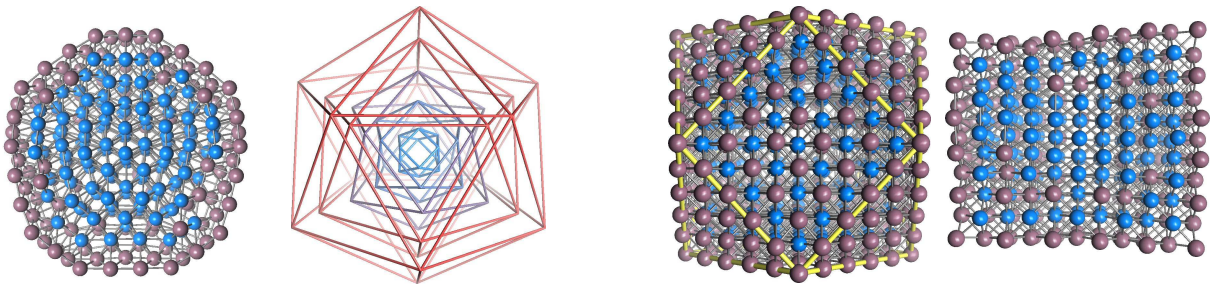

Core−shell icosahedron, fully segregated

Core−shell cuboctahedron with Pt−depleted subsurface shell

Figure 12: Two examples of structural transformations in chemically inhomogeneous clusters. Left: Fully segerated $Fe_{265}Pt_{296}$ icosahedral isomer (cross-section) The edge model obtained in the spirit of Fig. 4 clearly displays a shellwise Mackay-transformation of the pure iron core. Right: Core-shell cuboctahedron with Pt-depleted subsurface shell, full view and cross-section perpendicular to the viewing plane. This isomer is related to the corresponding icosahedral core-shell morphology by a full transformation along the Mackay-path and is represented in Fig. 10 by doubly nested squares. The Fe-core transforms along the Bain-path, inducing a strong tetragonal distortion of the overall cluster shape.

isomers are shown as cross-sections in Fig. 12. While in the first case a shell-wise Mackay-transformation of the iron core is observed as explained in the last section occurs, the cuboctahedral particle undergoes a (partial) transformation along the Bain-path. Common in both cases is that the transforming pure core is comparatively small and the presence of chemically mixed shells is not sufficient to prevent the transformations.

4.1.2 Chemical trends on structural stability

One suitable way to search for particles with improved properties with respect to magnetic recording applications and, at the same time, to learn more about the physical origin for twinning in FePt particles, is by systematically scanning the periodic table of elements for alternatives. A natural choice is to exchange the $3d$ element, iron, against the one to its right in the periodic table, cobalt, as bulk $L1_0$ CoPt is known to exhibit a comparably large magnetocrystalline anisotropy and is thus a reasonable choice as recording material as well. Therefore, the investigation on the size depence of magnetism and structural order has been repeated for Co-Pt in a similar fashion. Systematic replacements of Pt by other $4d$ and $5d$ elements are currently under consideration or will be published elsewhere [149]. Figure 13 summarizes the size dependence of the energetic relationship of CoPt clusters for most of the paradigmatic morphologies studied in the preceding section. The energetic order of the morphologies is practically the same as for the Fe-Pt case but appears on a different scale. Again, the $L1_0$ cuboctahdron of the respective size N serves as reference for the energies. In comparision to Fe-Pt, multiply twinned structures have now moved to considerably lower energies. The onion-type $Co_{265}Pt_{296}$ icosahedron, which corresponds to the lowest energy Fe-Pt isomer, lies 90 meV/atom lower in energy. This corresponds to approximately 1000 K (in comparison to $\approx$ 330 K in the case of Fe-Pt) and can certainly not be considered in the range of thermal energies. Both segeregated morpholgies (completly segregated and with Pt-depleted subsurface shell) are even found be-

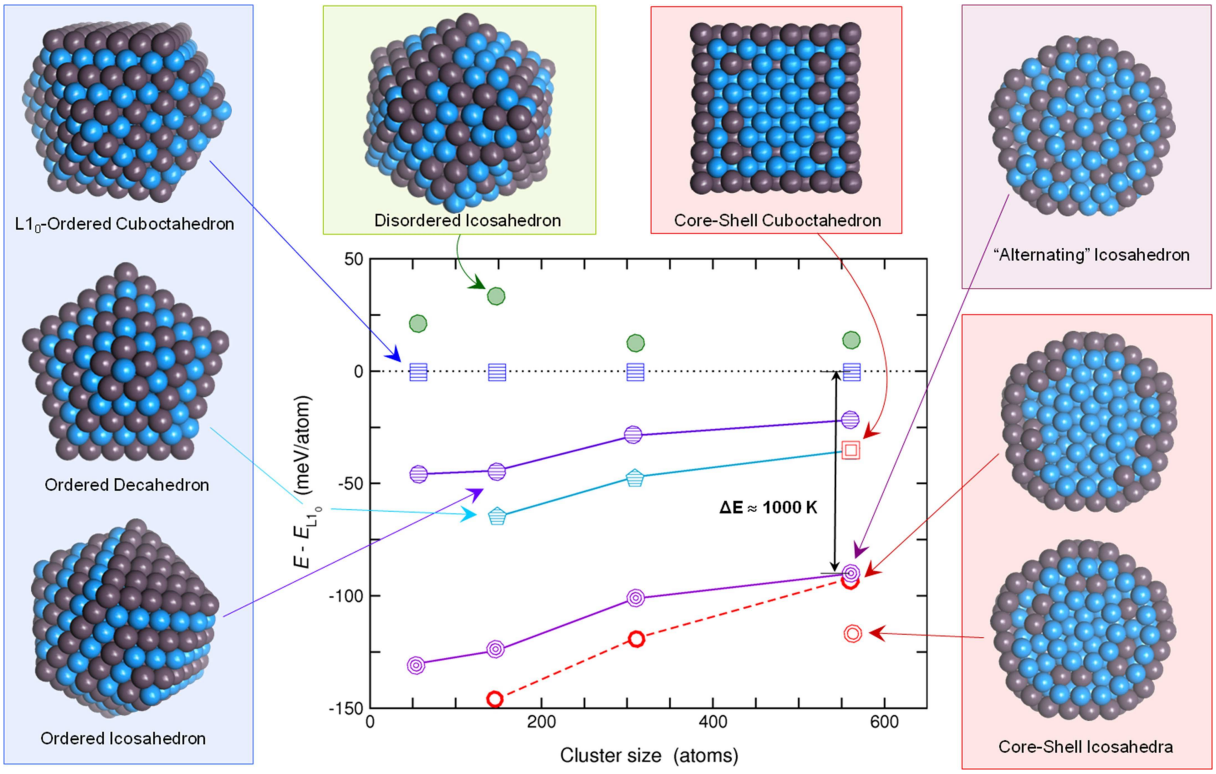

Figure 13: Energies of Co-Pt clusters of various morphologies and sizes. The energy reference is again marked by the $L1_0$ cuboctahedron. Symbols as in Fig. 10.

low. This demonstrates that segregation must be expected to be the dominant mechanism in thermodynamic equilibrium processes. Nevertheless, successfull synthesis of single crystalline $L1_0$ Co-Pt particles with diameters of a few nanometers by embedding them into a carbon environment has been reported recently [150, 151], stressing the importance of kinetic processes and the interaction with the substrate in this case, but the obtained magnetocrystalline anisotropy is again far below the expected values.

A qualitative understanding of the chemical trends on the energetic order of morphologies can be gained from a comparison of the respective element resolved electronic densities of states (DOS) [134, 136], as shown in Fig. 14. The DOS of the $L1_0$ ordered $Fe_{265}Pt_{296}$ isomer shares the basic features of bulk $L1_0$-FePt, which is already the case for much smaller cluster sizes [58]. Hovewer, there are certainly modifications by the surface states, involving still 45% of the atoms at this size. For the *alternating* icosahedron and the $L1_0$-ordered cuoctahedron, the Fermi level coincides with minima in the minority-spin DOS, arising from the minority-spin 3*d*-Fe electrons and is not washed out by the surface 3*d*-Fe states. This underlines the importance of the 3*d* electrons of the transition metal element for the stability of the clusters. Indeed, for each morphology, the Pt surface and core contributions remain largely unaltered upon changing the 3*d* constituent of the clusters. In case of the disordered clusters, the minimum in the minority-spin DOS is completely washed out, reflecting that these clusters have generally much higher energies [136].

In addition, characteristic features owing to the different morphologies can be discovered in the

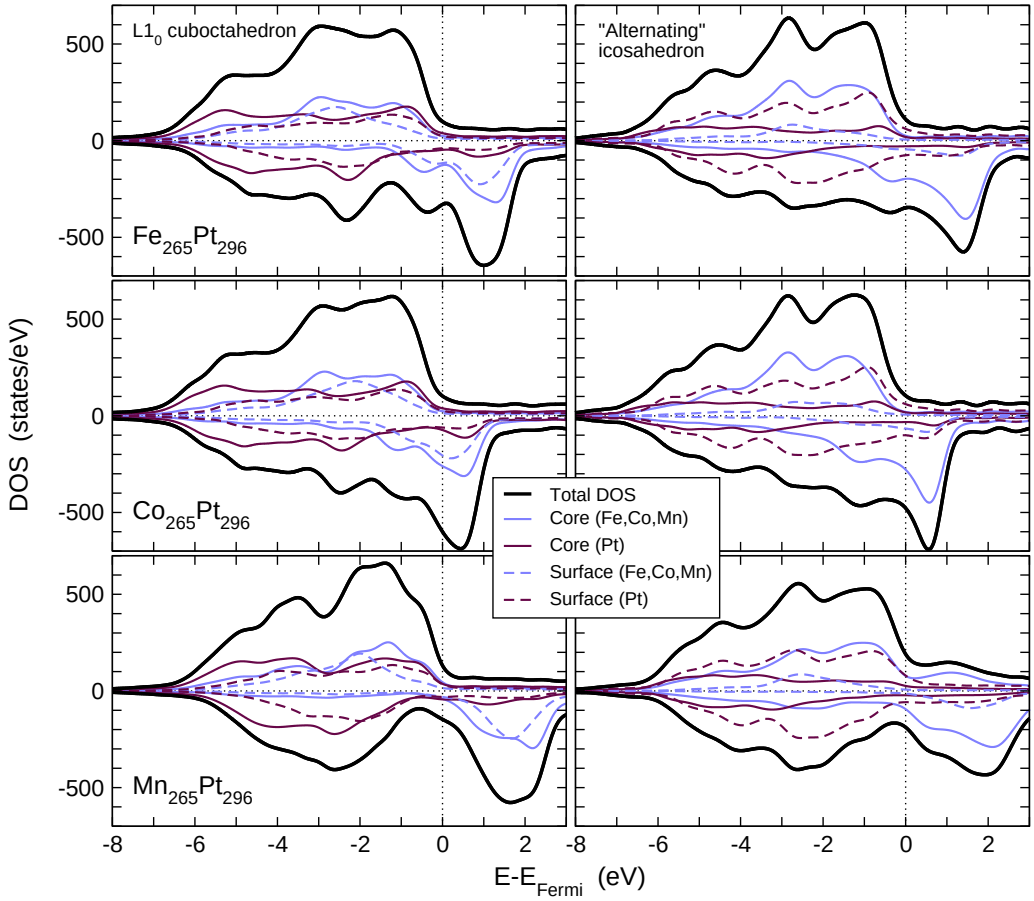

Figure 14: Spin polarized density of states (DOS) of selected $Fe_{265}Pt_{296}$, $Co_{265}Pt_{296}$ and $Mn_{265}Pt_{296}$ morphologies ($L1_0$ ordered cuboctahedron and icosahedron with alternating Fe/Co/Mn and Pt shells) according to Fig. 10 and 13. The thick lines denote the total DOS, the thinner lines the element-specific contributions of the 309 core atoms (full lines, blue for Fe/Co/Mn, brown for Pt). Dashed lines describe the contributions of the 252 surface atoms.

DOS. In the majority channel of the icosahedron there is a dip around $-2.25\,\mathrm{eV}$, surrounded by two maxima, which is only slightly shifted by the replacement of the $3d$ element. This dip nearly coincides with the hump in the minority channel of the $L1_0$ structures arising from the Pt-contributions. Such features could provide a measure to identify or rule out a population of specific morphologies in spectroscopic measurements [152]. As the Pt contribution remains nearly unaffected by changes of the $3d$ element, a discussion of chemical trends in terms of a simple rigind band picture appears justified. When replacing Fe by Co, the additional d-electrons of Co must fill up the states in the minority channel, as the $3d$ majority states are already occupied. This necessarily shifts the contributions of Co to lower energies. While the electron densities at the Fermi level E_F are nearly the same for both isomers, the density of the $L1_0$ minority $3d$-states encounter a steep increase above E_F. In consequence, there is a larger shift of the $3d$ minority states of the icosahedron, which results in a lower contribution to the band energy with respect to the $L1_0$ reference.

This simple relationship between the stability of the icosahedra with respect to the $L1_0$ and the filling of the $3d$ minority channel suggests that removing $3d$ minority spin electrons might work

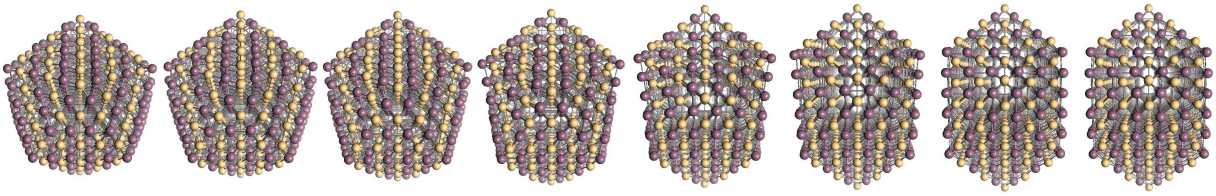

Figure 15: Snapshots of an MnPt cluster transforming from the ordered icosahedral structure (leftmost) to the $L1_0$ ordered cuboctahedron (right) during the conjugate gradient structure optimization. The snapshots were taken consecutively every 100 optimization steps.

in favor of the $L1_0$ structure. This seems in fact to be the case, if Fe is completely replaced by Mn. Here, the alternating icosahedron is located approximately 60 meV/atom above the 561 atom $L1_0$ cuboctahedron (as compared to ≈ 30 meV/atom below for FePt). The ferromagnetic, ordered icosahedron, which is nearly degenerate for $Fe_{265}Pt_{296}$, has become unstable in the Mn-Pt system. During the geometric optimization procedure it transforms downhill to a perfect $L1_0$ cuboctahedron proving that the Mackay path is a realistic transformation path for magic-number transition metal systems (Figure 15). Nevertheless, the simple rigid band picture does not hold quite as nicely as for the replacement of Fe by Co. For the alternating icosahedron, e.g., antiferromagnetic alignment of parts of the Mn spins could not be avoided, leading to contributions in the majority channel above the Fermi level and in the minority channel below, which alter the overall shape of the total DOS.

The drawback for using Mn as stabilizing agent for $L1_0$ particles for magnetic recording purposes is its preference for antiferromagnetic ordering, which is well known for the bulk system and also present in nanoparticles. The lowest energy isomer found so far, is an $L1_0$ cuboctahedron with staggered antiferromagnetic arrangement of the spins within the Mn layers. In order not to elicit the latent antiferromagnetic tendencies which are present in pure Fe-Pt as discussed above, only small admixtures of Mn can therefore be admissible.

5 Magnetic shape memory alloys – a new class of magnetomechanical actuators

Functional magnetic materials in a more conservative sense of the definition are materials where changes in magnetism – e.g., induced by an external magnetic field – directly relate to changes in other properties of interest, such as spatial extension or *vice versa*. One good example in this respect are magnetic shape memory (MSM) alloys, which transform martensitically below the Curie temperature in the ferromagnetic (FM) state. They represent a new class of actuators, which allow for giant magnetic field induced strains (MFIS) of up to about 10% in Ni_2MnGa [9, 153, 154]. These strains are associated with the super-elastic motion of twin boundaries in the modulated martensitic phase. In prototype Ni_2MnGa, the martensitic phase is stable below about 274 K, but the transformation temperature can be shifted above room temperature by changing stoichiometry. Depending on temperature and composition, Ni-Mn-Ga exhibits a variety of martensitic phases, each with different relevance to the MSM effect (e.g., [155–157]). Another important aspect, common to most MSM materials, is their compa-

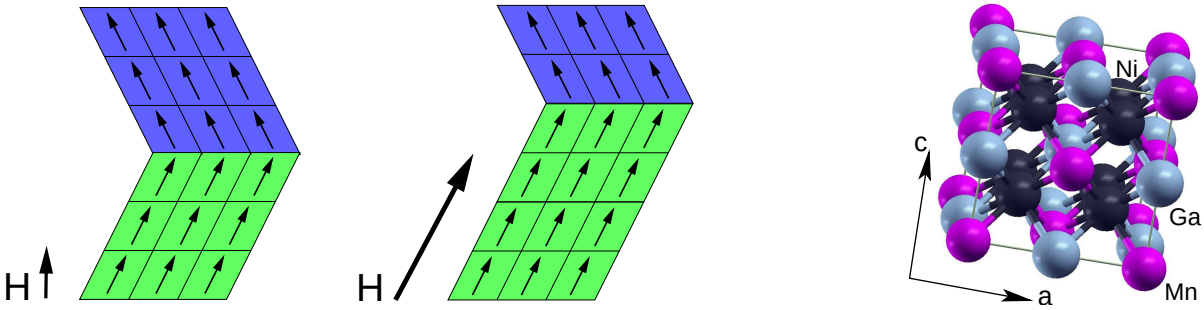

Figure 16: Left: Schematic visualization of the magnetic shape memory effect (magnetic field induced reorientation). Applying a magnetic field favors the martensitic twins with their easy axis parallel to that direction, causing a magnetic field induces strain (MFIS). Right: $L2_1$ Heusler structure of austenitic Ni_2MnGa (black spherse for Ni, purple for Mn, blue for Ga). Depending on temperature and stoichiometry, tetragonal martensitic phases exist with $c/a \approx 1.2$ as well as commensurate and incommensurate modulated phases with $c/a = 0.9 \ldots 0.94$.

rably large magnetocrystalline anisotropy in the martensitic phases (e.g., [158]). Together with the low activation energy for twin boundary motion, this is considered a key ingredient for the reversible growth of one martensitic variant on the expense of another in MSM alloys, which leads to the reported large strains. This MSM mechanism is usually referred to as *magnetic field induced reorientation* (MIR). There is another mechanism called *magnetic field induced martensite* (MIM), which can occur when martensitic and magnetic phase boundaries are coupled (for an introduction, see [159]). Such transitions do not necessarily require large uniaxial magnetocrystalline anisotropies and a high mobility of twin boundaries, but rather a martensitic transition temperature in the desired operation range and a large change in magnetization between both phases. In this case, the introduction of a sufficiently strong magnetic field can shift the martensitic transition temperatures and thus reversibly induce a martensitic transition. This effect was observed in polycrystalline Ni-Mn-In with a MFIS comparable to other polycrystalline MSM alloys [160, 161].

The development of novel sensor and actuator systems based on the MSM effect currently concentrates on two classes of materials: The archetypical Ni-based full-Heusler alloys and Fe-Pd based alloys [162] close to the bcc-fcc martensitic transformation. Although the Heusler systems are currently the best studied MSM-materials, several problems are to be solved before they can be used in large scale for industrial grade applications. First, the martensitic and magnetic transition temperatures are, although above room temperature in many cases, still too low for many fields of application, e.g., in the automotive sector. Furthermore, the material is very brittle and thus difficult to handle. For large strains, single crystals are needed, which are difficult and expensive to produce. The Fe-based systems have far better mechanical properties, the biocompatibility of Fe and Pd entitles them for applications within the human body. The Curie-temperatures are sufficiently large. However, the required reversible martensitic transition from the austenitic face centered cubic (fcc) to the intermediate martensitic face centered tetragonal (fct) phase, which is relevant for the MSM effect, takes place at even lower temperature than in the Ni-Mn-Ga system [163]. Fe-based MSM systems known so far are based on disordered $Fe_{70}Pd_{30}$ alloys, ordered Fe_3Pt and also Fe-Ni-Co alloys with an addition of a few at-% Ti [164].

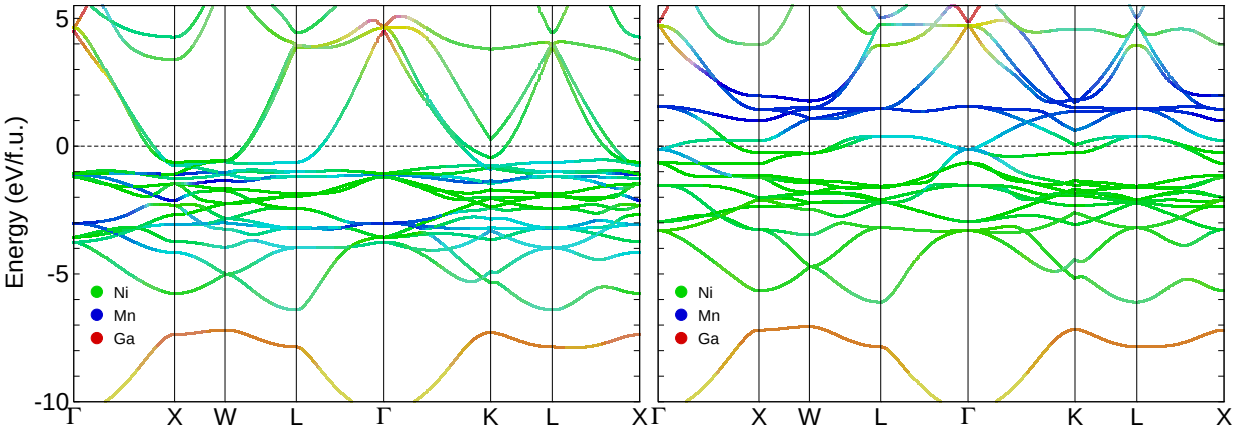

Figure 17: Element resolved band structure of Ni_2MnGa for the minority and the majority spin channel. The color coding refers to the contribution of the specified elements. Mixed contributions are marked by intermediate colors.

However, the considerable MFIS observed in the former two, 3.0 % for Fe-Pd and 2.3% For Fe_3Pt, are reported for low temperatures of 77 K and 4 K, respectively [165–167]. At higher temperatures, approaching the austenitic phase, the MFIS is decreasing as does also the c/a ratio, which determines the upper limit of the achievable strain. Electronic structure calculations [168–170] suggest that a band-Jahn-Teller mechanism is responsible for the transition from the fcc to the fct phase which is mandatory for the MSM effect. A similar mechanism is made responsible for the martensitic transition in Heusler-based shape memory alloys [171].

Many essential properties of MSM alloys have been successfully characterized up to now (for a review of previous experimental and theoretical work, see [1, 8–10]). However, one of the central questions, that remains unanswered up to now and is thus central part of our research, is about the origin of the high mobility of the twin boundaries and how a magnetic field allows to introduce large magnetic strains in MIR. Other important questions tackle the applicability of the materials, e.g., the shifting of the transition temperatures of the magnetic and structural phase transitions into the desired range or the optimization of the actuator properties in sub-Tesla magnetic fields. Within this review, we will concentrate on two aspects of the Ni-Mn-Ga system, namely the relationship between magnetism and phase stability and the influence of changes in stoichiometry on the mobility of twin boundaries.

5.1 Magnetism and phase stability in MSM Heusler alloys

The complex relationship between the austenitic and the various martensitic phases, which are present in MSM Heusler alloys, has been subject to numerous theoretical [10, 172–188] and experimental studies. A large fraction of the latter are related to the temperature dependent anomalies in the austenitic phonon dispersions when approaching the (pre-)martensitic transition temperature. This shows up as a temperature depending (incomplete) softening of TA_2 branch in [110] direction at a fraction of $\xi \approx 1/3$ of the way between the Γ- and the X-point of the Brillouin zone [189–194]. The instability of the TA_2 branch has been related to nesting features of the Fermi-surface in the austenitic phase in literature (see, e.g., [176, 177, 188, 195]) and has

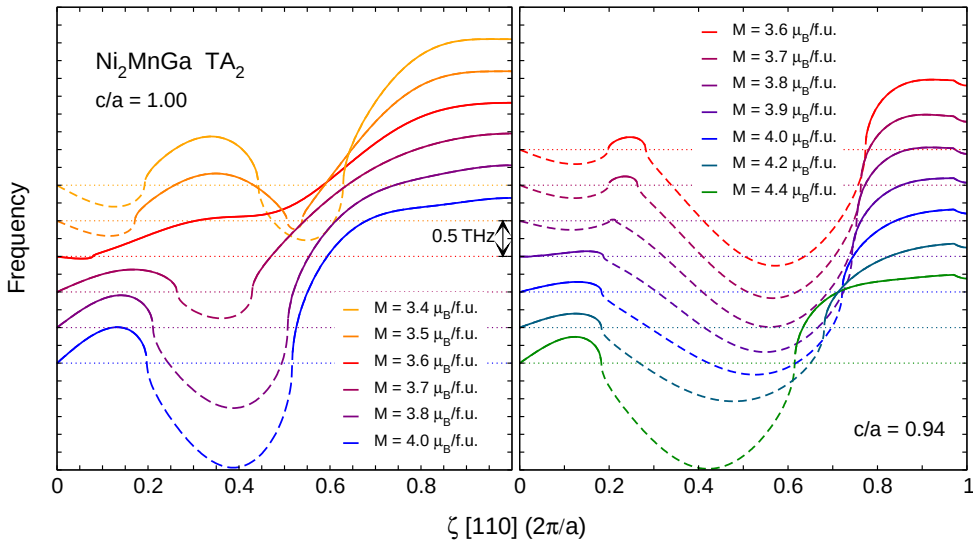

Figure 18: TA_2 branch of the phonon dispersion curves of cubic $L2_1$ (left) and unmodulated tetragonal Ni_2MnGa with c/a=0.94 (right) calculated along the [110]-direction for different fixed magnetic moments. To improve visibility, the individual branches are shifted in energy, instable parts (imaginary frequencies) are denoted by broken lines. For the $L2_1$ case, the branches for 3.6 μ_B/f.u. are nearly stable. The equilibrium moment is 4.06 μ_B per formula unit.

been reproduced by DFT calculations [177,181]. However, the softening here is complete, i.e., it leads to imaginary frequencies, which is not surprizing as the calculations refer to $T = 0$, where the cubic $L2_1$ structure of the austenitic phase is in fact unstable.

One central aspect of our work on Heusler alloys is to understand the relation between magnetism and the complex sequence of phases as a function of temperature. Such a relation has been first proposed by Lee *et al.* [176]. Later on, the energy landscape and the phonon spectra were evaluated for different magnetizations by using the fixed spin moment method [196]. These calculations highlight the importance of magnetic order as a stabilizing feature of the austenitic phase [183]. Consequently, we also examined the system at smaller values than the equilibrium moment of Ni_2MnGa [185]. This can be justified by a closer look at the spin and element resolved band structure of Ni_2MnGa (Fig. 17). Gallium states are present only several eV below and above the Fermi-level and are important to stabilize the Heusler-type structure. Manganese contributions are mainly found below the Fermi level (in the majority channel) or above (in the minority channel). Except for a small portion around the Γ-point, the Fermi surface is dominated by Ni-states in both, minority- and majority-spin channels. Subtle changes of the exchange-splitting can now have decisive effects on the Fermi surface. This can be easily modelled in a Stoner-like approach focusing on the description on the magnetism of the Ni-atoms. The Ni-atoms do not develop a stable magnetic moment on their own, as the coordination of the Ni-atoms in austenitic $L2_1$ Ni_2MnGa is rather body centered cubic than face centered cubic. The observed Ni-Moments are induced by the surrounding Mn atoms and these exhibit a stable, rather localized moment, which has been shown in detail by non-collinear spin-spiral calculations [197]. The Mn states, on the other hand, which are represented less well by this approach, are not expected to take part in the instabilities leading to the reconstruction of the Fermi-surface.

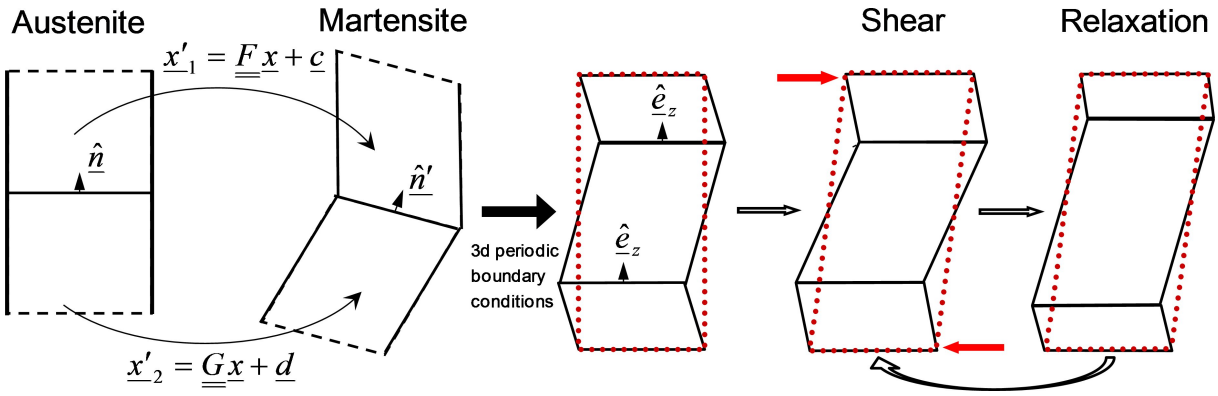

Figure 19: Schematic sketch visualizing the construction of an atomistic twin-boundary model for the martensitich phase, which is compatible with three-dimensional periodic boundary conditions, and the simulation of twin boundary movement by repeated shearing of the cell and relaxiation of the atomic positions as performed in our calculations.

For the resulting phonon dispersions, we found in the austenitic phase a narrow region around $3.6\,\mu_B$/f.u., in which the instability at finite $\xi \approx 0.4$ disappears (Fig. 18). This is only 10 % below and thus in realistic vicinity of the ground state magnetization of $4.06\,\mu_B$/f.u. and corresponds to a region of the binding surface, where the $L2_1$ and the $L1_0$ are close in energy, separated only by a tiny energy wall [185]. In the unmodulated tetragonal structures with $c/a = 0.94$, the instability at finite ξ is present for all magnetizations, but varies its position. This is in accordance with the observation that the pseudo-tetragonal martensite with $c/a = 0.94$ is only stable because of magnetism and modulations in the atomic positions [178, 180, 186] – in contrast to the martensitc $L1_0$ structure with $c/a \approx 1.25$, which is found stable at very low temperatures or off-stoichiometric compositions. All of these results demonstrate the extremely closely interrelation of electronic structure, magnetism and phase stability in the MSM Heusler systems.

5.2 Twin boundary mobility in magnetic shape memory alloys

The natural approach to look at finite temperature properties, which is also well suited to provide insight into the origin of the high mobility of twin boundaries on the atomistic level, would be, again, classical molecular dynamics simulations. These allow to deal with a sufficiently large number of atoms, but depend on the availability of reliable empirical model potentials. For the case of MSM alloys, up to now, either the Heusler-type or the Fe-based systems, suitable model potentials still do not exist and their development is a very delicate task, since the martensitic instability is closely related to the details of the electronic structure as shown above. Therefore, it remains necessary to perform *ab initio* molecular dynamics simulations to look at the materials properties at the atomic scale. Within this context, in a first step, the mathematical framework for simulating shear induced twin boundary mobility was set up making use of the continuum theory of martensitic transformations [198] and performing first *ab initio* simulations of comparatively small systems (256 atoms) [184] for the non-MSM relevant $L1_0$ phase as a test case. These calculations have meanwhile been extended to larger and non-stoichiometric systems.

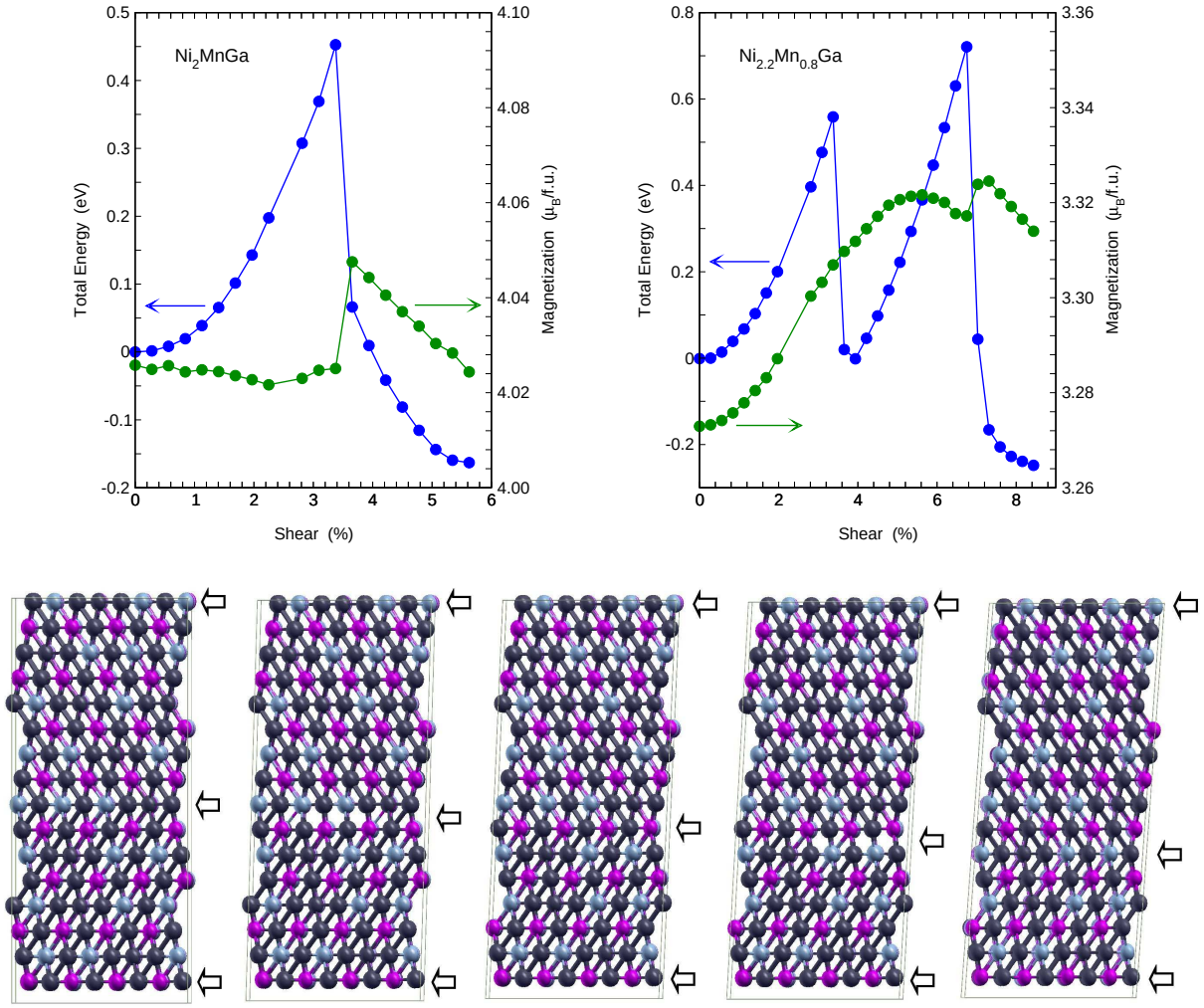

Figure 20: Total energy and magnetic moment are given as a function of the shear of the simulation cell for each completed quasistatic relaxation step for stoichiometric Ni_2MnGa (left) and off-stoichiometric $Ni_{2.2}Mn_{0.8}Ga$ (right). Bottom: Selected configurations (energy minima and transition states) of the 512 atom $Ni_{2.2}Mn_{0.8}Ga$ super-cell resulting from the geometric optimization processes after applying shear on the simulation box (in horizontal direction). The arrows denote the position of the twin boundaries. Same colors as in Fig. 16.

As the material undergoes a martensitic transformation from a high-symmetry parent phase at higher temperatures to a low-symmetry low-temperature phase, so-called twinning will occur. This is due to the different spatial possibilities in which the low symmetry phase can nucleate from the parent phase at the spatially separated seeds for the martensitic transformation. Following the continuum theory of martensitic transformations [198–200]), the transition can be described by a simple homogeneous transformation, characterized by a matrix $\underline{\underline{F}}$ and a vector $\underline{c}$ and, possibly, by an additional shuffle. The martensitic twins are in general represented by different homogeneous transformations, typically connected by symmetry operations, e.g., a rotation which is part of the point group of the parent phase but not of martensite. This information can be used to construct a model of a martensitic twin boundary suitable for atomistic simulations as depicted in Fig. 19 (left). Compatibility with the periodic boundary conditions can be achieved by rotating the system so that the twinning plane given by $\hat{\underline{n}}$ is parallel to one of boundary planes of the simulation cell. The periodic boundary conditions also imply that

there are at least two twin boundaries in the simulation cell. For the transformation to the $L1_0$ structure, the transformation matrix can be chosen in analogy to the Bain path as a (volume conserving) diagonal matrix with one of the diagonal elements different from the other two. For the transformation to the pseudo-tetragonal structure with $c/a < 1$, we follow the experimental findings from neutron diffraction data that two consecutive shears on (110) planes in the $[\bar{1}10]$ directions are involved [201]. As the direct *ab initio* simulation of twin boundary motion induced by a directional change of magnetic field including spin-orbit interactions is exceeding the current possibilities, we induce twin-boundary motion by applying shear on the simulation cell. The induced stress will be resolved in a subsequent relaxation step, as sketched in Fig. 19 (right), possibly leading to the introduction of defects or a shift of the twining plane. Then, in a number of consecutive shear and relaxation steps, a quasi-static picture of twin boundary motion can be achieved.

Fig. 20 shows the result of such a procedure applied to stoichiometric Ni_2MnGa and off-stoichiometric $Ni_{2.2}Mn_{0.8}Ga$. Here, a super-cell containing 512 atoms and two martensitic variants were used, the latter with a width of four unit cells each. Due to the periodic boundary condition in all three dimensions, two interfaces are contained in this system. The magnetization shows – unlike in previous simulations with 256 atoms [184] – only a small variation before and after the shifting process, indicating that finite size effects are considerably decreased and cells of 512 atoms may be sufficient to study the shear induced coherent motion process of the twin boundary. The activation energy in Fig. 20 is of the same magnitude as in the smaller case, being of one order larger than the MAE per atom multiplied with the system size [158, 184]. Disorder does apparently not change the energy scale. However, in the stoichiometric case, both twin boundaries move at the same time, while in the off-stoichiometric case, the same twin boundary (in the center) moves in two consecutive steps, while the other (at the cell boundary) remains immobile. The observed energy scale is in accordance with experimental observations and energetic considerations by Kakeshita *et al.* [167, 202, 203] of $Ni_{2.14}Mn_{0.92}Ga_{0.94}$ in the $L1_0$ phase with $c/a \approx 1.20$ and corroborates our previous finding, that despite of its considerably larger magnetocrystalline anisotropy for the $L1_0$ phase with the large c/a ratio, a magnetic field induced (coherent) rearrangement of twins is not a realistic process for this phase. It has to be noted at this point, that the current understanding is that interface defects like disconnections play a decisive role for the motion of realistic interfaces between phases and twins (see [204, 205] for recent reviews). Corresponding simulations require very large cells, containing more than 10 000 atoms and are currently only feasible on the basis of classical molecular dynamics simulations. As discussed above, it is unclear whether accurate empirical potentials can be developed soon. Thus, for now, only first-principles calculations can bring forward the understanding of the atomistic processes at the interface and might serve as helpful benchmarks in future.

While these results are encouraging in the sense that *ab initio* simulations of twin boundary mobility is possible, they also show that it is essential to explicitely consider the modulated phases, as attempts to approximate these by an unmodulated pseudo-tetragonal structure lead to a complete dissolution of the interfaces. This is certainly related to the instable phonon dispersions shown in Fig. 18 and demonstrates that these processes are taking place on a fairly small energy scale. The consideration of the rather large modulated unit cells and the required increase in numerical accuracy will boost the numerical demands, showing, once again, the importance of

state-of-the-art high-performance computing for practical materials science applications.

6 Conclusions

Within this contribution it is demonstrated in three examples, that first-principles investigations of the interplay between structural and magnetic properties on the nano-scale, covering systems with up to 923 (and, possibly, in future also 1415) spin-polarized transition metal atoms are feasible on current state-of-the-art supercomputers and how these calculations contribute to the understanding of key-properties of functional magnetic materials of technological interest:

- Iron clusters from around $N \approx 100$ atoms upwards have a bcc structure in the ground state. Icosahedra and cuboctahedra are instable against a partial transformation along the Mackay-path. For $N = 55$, a shell-wise Mackay-transformed structure is a good candidate for the ground state, and lies within the range of thermal energies for larger sizes. While retaining an icosahedral outer shape, this structure is characterized by a fcc-like coordination of the cluster core and bcc-like coordination of the sub-surface atoms; the corresponding pair distribution function exhibits typical features of amorphous systems. Due to the ferrimagnetic alignment of the spins in the core, the magnetic moment of this morphology is for $N = 561$ in much better agreement with the experimental data than the bcc isomers.

- For magic number Fe-Pt and Co-Pt nanoclusters, which are of technological interest for ultra-high density magnetic recording applications in their single crystalline $L1_0$ phase, multiply twinned morphologies are energetically favored up to diameters of at least 3 nm. The lowest energy morphology found for Fe-Pt is an onion-type structure with alternating Fe- and Pt-rich shells and a Pt-covered surface. For Co-Pt, segregated icosahedral morphologies are even more favored, exceeding the range of thermal energies with respect to the $L1_0$ reference structure. A comparison of the electronic densities of states suggests that the tendency to form multiply twinned morphologies can be controlled by the filling of the $3d$ minority spin channel. Consequnetly, multiply twinned morphologies are found suppressed in the case of Mn-Pt nano-clusters. Here, a staggered antiferromagnetic $L1_0$ structure is found to be lowest in energy.

- To address the mobility of twin interfaces in Ni_2MnGa shape memory alloys in its various phases, we proposed a simulation scheme, which allows us to get microscopic insight into a stress induced martensitic reorientation process in Ni_2MnGa by means of *ab initio* molecular statics calculations. Relating the results of the quasistatic simulations of shear-induced twin boundary motion in the $L1_0$ phase with $c/a \approx 1.25$ to previous calculations of the magnetocrystalline anisotropy energy, we see, that the energy scales encountered in the coherent reorientation processes of twins and magnetization are not of the same order of magnitude. So far, the simulations are restricted to – still – comparatively small system sizes and defect-free interfaces. Also the experimentally observed modulation in the pseudo-tetragonal and orthorhombic phases with $c/a < 1$, which are the relevant ones for the MSM effect, should be taken into account. All of these amendments are connected with increased numerical demands and still left open for future investigations.

Despite all the benefits which can be expected from the applications point of view, it should be acknowledged that the developers of the DFT packages on the other hand are confronted with the Sisyphean challenge to constantly adapt their codes in order to keep their parallel performance at pace with an exponential development of computing resources. However, regarding the perspectives for the field of materials science, this might be worth the effort. There is plenty of room at the TOP500.

Acknowledgements

The vast majority of the calculations has been performed on the IBM Blue Gene/L and Blue Gene/P supercomputers of the John von Neumann Institute for Computing (NIC) in Jülich. Without the access to these resources, the work presented above certainly would not have been possible. We thank the staff of the Jülich Supercomputing Center (JSC) and IBM for their continuous support, especially P. Vezolle (IBM) and I. Gutheil (JSC) for their substantial help in making the VASP code run efficiently on the Blue Gene systems. This work also depends on many stimulating discussions and helpful comments. In this respect we would like to gratefully acknowledge the contributions of G. Rollmann, A. Hucht, R. Meyer, J. R. Chelikowsky and M. L. Tiago (iron nanoparticles), M. Farle, O. Dmitrieva, D. Sudfeld, N. Friedenberger, C. Antoniak, M. Spasova, K. Albe and U. Wiedwald (binary particles for ultra-high density magnetic recording), A. T. Zayak, W. A. Adeagbo, U. K. Rößler, I. Opahle, M. Richter, R. C. Pond, S. Fähler, M. Acet and E. F. Wassermann (magnetic shape memory Heusler alloys). Financial support was granted by the Deutsche Forschungsgemeinschaft through the Priority Programme SPP 1239, *Change of microstructure and shape of solid materials by external magnetic fields* and SFB 445, *Nanoparticles from the Gasphase: Formation, Structure, Properties*.

References

[1] A. Planes, L. Mañosa and A. Saxena, eds., *Magnetism and Structure in Functional Materials*, vol. 79 of *Springer Series in Materials Science*, Springer, Berlin, Heidelberg, New York 2005.

[2] Q. A. Pankhurst, J. Conolly, S. K. Jones and J. Dobson, *Application of magnetic nanoparticles in biomedicine*, J. Phys. D: Appl. Phys. **36**, R167 (2003).

[3] P. Tartaj, M. del Puerto Morales, S. Veintemillas-Verdaguer, T. Gonzáles-Carreño and C. J. Serna, *The preparation of magnetic nanoparticles for application in biomedicine*, J. Phys. D: Appl. Phys **36**, R182 (2003).

[4] I. Šafařík and M. Šafaříková, *Magnetic nanoparticles and biosciences*, Monatshefte für Chemie **737**, 133 (2002).

[5] S. Sun, C. B. Murray, D. Weller, L. Folks and A. Moser, *Monodisperse FePt nanoparticles and ferromagnetic* FePt *nanocrystal superlattices*, Science **287**, 1989 (2000).

[6] S. Sun, *Recent advances in chemical synthesis, self-assembly, and applications of* FePt *Nanoparticles*, Adv. Mater. **18**, 393 (2006).

[7] D. Weller and A. Moser, *Thermal effect limits in ultrahigh-density magnetic recording*, IEEE Trans. Magn. **35**, 4423 (1999).

[8] A. N. Vasil'ev, V. D. Buchel'nikov, T. Takagi, V. V. Khovailo and E. I. Estrin, *Shape memory ferromagnets*, Physics Uspekhi **46**, 559 (2003).

[9] O. Söderberg, Y. Ge, A. Szinov, S.-P. Hannula and V. V. Lindroos, *Recent breakthrough development of the shape memory effect in* Ni-Mn-Ga *alloys*, Smart Mater. Struct. **14**, 223 (2005).

[10] P. Entel, V. D. Buchelnikov, V. V. Khovailo, A. T. Zayak, W. A. Adeagbo, M. E. Gruner, H. C. Herper and E. F. Wassermann, *Modelling the phase diagram of magnetic shape memory Heusler alloys*, J. Phys. D: Appl. Phys. **39**, 865 (2006).

[11] G. M. Pastor, J. Dorantes-Dávila and K. H. Bennemann, *Size and structural dependence of the magnetic properties of small* 3*d-transition-metal clusters*, Phys. Rev. B **40**, 7642 (1989).

[12] A. N. Andriotis and M. Menon, *Tight-binding molecular-dynamics study of ferromagnetic clusters*, Phys. Rev. B **57**, 10069 (1998).

[13] C. Barreteau, M. Desjonquieres and D. Spanjaard, *Theoretical study of the icosahedral to cuboctahedral structural transition in* Rh *and* Pd *clusters*, Eur. Phys. J. D **11**, 395 (2000).

[14] R. A. Guirado-López, J. Dorantes-Dávila and G. M. Pastor, *Orbital magnetism in transition-metal clusters: From Hund's rule to bulk quenching*, Phys. Rev. Lett. **90**, 226402 (2003).

[15] Y. Xie and J. A. Blackman, *Universal tight-binding model for transition metals: From bulk to cluster*, J. Phys. Condens. Matter **16**, 8589 (2004).

[16] C. Köhler, G. Seifert and T. Frauenheim, *Magnetism and the potential energy hypersurfaces of* Fe_{53} *to* Fe_{57}, Comp. Mat. Sci. **35**, 297 (2006).

[17] S. L. Dudarev and P. M. Derlet, *A 'magnetic' interatomic potential for molecular dynamics simulations*, J. Phys. Condens. Matter **17**, 7097 (2005).

[18] P.-W. Ma, C. H. Woo and S. L. Dudarev, *Large-scale simulation of the spin-lattice dynamics in ferromagnetic iron*, Physical Review B - Condensed Matter and Materials Physics **78**, 024434 (2008).

[19] S. Goedecker, *Linear scaling electronic structure methods*, Rev. Mod. Phys. **71**, 1085 (1999).

[20] J. M. Soler, E. Artacho, J. D. Gale, A. Garciá, J. Junquera, P. Ordejón and D. Sánchez-Portal, *The SIESTA method for ab initio order-N materials simulation*, J. Phys. Cond. Matter **14**, 2745 (2002).

[21] D. R. Bowler, R. Choudhury, M. J. Gillan and T. Miyazaki, *Recent progress with large-scale ab initio calculations: The CONQUEST code*, phys. stat. sol. (b) **243**, 989 (2006).

[22] R. Zeller, *Towards a linear-scaling algorithm for electronic structure calculations with the tight-binding Korringa-Kohn-Rostoker Green function method*, J. Phys. Cond. Matter **20**, 294215 (2008).

[23] M. E. Gruner, G. Rollmann and P. Entel, *Large-scale first-principles calculations of magnetic nanoparticles*, in *Proceedings of the NIC Symposion 2008*, edited by G. Münster, D. Wolf and M. Kremer, vol. 39 of *NIC Series*, p. 161, Jülich 2008.

[24] http://www.top500.org.

[25] F. Viñes, F. Illas and K. M. Neyman, *On the mechanism of formation of metal nanowires by self-assembly*, Angew. Chem. Int. Ed. **46**, 7094 (2007).

[26] J. Akola and R. O. Jones, *Structural phase transitions on the nanoscale: The crucial pattern in the phase-change materials* $Ge_2Sb_2Te_5$ *and* GeTe, Phys. Rev. B **76**, 235201 (2007).

[27] J. Akola and R. O. Jones, *Binary alloys of* Ge *and* Te*: Order, voids, and the eutectic composition*, Phys. Rev. Lett. **100**, 205502 (2008).

[28] F. Gygi, E. W. Draeger, M. Schulz, B. R. de Supinski, J. A. Gunnels, V. Austel, J. C. Sexton, F. Franchetti, S. Kral, C. W. Ueberhuber and J. Lorenz, *Large-Scale electronic strucutre calculation of high-Z metals on the BlueGene/L Platform*, in *Proceedings of the ACM/IEEE Conference on Supercomputing, Tampa, FL* 2006.

[29] F. Gygi, *Architecture of Qbox: A scalable first-principles molecular dynamics code*, IBM J. Res. & Dev. **52**, 137 (2008).

[30] R. Laskowski, P. Blaha, T. Gallauner and K. Schwarz, *Single-layer model of the hexagonal boron nitride nanomesh on the* Rh(111) *surface*, Phys. Rev. Lett. **98**, 106802 (2007).

[31] R. Laskowski and P. Blaha, *Unraveling the structure of the* h-BN/Rh(111) *nanomesh with ab initio calculations*, J. Phys.: Condens. Matter. **20**, 064207 (2008).

[32] P. Hohenberg and W. Kohn, *Inhomogeneous electron gas*, Phys. Rev. **136**, B864 (1964).

[33] G. Kresse and J. Furthmüller, *Efficient iterative schemes for ab initio total-energy calculations using a plane-wave basis set*, Phys. Rev. B **54**, 11169 (1996).

[34] G. Kresse and D. Joubert, *From ultrasoft pseudopotentials to the projector augmented-wave method*, Phys. Rev. B **59**, 1758 (1999).

[35] J. Hafner, *Ab-initio simulations of materials using VASP: Density-functional theory and beyond*, Journal of Computational Chemistry **29**, 2044 (2008).

[36] J. P. Perdew, in *Electronic Structure of Solids '91*, edited by P. Ziesche and H. Eschrig, Akademie Verlag, Berlin 1991.

[37] J. P. Perdew, K. Burke and Y. Wang, *Generalized gradient approximation for the exchange-correlation hole of a many-electron system*, Phys. Rev. B **54**, 16533 (1996).

[38] S. H. Vosko, L. Wilk and M. Nusair, *Accurate spin-dependent electron liquid correlation energies for local spin density calculations: A critical analysis*, Can. J. Phys. **58**, 1200 (1980).

[39] K. Parlinski, Z. Q. Li and Y. Kawazoe, *First-principles determination of the soft mode in cubic* ZrO_2, Phys. Rev. Lett. **78**, 4063 (1997).

[40] J. P. Perdew, K. Burke and M. Ernzerhoff, *Generalized gradient approximation made simple*, Phys. Rev. Lett. **77**, 3865 (1996).

[41] A. Gara, M. A. Blumrich, D. Chen, G. L.-T. Chiu, P. Coteus, M. E. Giampapa, R. A. Haring, P. Heidelberger, D. Hoenicke, G. V. Kopcsay, T. A. Liebsch, M. Ohmacht, B. D. Steinmacher-Burow, T. Takken and P. Vranas, *Overview of the Blue Gene/L system architecture*, IBM J. Res. & Dev. **49**, 195 (2005).

[42] J. A. Alonso, *Electronic and atomic structure, and magnetism of transition metal clusters*, Chem. Rev. **100**, 637 (2000).

[43] F. Baletto and R. Ferrando, *Structural properties of nanoclusters: Energetic, thermodynamic, and kinetic effects*, Rev. Mod. Phys. **77**, 371 (2005).

[44] J. Bansmann, S. H. Baker, C. Binns, J. A. Blackman, J.-P. Bucher, J. Dorantes-Dávila, V. Dupuis, L. Favre, D. Kechrakos, A. Kleibert, K.-H. Meiwes-Broer, G. M. Pastor, A. Perez, O. Toulemonde, K. N. Trohidou, J. Tuaillon and J. Xie, *Magnetic and structural properties of isolated and assembled clusters*, Surf. Sci. Rep. **56**, 189 (2005).

[45] C. Binns, K. N. Trohidou, J. Bansmann, S. H. Baker, J. A. Blackman, J.-P. Bucher, D. Kechrakos, A. Kleibert, S. Louch, K.-H. Meiwes-Broer, G. M. Pastor, A. Perez and Y. Xie, *The behaviour of nanostructured magnetic materials produced by depositing gas-phase nanoparticles*, J. Phys. D: Appl. Phys. **38**, R357 (2005).

[46] I. M. L. Billas, J. A. Becker, A. Châtelain and W. A. de Heer, *Magnetic moments of iron clusters with 25 to 700 atoms and their dependence on temperature*, Phys. Rev. Lett. **71**, 4067 (1993).

[47] I. M. L. Billas, A. Châtelain and W. A. de Heer, *Magnetism from the atom to the bulk in iron, cobalt, and nickel clusters*, Science **265**, 1682 (1994).

[48] I. M. L. Billas, A. Châtelain and W. A. de Heer, *Magnetism of* Fe, Co *and* Ni *in molecular beams*, J. Magn. Magn. Mater **168**, 64 (1997).

[49] B. W. van de Waal, *Stability of face-centered cubic and icosahedral Lennard-Jones clusters*, J. Chem. Phys. **90**, 3407–3408 (1988).

[50] B. Raoult, J. Farges, M.-F. de Feraudy and G. Torchet, *Comparison between icosahedral, decahedral and crystalline Lennard-Jones models containing 500 to 6000 atoms*, Phil. Mag. B **60**, 881–906 (1989).

[51] J. P. K. Doye and F. Calvo, *Entropic effects on the size dependence of cluster structure*, Phys. Rev. Lett. **86**, 3570 (2001).

[52] X. Shao, Y. Xiang and W. Cai, *Structural transition from icosahedra to decahedra of large Lennard-Jones clusters*, J. Phys. Chem. A **109**, 5193–5197 (2005).

[53] C. L. Cleveland and U. Landmann, *The energetics and structure of nickel clusters: Size dependence*, J. Chem. Phys. **94**, 7376 (1991).

[54] H. M. Duan and Q. Q. Zheng, *Symmetry and magnetic properties of transition metal clusters*, Phys. Lett. A **280**, 333 (2001).

[55] A. V. Postnikov, P. Entel and J. M. Soler, *Density functional simulation of small* Fe *nanoparticles*, Eur. Phys. J. D **25**, 261 (2003).

[56] O. Šipr, M. Košuth and H. Ebert, *Magnetic structure of iron clusters and iron crystal surfaces*, Surf. Sci. **566-568**, 268 (2004).

[57] O. Šipr, M. Košuth and H. Ebert, *Magnetic structure of free iron clusters compared to iron crystal surfaces*, Phys. Rev. B **70**, 174423 (2004).

[58] H. Ebert, S. Bornemann, J. Minár, P. H. Dederichs, R. Zeller and I. Cabria, *Magnetic properties of* Co- *and* FePt-*Clusters*, Comp. Mat. Sci. **35**, 279 (2006).

[59] V. Kumar and Y. Kawazoe, *Icosahedral growth, magnetic behavior, and adsorbate-induced metal-nonmetal transition in palladium clusters*, Phys. Rev. B **66**, 144413 (2002).

[60] V. Kumar and Y. Kawazoe, *Evolution of electronic states and abnormal multishell relaxations in strontium clusters*, Phys. Rev. B **63**, 075410 (2001).

[61] P. Nava, S. M. and A. R., *Density functional study of palladium clusters*, Phys. Chem. Chem. Phys. **5**, 3372 (2003).

[62] M. L. Tiago, Y. Zhou, M. M. G. Alemany, Y. Saad and J. R. Chelikowsky, *Evolution of magnetism in iron from the atom to the bulk*, Phys. Rev. Lett. **97**, 147201 (2006).

[63] J. Guevara, F. Parisi, A. M. Llois and M. Weissmann, *Electronic properties of transition-metal clusters: Consideration of the spillover in a bulk parametrization*, Phys. Rev. B **55**, 13283 (1997).

[64] J. A. Franco, A. Vega and F. Aguilera-Granja, *Average magnetization and local magnetic moments of* Fe_N *clusters* ($N < 230$), Phys. Rev. B **60**, 434 (1999).

[65] G. Rollmann, M. E. Gruner, A. Hucht, P. Entel, M. L. Tiago and J. R. Chelikowsky, *Shell-wise Mackay transformation in iron nano-clusters*, Phys. Rev. Lett. **99**, 083402 (2007).

[66] P. J. Jensen and K. H. Bennemann, *Theory for the atomic shell structure of the cluster magnetic moment and magnetoresistance of a cluster ensemble*, Z. Phys. D **35**, 273–278 (1995).

[67] F. Aguilera-Granja, J. M. Montejano-Carrizales and J. L. Morán-López, *Magnetic moments of iron clusters: A simple theoretical model*, Phys. Lett. A **242**, 255 (1998).

[68] Y. Xie and J. A. Blackman, *On the oscillation of the magnetic moment of free transition metal clusters*, J. of Phys. Condens. Matter **15**, L615 (2003).

[69] Y. Xie and J. A. Blackman, *Enhanced effect of magnetic anisotropy on free clusters*, Appl. Phys. Lett. **82**, 1446 (2003).

[70] M. E. Gruner, G. Rollmann, A. Hucht and P. Entel, *Structural and magnetic properties of transition metal nanoparticles from first principles*, vol. 47 of *Advances in Solid State Physics*, p. 117, Springer, Berlin 2008.

[71] G. Rollmann, *Ab initio Simulationen eisenhaltiger Systeme: Vom Festkörper zum Cluster*, Ph.D. thesis, Universität Duisburg-Essen (2007).

[72] D. L. Huber, *Synthesis, properties, and applications of iron nanoparticles*, Small **1**, 482 (2005).

[73] M. Pellarin, B. Baguenard, J. L. Vialle, J. Lerme, M. Broyer, J. Miller and A. Perez, *Evidence for icosahedral atomic shell structure in nickel and cobalt clusters - comparison with iron clusters*, Chem. Phys. Lett. **217**, 349 (1994).

[74] A. L. Mackay, *A dense non-crystallographic packing of equal spheres*, Acta Cryst. **15**, 916 (1962).

[75] S. Ino, *Stability of multiply-twinned particles*, J. Phys. Soc. Jpn. **27**, 941 (1969).

[76] E. C. Bain, *The nature of martensite*, Trans. AIME **70**, 25 (1926).

[77] G. Wulff, *Zur Frage der Geschwindigkeit des Wachsthums und der Auflösung von Krystallflächen*, Z. Kristallogr. **34**, 29 (1901).

[78] L. D. Marks, *Modified Wulff construction for multiply twinned particles*, J. Cryst. Growth **61**, 556 (1983).

[79] H. C. Herper, E. Hoffmann and P. Entel, *Ab initio full-potential study of the structural and magnetic phase stability of iron*, Phys. Rev. B **60**, 3839 (1999).

[80] T. Vystavel, G. Palasantzas, S. A. Koch and J. T. M. De Hosson, *Nanosized iron clusters investigated with in situ transmission electron microscopy*, Appl. Phys. Lett. **82**, 197 (2003).

[81] P. Bobadova-Parvanova, K. A. Jackson, S. Srinivas and M. Horoi, *Density-functional investigations of the spin ordering in Fe_{13} clusters*, Phys. Rev. B **66**, 195402 (2002).

[82] G. Rollmann, P. Entel and S.Sahoo, *Competing structural and magnetic effects in small iron clusters*, Comp. Mat. Sci. **35**, 275–278 (2005).

[83] N. A. Besley, R. L. Johnston, A. J. Stace and J. Uppenbrinck, *Theoretical study of the structures and stabilities of iron clusters*, J. Mol. Struct. (Theochem) **341**, 75 (1995).

[84] M. E. Gruner, G. Rollmann, S. Sahoo and P. Entel, *Magnetism of close packed* Fe_{147} *clusters*, Phase Trans. **79**, 701 (2006).

[85] S. H. Baker, A. M. Asaduzzaman, M. Roy, S. J. Gurman, C. Binns, J. A. Blackman and Y. Xie, *Atomic structure and magnetic moments in cluster-assembled nanocomposite* Fe/Cu *films*, Phys. Rev. B **78**, 014422 (2008).

[86] P. Entel, M. E. Gruner, G. Rollmann, A. Hucht, S. Sahoo, A. T. Zayak, H. C. Herper and A. Dannenberg, *First-principles investigations of multimetallic transition metal clusters*, Phil. Mag. (2008), in print, DOI: 10.1080/14786430802398040.

[87] R. Meyer and P. Entel, *Martensite - austenite transition and phonon dispersion curves of* $Fe_{1-x}Ni_x$ *studied by molecular dynamics simulations*, Phys. Rev. B **57**, 5140 (1998).

[88] P. Entel, M. E. Gruner, A. Hucht, R. Meyer, G. Rollmann, S. Sahoo and S. K. Nayak, *Simulating structure, magnetism and electronic properties of monoatomic, binary and ternary transition metal nanoclusters*, in *MESOSCOPIC, NANOSCOPIC AND MACROSCOPIC MATERIALS: Proceedings of the International Workshop on Mesoscopic, Nanoscopic and Macroscopic Materials (IWMNMM-2008)*, edited by S. M. Bose, S. N. Behera and B. K. Roul, vol. 1063 of *AIP Conference Proceedings*, p. 3 (2008).

[89] C. M. Wei, C. Cheng and C. Chang, *Transition between icosahedral and cuboctahedral nanoclusters of lead*, J. Phys. Chem. B **110**, 24642 (2006).

[90] N. Lümmen and T. Kraska, *Investigation of the formation of iron nanoparticles from the gas phase by molecular dynamics simulation*, Nanotechnology **15**, 525 (2004).

[91] H. Jónsson and H. C. Andersen, *Icosahedral ordering in the Lennard-Jones liquid and glass*, Phys. Rev. Lett. **60**, 2295 (1988).

[92] D. Faken and H. Jónsson, *Systematic analysis of local atomic structure combined with 3D computer graphics*, Comp. Mat. Sci. **2**, 279 (1994).

[93] J. Kübler, *Theory of Itinerant Electron Magnetism*, Oxford University Press, Oxford 2000.

[94] T. Ichikawa, *Electron diffraction study of the local atomic arrangement in amorphous iron and nickel films*, phys. stat. sol. (a) **19**, 707 (1973).

[95] K. S. Suslick, S.-B. Choe, A. A. Cichowlas and M. W. Grinstaff, *Sonochemical synthesis of amorphous iron*, Nature **353**, 414 (1991).

[96] N. P. Kovalenko, Y. P. Krasny and U. Krey, *Physics of Amorphous Metals*, Wiley-VCH, Berlin 2001.

[97] E. Aprà, F. Baletto, R. Ferrando and A. Fortunelli, *Amorphization mechanism of Icosahedral Metal Nanoclusters*, Phys. Rev. Lett. **93**, 065502 (2004).

[98] L. E. Kar'kina, I. N. Kar'kin and Y. N. Gornostyrev, *Structural Transformations in* Fe-Ni-*alloy nanoclusters: Results of molecular-dynamics-simulations*, Phys. Met. Met. **101**, 130 (2006).

[99] Y. Xie and J. A. Blackman, *On the anomalous temperature dependence of the magnetic moment of cobalt clusters*, J. Phys. Condens. Matter **16**, 4373 (2004).

[100] Y. Xie and J. A. Blackman, *Magnetic anisotropy of nanoscale cobalt particles*, J. Phys. Condens. Matter **16**, 3163 (2004).

[101] M. L. Plumer, J. van Ek and D. Weller, eds., *The Physics of Ultra-High-Density Magnetic Recording*, Springer, Berlin 2001.

[102] H. Kodama, S. Momose, N. Ihara, T. Uzumaki and T. Atsushi, *Disk substrate deposition techniques for monodisperse chemically sythesized* FePt *nanoparticle media*, Appl. Phys. Lett. **83**, 5253 (2003).

[103] A. Perez, V. Dupuis, J. Tuaillon-Combes, L. Bardotti, B. Prével, E. Bernstein, P. Mélinon, L. Favre, A. Hannour and M. Jamet, *Functionalized cluster-assembled magnetic nanostructures for application to high integration-density devices*, Adv. Eng. Mater. **7**, 475 (2005).

[104] X. Yang, C. Liu, J. Yu, T. Klemmer, E. Johns and D. Weller, *Fabrications of* FePt *nanoparticles for self-organized magnetic array*, J. Vac. Sci. Technol. B **22**, 31 (2004).

[105] G. A. Held, H. Zeng and S. Sun, *Magnetics of ultrathin* FePt *nanoparticle films*, J. Appl. Phys. **95**, 1481 (2004).

[106] C. Antoniak and M. Farle, *Magnetism at the nanoscale: The case of* FePt, Mod. Phys. Lett. **18**, 1111 (2007).

[107] J. Lyubina, I. Opahle, K.-H. Müller, O. Gutfleisch, M. Richter, M. Wolf and L. Schultz, *Magnetocrystalline anisotropy in* $L1_0$ FePt *and exchange coupling in* FePt/Fe_3Pt *nanocomposites*, J. Phys. Condens. Matter **17**, 4157 (2005).

[108] S. Stappert, B. Rellinghaus, M. Acet and E. F. Wassermann, *Gas-phase preparation of* $L1_0$ *ordered* FePt *nanoparticles*, J. Cryst. Growth **252**, 440 (2003).

[109] B. Rellinghaus, S. Stappert, M. Acet and E. F. Wassermann, *Magnetic properties of* FePt *nanoparticles*, J. Magn. Magn. Mater. **266**, 142 (2003).

[110] B. Stahl, J. Ellrich, R. Theissmann, M. Ghafari, S. Bhattacharya, H. Hahn, N. S. Gajbhiye, D. Kramer, R. N. Viswanath, J. Weissmüller and H. Gleiter, *Electronic properties of 4-nm* FePt *particles*, Phys. Rev. B **67**, 014422 (2003).

[111] V. Salgueiriño Maceira, L. M. Liz-Marzán and M. Farle, *Water-based ferrofluids from* Fe_xPt_{1-x} *nanoparticles synthesized in organic media*, Langmuir **20**, 6946 (2004).

[112] G. A. Held, H. Zeng and S. Sun, *Magnetics of ultrathin* FePt *nanoparticle films*, J. Appl. Phys. **95**, 1481 (2004).

[113] T. Miyazaki, O. Kitakami, S. Okamoto, Y. Shimada, Z. Akase, Y. Murakami, D. Shindo, Y. K. Takahashi and K. Hono, *Size effect on the ordering of* $L1_0$ FePt *nanoparticles*, Phys. Rev. B **72**, 144419 (2005).

[114] O. Dmitrieva, B. Rellinghaus, J. Kästner, M. O. Liedke and J. Fassbender, *Ion beam induced destabilisation of icosahedral structures in gas phase prepared* FePt *nanoparticles*, J. Appl. Phys. **97**, 10N112 (2005).

[115] C. Antoniak, J. Lindner, M. Spasova, D. Sudfeld, M. Acet, M. Farle, K. Fauth, U. Wiedwald, H.-G. Boyen, P. Ziemann, F. Wilhelm, A. Rogalev and S. Sun, *Enhanced orbital magnetism in* $Fe_{50}Pt_{50}$ *Nanoparticles*, Phys. Rev. Lett. **97**, 117201 (2006).

[116] C. Rong, D. Li, V. Nandwana, N. Poudyal, Y. Ding and Z. L. Wang, *Size-dependent chemical and magnetic ordering in* $L1_0$-FePt *nanoparticles*, Adv. Mater. **18**, 2984 (2006).

[117] A. Ethirajan, U. Wiedwald, H.-G. Boyen, B. Kern, A. Klimmer, F. Weigl, G. Kästle, P. Ziemann, K. Fauth, J. Cai, J. Behm, A. Romanyuk, P. Oelhafen, P. Walther, J. Biskupek and U. Kaiser, *A micellar approach to magnetic ultrahigh-density data-storage media: Extending the limits of current colloidal methods*, Adv. Mater. **19**, 406 (2007).

[118] U. Wiedwald, A. Klimmer, B. Kern, H.-G. Han, L.and Boyen, P. Ziemann and K. Fauth, *Lowering of the* $L1_0$ *ordering temperature of* FePt *nanoparticles by* He^+ *ion irradiation*, Appl. Phys. Lett. **90**, 062508 (2007).

[119] B. Rellinghaus, S. Stappert, M. Acet and E. F. Wassermann, *Magnetic properties of* FePt *nanoparticles*, Journal of Magnetism and Magnetic Materials **266**, 142 (2003).

[120] Z. R. Dai, S. Sun and Z. L. Wang, *Shapes, multiple twins and surface structures of monodisperse* FePt *magnetic nanocrystals*, Surf. Sci. **505**, 325 (2002).

[121] D. Sudfeld, O. Dmitrieva, N. Friedenberger, G. Dumpich, M. Farle, C. Song, C. Kisielowski, M. E. Gruner and P. Entel, *HR-TEM studies of* FePt *nanoparticles by exit wave reconstruction*, Mater. Res. Soc. Symp. Proc. **998E**, 0998–J01–06 (2007).

[122] R. Wang, O. Dmitrieva, M. Farle, G. Dumpich, H. Q. Ye, H. Poppa, R. Kilaas and C. Kisielowski, *Layer resolved structural relaxation at the surface of magnetic* FePt *icosahedral nanoparticles*, Phys. Rev. Lett. **100**, 017205 (2008).

[123] R. Ferrando, J. Jellinek and R. L. Johnston, *Nanoalloys: From theory to applications of alloy clusters and nanoparticles*, Chem. Rev. **108**, 845 (2008).

[124] M. Müller and K. Albe, *Structural stability of multiply twinned* FePt *nanoparticles*, Acta Mater. **55**, 6617 (2007).

[125] M. Müller and K. Albe, *Lattice Monte Carlo simulations of* FePt *nanoparticles: Influence of size, composition, and surface segregation on order-disorder phenomena*, Phys. Rev. B **72**, 094203 (2005).

[126] B. Yang, M. Asta, O. N. Mryasov, T. J. Klemmer and R. W. Chantrell, *Equilibrium Monte Carlo simulations of A1-*$L1_0$ *ordering in* FePt *nanoparticles*, Scripta Mater. **53**, 417 (2005).

[127] B. Yang, M. Asta, O. N. Mryasov, T. J. Klemmer and R. W. Chantrell, *The nature of A1-$L1_0$ ordering transition in alloy nanoparticles: A Monte Carlo study*, Acta Materialia **54**, 4201 (2006).

[128] S. Heinrichs, W. Dieterich and P. Maass, *Kinetic growth of nano clusters with perpendicular magnetic anisotropy*, Europhys. Lett. **75**, 167 (2006).

[129] N. Lümmen and T. Kraska, *Homogeneous nucleation and growth in iron-platinum vapour investigated by molecular dynamics simulations*, Eur. Phys. J. D **41**, 247 (2007).

[130] G. Rossi, R. Ferrando and C. Mottet, *Structure and chemical ordering in* CoPt *nanoalloys*, Faraday Discussions **138**, 193–210 (2008).

[131] A. Fortunelli and A. M. Velasco, *Structural and electronic properties of* Pt/Fe *nanoclusters from EHT calculations*, J. Mol. Struct. (Theochem) **487**, 251 (1999).

[132] A. Fortunelli and A. M. Velasco, *Local properties of* Pt/Fe *nanoclusters by EHT calculations*, J. Mol. Struct. (Theochem) **528**, 1 (2000).

[133] Y. Wang, G. M. Stocks, A. Rusanu, D. M. C. Nicholson, M. Eisenbach, Q. Zhang and J. P. Liu, *Electronic and magnetic structure of* $L1_0$-FePt *nanoparticle embedded in* FePt *random alloy*, IEEE Trans. Magn. **43**, 3103 (2007).

[134] M. E. Gruner, G. Rollmann, P. Entel and M. Farle, *Multiply twinned morphologies of Fe-Pt and Co-Pt nanoparticles*, Phys. Rev. Lett. **100**, 087203 (2008).

[135] M. E. Gruner, *Antiferromagnetism and segregation in cuboctahedral* FePt *nanoparticles*, J. Phys. D: Appl. Phys. **41**, 134015 (2008).

[136] P. Entel and M. E. Gruner, *Large-scale ab initio simulations of binary transition metal clusters for storage media materials*, J. Phys. Cond. Matter (2009), in print.

[137] J. F. Clark, F. J. Pinski, D. D. Johnson, P. A. Sterne, J. B. Staunton and B. Ginatempo, *Van Hove Singularity induced* $L1_1$ *ordering in* CuPt, Phys. Rev. Lett. **74**, 3225 (1995).

[138] J. Lyubina, I. Opahle, M. Richter, O. Gutfleisch, K.-H. Müller, L. Schultz and O. Isnard, *Influence of composition and order on the magnetism of* Fe-Pt *alloys: Neutron powder diffraction and theory*, Appl. Phys. Lett. **89**, 032506 (2006).

[139] H. Zeng, R. Sabirianov, O. Mryasov, M. L. Yan, K. Cho and D. J. Sellmyer, *Curie temperature of FePt:*B_2O_3 *nanocomposite films*, Phys. Rev. B **66**, 184425 (2002).

[140] G. Brown, B. Kraczek, A. Janotti, T. C. Schulthess, G. M. Stocks and D. D. Johnson, *Competition between ferromangetism and antiferromagnetism in* FePt, Phys. Rev. B **68**, 052405 (2003).

[141] O. N. Mryasov, *Magnetic interactions in* 3*d*-5*d layered ferromagnets*, J. Magn. Magn. Mater. **272**, 800 (2004).

[142] J. M. MacLaren, R. R. Duplessis, R. A. Stern and S. Willoughby, *First principles calculations of* FePt*,* CoPt*,* Co_3Pt*, and* Fe_3Pt *alloys*, IEEE Trans. Magn. **41**, 4347 (2005).

[143] O. N. Mryasov, *Magnetic interactions and phase transformations in* FeM, M = (Pt, Rh) *ordered alloys*, Phase Transitions **78**, 197 (2005).

[144] M. Fallot, *Les alliages du fer avec les métaux de la famille du platine*, Ann. Phys. (Paris) **10**, 291 (1938).

[145] O. N. Mryasov, U. Nowak, K. Y. Guslienko and R. W. Chantrell, *Temperature-dependent magnetic properties of* FePt*: Effective spin Hamiltonian model*, Europhys. Lett. **69**, 805 (2005).

[146] P. Tu, A. J. Heeger, J. S. Kouvel and J. B. Comly, *Mechanism for the first-order magnetic transition in the* FeRh *System*, J. Appl. Phys. **40**, 1368 (1969).

[147] M. E. Gruner, E. Hoffmann and P. Entel, *Instability of the rhodium magnetic moment as origin of the metamagnetic phase transition in* α-FeRh, Phys. Rev. B **67**, 064415 (2003).

[148] G. Ju, J. Hohlfeld, R. J. M. van de Veerdonk, O. N. Mryasov, J.-Y. Kim, X. Wu, D. Weller and B. Koopmanns, *Ultrafast generation of ferromagnetic order via a laser-induced phase transformation in* FeRh *thin films*, Phys. Rev. Lett. **93**, 197403 (2004).

[149] M. E. Gruner and A. Dannenberg, *Structure and magnetism in near-stoichiometric* FePd *nanoparticles*, J. Magn. Magn. Mater., accepted for publication.

[150] J. Penuelas, C. Andreazza-Vignolle, P. Andreazza, A. Ouerghi and N. Bouet, *Temperature effect on the ordering and morphology of* CoPt *nanoparticles*, Surf. Sci. **602**, 545 (2008).

[151] F. Tournus, A. Tamion, N. Blanc, A. Hannour, L. Bardotti, B. Prével, P. Ohresser, E. Bonet, T. Epicier and V. Dupuis, *Evidence of* $L1_0$ *chemical order in* CoPt *nanoclusters: Direct observation and magnetic signature*, Phys. Rev. B **77**, 144411 (2008).

[152] H.-G. Boyen, K. Fauth, B. Stahl, P. Ziemann, G. Kästle, F. Weigl, F. Banhart, M. Hessler, G. Schütz, N. S. Gajbhiye, J. Ellrich, H. Hahn, M. Büttner, M. G. Garnier and P. Oelhafen, *Electronic and magnetic properties of ligand-free* FePt *nanoparticles*, Adv. Mater. **17**, 574 (2005).

[153] K. Ullakko, J. K. Huang, C. Kantner, R. C. O'Handley and V. V. Kokorin, *Large magnetic-field-induced strains in* Ni_2MnGa *single crystals*, Appl. Phys. Lett. **69**, 1966 (1996).

[154] A. Sozinov, A. A. Likhachev, N. Lanska and K. Ullakko, *Giant magnetic-field-induced strain in* NiMnGa *seven-layered martensitic phase*, Appl. Phys. Lett. **80**, 1746 (2002).

[155] V. Chernenko, C. Segui, E. Cesari, J. Pons and V. Kokorin, *Sequence of martensitic transformations in* Ni-Mn-Ga *alloys*, Phys. Rev. B **57**, 2659 (1998).

[156] V. V. Khovaylo, V. D. Buchelnikov, R. Kainuma, V. V. Koledov, M. Ohtsuka, V. G. Shavrov, T. Takagi, S. V. Taskaev and A. N. Vasiliev, *Phase transitions in* $Ni_{2+x}Mn_{1-x}Ga$ *with a high* Ni *excess*, Phys. Rev. B **72**, 224408 (2005).

[157] M. Richard, J. Feuchtwanger, D. Schlagel, T. Lograsso, S. Allen and R. O'Handley, *Crystal structure and transformation behavior of Ni-Mn-Ga martensites*, Scr. Mater. **54**, 1797 (2006).

[158] J. Enkovaara, A. Ayuela, L. Nordström and R. M. Nieminen, *Magnetic anisotropy in Ni_2MnGa*, Phys. Rev. B **65**, 134422 (2002).

[159] S. Fähler, *An introduction to actuation mechanisms in magnetic shape memory alloys*, ECS Transactions **3**, 155 (2007).

[160] T. Krenke, M. Acet, E. F. Wassermann, X. Moya, L. Mañosa and A. Planes, *Ferromagnetism in the austenitic and martensitic states of Ni-Mn-In alloys*, Phys. Rev. B **73**, 174413 (2006).

[161] T. Krenke, E. Duman, M. Acet, E. F. Wassermann, X. Moya, L. Mañosa, A. Planes, E. Suard and B. Ouladdiaf, *Magnetic superelasticity and inverse magnetocaloric effect in Ni-Mn-In*, Phys. Rev. B **75**, 104414 (2007).

[162] R. D. James and M. Wuttig, *Magnetostriction of martensite*, Phil. Mag. A **77**, 1273 (1998).

[163] J. Cui, T. W. Shield and R. D. James, *Phase transformation and magentic anisotropy of an iron-palladium ferromagnetic shape-memory alloy*, Acta Mater. **52**, 35 (2004).

[164] R. Hayashi, S. Murray, M. Marioni, S. Allen and R. O´Handley, *Magnetic and mechanical properties of FeNiCoTi magnetic shape memory alloy*, Sensors and Actuators **81**, 219 (2000).

[165] T. Kakeshita and T. Fukuda, *Giant Magnetostriction in Fe_3Pt and FePd Ferromagnetic Shape Memory Alloys*, Mater. Sci. Forum **394-395**, 531 (2002).

[166] T. Fukuda, T. Sakamoto, T. Kakeshita, T. Takeuchi and K. Kishio, *Rearrangement of martensite variants in iron-based ferromagnetic shape memory alloy under magnetic field*, Mater. Trans. **45**, 188 (2004).

[167] T. Kakeshita, T. Fukuda and T. Takeuchi, *Magneto-mechanical Evaluation for Twinning Plane Movement Driven by Magnetic Field in Ferromagnetic Shape Memory Alloys*, Mater. Sci. Eng. A **438-440**, 12 (2006).

[168] I. Opahle, K. Koepernik, U. Nitzsche and M. Richter, in preparation.

[169] R. A. Stern, S. D. Willoughby, A. Ramirez, J. M. MacLaren, J. Cui, Q. Pan and R. D. James, *Electronic and structural properties of* Fe_3Pd-Pt *ferromagnetic shape memory alloys*, J. Appl. Phys. **91**, 7818 (2002).

[170] R. A. Stern, S. D. Willoughby, J. M. MacLaren, J. Cui, Q. Pan and R. D. James, Fe_3Pd *ferromagnetic shape memory alloys*, J. Appl. Phys. **93**, 8644 (2003).

[171] P. J. Brown, A. Y. Bargawi, J. Crangle, K.-U. Neumann and K. R. A. Ziebeck, *Direct observation of a band Jahn-Teller effect in the martensitic phase transition of* Ni_2MnGa, J. Phys.: Condens. Matter **11**, 4715 (1999).

[172] A. Ayuela, J. Enkovaara, K. Ullakko and R. Nieminen, *Structural properties of magnetic Heusler alloys*, J. Phys.: Condens. Matter **11**, 2017 (1999).

[173] O. I. Velikokhatnyi and I. I. Naumov, *Electronic structure and instability of* Ni_2MnGa, Fiz. Tverd. Tela **41**, 684 (1999), [Physics of the Solid State **41**, 617 (1999)].

[174] J. Enkovaara, A. Ayuela, L. Nordström and R. M. Nieminen, *Structural, thermal, and magnetic properites of* Ni_2MnGa, J. Appl. Phys. **91**, 7798 (2002).

[175] A. Ayuela, J. Enkovaara and R. M. Nieminen, *Ab initio study of tetragonal variants in* Ni_2MnGa *alloy*, J. Phys.: Condens. Matter **14**, 5325 (2002).

[176] Y. Lee, J. Y. Rhee and B. N. Harmon, *Generalized susceptibility of the magnetic shape-memory alloy* Ni_2MnGa, Phys. Rev. B **66**, 054424 (2002).

[177] C. Bungaro, K. M. Rabe and A. Dal Corso, *First-principles study of lattice instabilities in ferromagnetic* Ni_2MnGa, Phys. Rev. B **68**, 134104 (2003).

[178] A. T. Zayak, P. Entel, J. Enkovaara, A. Ayuela and R. M. Nieminen, *A first-principles investigation of phonon softenings and lattice instabilities in the shape-memory system* Ni_2MnGa, Phys. Rev. B **68**, 132402 (2003).

[179] A. T. Zayak, P. Entel, K. M. Rabe, W. A. Adeagbo and M. Acet, *Anomalous vibrational effects in nonmagnetic and mangetic Heusler alloys*, Phys. Rev. B **72**, 0541113 (2005).

[180] A. T. Zayak and P. Entel, *A critical discussion of calculated modulated structures, Fermi surface nesting and phonon softening in magnetic shape memory alloys* Ni_2Mn(Ga, Ge, Al) *and* Co_2Mn(Ga, Ge), J. Magn. Magn. Mater. **290-291**, 874 (2005).

[181] A. T. Zayak, W. A. Adeagbo, P. Entel and K. M. Rabe, *e/a dependence of the lattice instability of cubic Heusler alloys from first principles*, Appl. Phys. Lett. **88**, 111903 (2006).

[182] P. Entel, M. E. Gruner, W. A. Adeagbo, C.-J. Eklund, A. T. Zayak, H. Akai and M. Acet, *Ab initio modeling of martensitic transformations (MT) in magnetic shape memory alloys*, J. Magn. Magn. Mater **310**, 2761 (2007).

[183] P. Entel, M. E. Gruner, W. A. Adeagbo and A. Zayak, *Magnetic field-induced changes in magnetic shape memory alloys*, Mater. Sci. Eng. A **481-482**, 258 (2008).

[184] M. E. Gruner, P. Entel, I. Opahle and M. Richter, *Ab initio investigation of twin boundary motion in the magnetic shape memory Heusler alloy* Ni_2MnGa, J. Mater. Sci. **43**, 3825 (2008).

[185] M. E. Gruner, W. A. Adeagbo, A. T. Zayak, A. Hucht, S. Buschmann and P. Entel, *Influence of magnetism on the structural stability of cubic* $L2_1$ Ni_2MnGa, Eur. Phys. J. – Special Topics **158**, 193 (2008).

[186] P. Entel, V. D. Buchelnikov, M. E. Gruner, A. Hucht, V. V. Khovailo, S. K. Nayak and A. T. Zayak, *Shape memory alloys: A summary of recent achievements*, Mater. Sci. Forum **583**, 21 (2008).

[187] A. Zayak, P. Entel and J. Chelikowsky, *Minority-spin polarization and surface magnetic enhancement in Heusler clusters*, Phys. Rev. B (2008).

[188] C. P. Opeil, B. Mihaila, R. K. Schulze, L. Mañosa, A. Planes, W. L. Hults, R. A. Fisher, P. S. Riseborough, P. B. Littlewood, J. L. Smith and J. C. Lashley, *Combined experimental and theoretical investigation of the premartensitic transition in* Ni_2MnGa, Phys. Rev. Lett. **100**, 165703 (2008).

[189] A. Zheludev, S. Shapiro, P. Wochner, A. Schwartz, M. Wall and L. Tanner, *Phonon anomaly, central peak, and microstructures in Ni_2MnGa*, Phys. Rev. B **51**, 11310 (1995).

[190] A. Zheludev, S. Shapiro, P. Wochner and L. Tanner, *Precursor effects and premartensitic transformation in Ni_2MnGa*, Phys. Rev. B, **54**, 15045 (1996).

[191] U. Stuhr, P. Vorderwisch, V. Kokorin and P.-A. Lindgard, *Premartensitic phenomena in the ferro- and paramagnetic phases of Ni_2MnGa*, Phys. Rev. B, **56**, 14360 (1997).

[192] L. Manosa, A. Planes, J. Zarestky, T. Lograsso, D. Schlagel and C. Stassis, *Phonon softening in* Ni-Mn-Ga *alloys*, Phys. Rev. B **64**, 024305 (2001).

[193] X. Moya, L. Mañosa, A. Planes, T. Krenke, M. Acet, V. O. Garlea, T. A. Lograsso, D. L. Schlagel and J. L. Zarestky, *Lattice dynamics and phonon softening in* Ni-Mn-Al *Heusler alloys*, Phys. Rev. B **73**, 064303 (2006).

[194] S. M. Shapiro, P. Vorderwisch, K. Habicht, K. Hradil and H. Schneider, *Observations of phasons in magnetic shape memory alloy* Ni_2MnGa, Europhys. Lett. **77**, 56004 (2006).

[195] P. Entel, M. E. Gruner and A. Hucht, *A first-principles study of the martensitic instabilities in magnetic shape memory alloys*, Mater. Res. Soc. Symp. Proc. **1050E**, 1050–BB03–01 (2008).

[196] V. L. Moruzzi, P. M. Marcus, K. Schwarz and P. Mohn, *Ferromagnetic phases of bcc and fcc* Fe*,* Co*, and* Ni, Phys. Rev. B **34**, 1784 (1986).

[197] J. Enkovaara, A. Ayuela, J. Jalkanen, L. Nordström and R. M. Nieminen, *First-principles calculations of spin spirals in* Ni_2MnGa *and* Ni_2MnAl, Phys. Rev. B **67**, 544171 (2003).

[198] K. Bhattacharya, *Microstructure of Martensite – why it Forms and how it Gives Rise to the Shape-Memory Effect*, Oxford University Press, Oxford 2003.

[199] J. M. Ball and R. D. James, *Fine phase mixtures as minimizers of energy*, Arch. Rat. Mech. Anal. **100**, 13 (1987).

[200] M. Pitteri and G. Zanzotto, *Continuum Models for Phase Transitions and Twinning in Crystals*, Chapman & Hall/CRC, Boca Raton 2003.

[201] P. J. Brown, B. Dennis, J. Crangle, T. Kanomata, M. Matsumoto, K.-U. Neumann, L. M. Justham and K. R. A. Ziebeck, *Stability of martensitic domains in the ferromagnetic alloy* Ni_2MnGa*: a mechanism for shape memory behaviour*, J. Phys.: Cond. Mat. **16**, 65 (2004).

[202] N. Okamoto, T. Fukuda, T. Kakeshita and T. Takeuchi, *Magnetocrystalline anisotropy constant and twinning stress in martensite phase of* Ni-Mn-Ga, Mater. Sci. Eng. A **438-440**, 948 (2006).

[203] T. Kakeshita and T. Fukuda, *Energy evaluation for twinning plane movement in ferromagnetic shape memory alloys*, Int. J. Appl. Electrom. **23**, 45 (2006).

[204] R. C. Pond and S. Celotto, *Special interfaces: Military transformations*, Int. Mater. Rev. **48**, 225 (2003).

[205] P. Müllner and G. Kostorz, *Microstructure of magnetic shape-memory alloys: Between magnetoelasticity and magnetoplasticity*, Mater. Sci. Forum **583**, 43 (2008).